

Subhasis Chaudhuri
Tanmay D. Pawar
Siddhartha Duttagupta

Ambulation Analysis in Wearable ECG

Ambulation Analysis in Wearable ECG

Subhasis Chaudhuri · Tanmay D. Pawar
Siddhartha Duttagupta

Ambulation Analysis in Wearable ECG

Subhasis Chaudhuri
Department of Electrical Engineering
Indian Institute of Technology, Bombay
Powai, Mumbai-400076
India
sc@ee.iitb.ernet.in

Tanmay D. Pawar
Department of Electrical Engineering
Indian Institute of Technology, Bombay
Powai, Mumbai-400076
India

Siddhartha Duttagupta
Department of Electrical Engineering
Indian Institute of Technology, Bombay
Powai, Mumbai-400076
India

ISBN 978-1-4419-0723-3 e-ISBN 978-1-4419-0724-0
DOI 10.1007/978-1-4419-0724-0
Springer Dordrecht Heidelberg London New York

Library of Congress Control Number: 2009928038

© Springer Science+Business Media, LLC 2009

All rights reserved. This work may not be translated or copied in whole or in part without the written permission of the publisher (Springer Science+Business Media, LLC, 233 Spring Street, New York, NY 10013, USA), except for brief excerpts in connection with reviews or scholarly analysis. Use in connection with any form of information storage and retrieval, electronic adaptation, computer software, or by similar or dissimilar methodology now known or hereafter developed is forbidden.

The use in this publication of trade names, trademarks, service marks, and similar terms, even if they are not identified as such, is not to be taken as an expression of opinion as to whether or not they are subject to proprietary rights.

Illustrations used in the text: Figures 1.3, 3.6, 3.7, 6.2, 6.3, 6.4, 6.6, 7.1, 7.6, 7.7, 7.8, 7.9, 7.12, 8.4, 8.5, 8.6, 8.8, 8.11, 8.12, 8.13, © Institute of Electrical and Electronics Engineers. Reproduced with permission.

Printed on acid-free paper

Springer is part of Springer Science+Business Media (www.springer.com)

To

My father for casting an everlasting shadow of his life on mine, and
my father-in-law for teaching me the value of simplicity.

-SC

My parents with love.
-TP

My closest circle of friends: my family.
-SD

Preface

We live in a fast-paced world today and, very often, we do not even have enough time for ourselves to recuperate fully after suffering from ailments. We also suffer from many lifestyle diseases, inconveniencing us slowly and silently. These are proving to be a big burden to our health care system. Quite naturally, researchers in the health care sector are trying their best to come up with technologies that provide help to those who would like to live a normal life despite their health problems.

Pervasive health care in the area of cardiac abnormalities is perhaps the most important one. One requires constant monitoring of the cardiac condition of a subject who is known to have had difficulties earlier. Holter monitoring had been one of the major steps in this direction, although it is not meant to be a fully wearable yet pervasive system. Over the last decade, attempts are being made to build a device which is truly wearable and provides various pre- and post-processing facilities.

Electrocardiography is the simplest non-invasive method of collecting signal from the beating heart that provides extremely useful information to the doctors. Hence ECG data collection is almost routine in any clinic dealing with heart patients. The procedure is highly standardized and the recorder is well calibrated so that any doctor anywhere in the world can interpret the data. The protocol requires that the patient lies down and be completely immobile so that skin to electrode contact is never disturbed. Any such disturbance will produce spurious signals in the ECG data obliterating the true interpretation by the doctor, making ECG presumably unsuitable for wearable applications.

Efforts have been made to improve the quality of ECG recorders. The weight and size have come down drastically. Data storage and on-chip processing power have improved manifold. The power consumption level has been reduced substantially such that the battery life is now prolonged to several days. The functionality now also includes wireless connectivity among others. All these recent developments make the wearable ECG recorder an ideal candidate for 24×7 monitoring of cardiac patients trying to maintain an active lifestyle.

VIII Preface

Notwithstanding above, various types of body movement activities, called BMA in this monograph, continue to plague the usefulness of such recorders due to the motion artifact it generates in the collected ECG data. The skin stretches and contracts due to body movement, changing the contact resistance at the electrode. Any change in skin humidity would also affect the resistivity of the skin but it is not considered in this monograph. The recorded signal is thus very different from the sedentary ECG when the subject is under ambulation. Since the true ECG signal and the motion artifact overlap in the spectrum, it is not possible to filter out these artifacts without affecting the morphology of the ECG signal.

Is pervasive cardiac monitoring using W-ECG recorder at all feasible? This is the key focus of this monograph. Although the industry focus has primarily been in developing such recorders, the signal processing aspects of the corresponding recordings have been mostly overlooked and the corresponding area is still largely unexplored. Needless to say, the final utility of such devices would depend on how useful are these signals to the clinicians.

We observe that most physical activities involve certain repetitive motions of our muscles and hence there must be some structure to the motion artifact signal which is superposed on the true cardiac signal. We ask the question if such a structure can at all be discovered from the recorded ECG signal. If it is so then that particular body movement can be recognized from the recorded ambulatory ECG signal itself. If the structure of the artifact signal is known for a given activity, this should also help us in cleaning the corrupted ECG signal. Further, in order that the above statement makes sense to the clinicians, there has to be some experimental validation that must bring out explicit correlation between this structured noise or artifacts and the actual motion (as measured by some device, say, an accelerometer) of the limb(s). The primary aim of the monograph is to demonstrate through development of appropriate signal processing techniques and experimental procedures that it is, indeed, possible to develop a truly pervasive, W-ECG based, cardiac monitoring system.

As mentioned earlier, the current state of research in this area of ambulatory ECG analysis is still in its infancy. A lot remains to be done before a firm recommendation of the new technology can be made for absorption by the health care industry. This book is meant to initiate the necessary dialog among researchers and practicing engineers to carry the concept further.

Any technical document in the form of a book or a monograph may suffer from the problem of being superfluous and unsubstantiated as there is very little opportunity for complete reviewing by peers. In order to avoid such a problem we made sure that the key concepts are first peer reviewed in the form of publications in appropriate journals. The publications that overlap with the contents of the book are given in the references [99, 100, 101, 102, 103]. We have modified and enhanced them to suit the demand of this book. Needless to say, the copyrights of various figures reproduced from our earlier publications rest with the original publishers.

The book is addressed to a broad audience. It should be useful to both practitioners and researchers in the area of biomedical engineering. We have tried to make the book self-contained and hence there is no specific prerequisite. Any one with basic familiarity with digital signal processing and linear algebra, will find the content quite readable. In order to bridge the gap between hardware and algorithmic developments, we have included chapters that specifically discuss the hardware aspects and the corresponding calibration issues. We have invited our colleagues who have actually developed such a hardware to write a chapter on hardware details. This particular aspect should be specifically useful to the practitioners in technology development.

We hope that the readers will find the book useful. We welcome comments and suggestions from readers.

Mumbai
March 2009

*Subhasis Chaudhuri
Tanmay Pawar
Siddhartha Duttagupta*

Acknowledgments

The authors are truly indebted to Prof. Soumyo Mukherji at IIT Bombay for suggesting to us that we investigate the possibility of identifying the nature of motion artifacts in ECG signals. Our discussions with him had always been very fruitful. The authors are also thankful to Profs. Harish Pillai and S. N. Merchant, both at IIT Bombay, for their insightful comments and suggestions. Thanks are also due to Profs. Maryam Shoejai-Baghini, Dinesh K. Sharma, both at IIT Bombay and Prof. Rakesh Lal who is currently at University of California, Santa Barbara, for having provided us with all necessary hardware support as well as for having accepted to write an invited chapter for this monograph.

The authors thank N. S. Ananthakrishnan for his help in data collection and running some experiments for developing the contents of Chapter 8. Thanks are due to Dr. Gandhi, Dr. Mohanty and their staff at Nanavati Hospital in Mumbai for their enthusiastic help and support in collecting relevant data from cardiac patients. We are also thankful to Prof. G. G. Ray of IITB for his help in data collection. Needless to say, the authors are thankful to all subjects who volunteered in the experiments.

Jennifer Evans and her staff at Springer, particularly Kelly Moritz, deserve to be thanked for making sure that we do complete the manuscript. Authors are also thankful to IEEE and Springer for their generous policy of allowing the authors to use figures published in their journals in the monograph.

The authors thank the Bharti Center for Communication in EE department at IIT Bombay for help and support.

The authors thank the Department of Science and Technology (DST) for the financial help in the form of J. C. Bose National Fellowship to the first author. The acknowledgment is incomplete without mentioning the constant support and encouragement received by the authors from their family members.

IIT Bombay
March 2009

*Subhasis Chaudhuri
Tanmay Pawar
Siddhartha Duttagupta*

Contents

1	Introduction	1
1.1	Basics of Electrocardiogram (ECG)	1
1.2	Artifacts in ECG	5
1.2.1	EMG Noise	5
1.2.2	Baseline Wandering	5
1.2.3	Powerline Interference	6
1.2.4	Motion Artifacts	6
1.3	Ambulatory Monitoring	6
1.4	Challenges in Ambulatory ECG Processing	8
1.5	Mathematical Model of Ambulatory ECG Signal	9
1.6	Tour of the Book	10
2	Review of ECG Analysis	15
2.1	QRS Detection Methods	16
2.2	Delineation of Wave Boundaries	18
2.3	Beat Alignment	20
2.4	Noise Reduction in ECG	21
2.5	Detection of Body Posture Changes	23
2.6	Overview of Wearable ECG Recorders	24
2.7	Analysis of Ambulation in ECG	25
3	Hardware Development of Wearable ECG Devices	27
3.1	Introduction	27
3.2	Basics of Personal ECG Instruments	28
3.2.1	System Modules and Operation	28
3.2.2	System Requirements	29
3.3	Electrodes	29
3.4	Signal Conditioning	30
3.4.1	Implementation Using General-Purpose ICs	31
3.4.2	ASIC (Application-Specific Integrated Circuit) Design for Signal Conditioning	33

3.5	Analog to Digital Converter	39
3.6	Digital Modules	42
3.6.1	Microcontroller	42
3.6.2	Data Storage	42
3.6.3	Data Retrieval	43
3.7	Discussion	43
4	Calibration of Locket	45
4.1	Calibration Requirements.....	46
4.2	Experimental Set-up	47
4.3	Calibration Technique.....	48
4.4	Results and Discussion	49
5	Data Acquisition	53
5.1	Introduction	53
5.2	Commonplace Body Movement Activities.....	54
5.3	Activity Transition	55
5.4	Motion Sensing	57
5.4.1	Data Collection using Accelerometer	57
5.4.2	Processing of Accelerometer Data	59
5.5	Variation of Activity Levels	60
5.6	Protocols for Treadmill Tests	60
6	Detection of Activity Transition	63
6.1	Introduction	64
6.2	Transition Detection	66
6.3	Experimental Results	70
6.4	Discussion	77
7	Activity Recognition.....	79
7.1	Introduction	80
7.2	Nonparametric Classification	82
7.2.1	Preprocessing	84
7.2.2	Principal Component Analysis (PCA).....	86
7.2.3	Supervised Learning of Body Movement	88
7.2.4	Activity Classification.....	90
7.2.5	Removal of Motion Artifacts	91
7.3	Parametric classification	91
7.3.1	Pre-processing	93
7.3.2	Feature Extraction	95
7.3.3	Hidden Markov Model (HMM) and Training	97
7.3.4	Activity Classification.....	99
7.4	Experimental Results	100
7.4.1	PCA-based Recognition	100
7.4.2	HMM-based Recognition	111

7.5 Discussion	120
8 Impact of Ambulation	123
8.1 Introduction	124
8.2 Derivation of Impact Signal	125
8.3 Synchronization of Impact and Motion Data	126
8.4 Experimentations	127
8.4.1 Experiments on the Treadmill	127
8.4.2 Experiments with Motion Sensors	130
8.5 Discussions	138
9 Conclusions	143
9.1 Conclusions	143
9.2 Scopes for Future Work	145
References	149
Index	159

Introduction

A surface electrocardiogram (ECG) is a plot of surface bio-potential caused due to electrical activity of the heart. It is a noninvasive tool widely used for many years for basic cardiac monitoring in a clinical set-up. With advances in technology, the ECG recording equipment are available in a smaller form-factor with some useful features like digital storage and wireless transmission of the recorded signals. Due to this improvement it is now practically possible to develop wearable ECG equipment for cardiac monitoring in ambulatory conditions. In this chapter we provide some background on electrocardiogram (ECG) signal and the relevant topics in the work related to analysis of ambulatory ECG signal. A brief summary on electrocardiogram (ECG), a discussion on a distinct set of artifacts in ECG signal, challenges in analysis of ECG due to the motion artifacts, a mathematical model of ambulatory ECG signal adopted in this work, and a tour of the monograph are given here in the subsequent sections.

1.1 Basics of Electrocardiogram (ECG)

A surface electrocardiogram (ECG) is a temporally evolving bio-potential signal caused due to the electrical activity of the cardiac muscles of the heart. This signal, called ECG, is recorded from the body surface itself by placing Ag/AgCl electrodes (for making electrical contacts with the skin surface) at specific locations without requiring any invasion. A human heart under normal conditions beats 72 times per minute. Under normal conditions, during every beat the cardiac muscles go through specifically ordered electrical activities which are distinctly identifiable from the patterns in the ECG signal. Thus the ECG signal is very important in cardiac monitoring. Moreover, it is the most simple, non-invasive and cost effective method and hence it is being used as a primary tool for cardiac monitoring.

Many types of cardiac disorders can be detected from the patterns in the ECG signal, in particular, those due to improper electric conduction through

damaged cardiac muscles. Some of the abnormal patterns in the ECG signal can be visually identified by a qualified professional and related to the damages in certain region of the heart. It is thus required to analyze signals from different leads of the ECG for determining the location of the damaged region. Here the lead refers to the signal acquired from a specific pair of ECG electrodes placed at predefined locations on the body. Thus every ECG lead looks at the specific area of the heart and, in order to cover different areas of the heart, different ECG leads are required. The ECG equipment commonly uses the standard 12-lead configuration. This standard configuration has three primary limb leads called lead - I (right arm (RA) with respect to left arm (LA)), II (RA with respect to left leg (LL)) and III (LA with respect to LL), which follow the triangular law of vector addition in the frontal plane, for example, $ECG_{II} = ECG_I + ECG_{III}$. There are three other leads derived in the frontal plane called augmented leads, aV_R , aV_L and aV_F . The speciality of the augmented leads is that the potential at one of the RA, LA and LL locations is measured with respect to the middle potential of the rest of the two locations. This way the electrical vectors of the augmented leads are rotated by 30° (and also that their amplitudes are enhanced) with respect to that of the primary leads in the frontal plane. Thus the signals from six limb leads represent six different views of the cardiac cycle which are taken from the angles equally spaced by 30° in the frontal plane. This helps to locate the exact orientation of the cardiac cycle in the frontal plane. The remaining six leads are called chest or pre-cordial leads: V_1 , V_2 , V_3 , V_4 , V_5 and V_6 , which are placed on the chest with respect to a negative terminal derived as the central potential point of RA, LA and LL, also known as Wilson's central terminal. The limb leads look into the frontal vertical plane whereas the pre-cordial leads look into the azimuth (horizontal or transverse) plane. The leads V_1 , V_2 , V_3 are called right pre-cordial leads and V_4 , V_5 and V_6 are called left pre-cordial leads. The basics of the electrocardiography discussed above are explained in more detail in [75, 138].

As we have seen, the ECG signal is acquired from a pair of specific locations on the body and Ag/AgCl electrodes are used for making electrical contact with the skin surface. There are two types of electrodes that can be used for acquiring ECG: reusable suction electrodes, and disposable foam pad electrodes. For long term continuous monitoring applications, pre-gelled foam pad electrodes are preferred due to the ease in usage. Suction electrodes are used for saving cost over multiple usage for short time periods as they can be reused after cleaning them. However, the use of suction electrodes is limited to the sedentary and short time recording/monitoring applications due to the following reasons.

1. In a suction electrode, the electrolyte gel applied on the contacting surface dries out quickly and hence it is unreliable for long term cardiac monitoring.

2. The suction against the skin can be sustained for a short while only. Therefore, the suction electrodes cannot be held in a fixed position for a long time.
3. The suction type electrode is bulky as compared to a foam pad electrode and hence for a wearable device the foam pad electrodes are more comfortable for the patient.

Thus from reliability and patient comfort view points the disposable foam pad electrodes are preferred in long term cardiac monitoring applications. A picture of a disposable foam pad adhesive ECG electrode is depicted in Fig. 1.1. The silver colored center in front is a male snap provided for connecting the lead wire with a female snap. The rear side of the connector is pre-gelled. The adhesive on the white foam on the rear side helps the electrode to be held at a fixed position on the skin.



Fig. 1.1. A pre-gelled foam pad electrode for acquiring ECG signal from the body.

A typical cardiac cycle (ECG beat) in the ECG signal has the following distinct characteristic segments called P wave, QRS complex and T wave occurring in a sequence as depicted in Fig. 1.2, which are important for in depth analysis. This particular cardiac cycle is acquired from ECG signal of lead II. Here the constant horizontal level of the line segments in between the ECG waves is called the baseline signal of the ECG and usually it is at an isoelectric level. Each of the ECG waves in a cardiac cycle represents a physiological activity of the heart. The cycle of the electrical activity of the heart starts with P wave, which represents atrial depolarization (contraction). Typically, the P wave is of less than 110ms duration. Some the abnormalities related to the atria like left/right atrial hypertrophy, atrial premature beat, etc. can be detected from the the P wave. There is a horizontal line segment at isoelectric level followed by the Q wave, called PQ (or PR when Q is absent) interval. Typically, the PQ interval is of 120-200ms duration. Some of the heart diseases (like Wolf-Parkinson-White syndrome or first degree heart block) may cause a shorter or longer PR interval. Next to the PQ wave in the

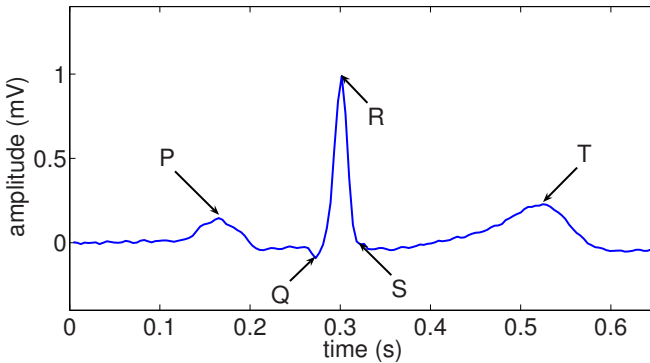


Fig. 1.2. A typical cardiac cycle of ECG signal, captured in a sedentary condition by a wearable ECG recorder.

graph is QRS complex which is with a sharp peak at middle, called R wave. The QRS complex represents the ventricular depolarization which may be typically of 60-100ms duration. In fact, the atrial repolarization (deactivation) occurs during the same interval but it is not noticeable. Many ailments like cardiac arrhythmias, myocardial infarction, conduction abnormalities can be detected from the QRS complex. Since QRS complex is the most dominant feature of the ECG cycle, it is used for determining the heart rate for a normal cardiac rhythm. The next important wave representing the ventricular repolarization is called T wave. The interval between the start of QRS complex and peak of the T wave is called absolute refractory period. The segment between the end of the QRS complex and the beginning of the T wave is called ST segment which lies at the same level as PQ segment. ST and T waves are analyzed for detection of myocardial infarction and ischemia.

For a normal functioning heart the cardiac cycle repeats continuously in the same ordered manner and time of repetition of the cardiac cycle determines the heart rate, which is variable due to many different physiological aspects, for example, respiration rate, physical stress, anxiety, etc.

The morphology of an ECG beat is specific to a particular lead since each of the leads represents a specific view of the electric field due to the cardiac activity. A trained expert (cardiologist) can visually detect most abnormalities in the morphology of the ECG and thereby diagnoses the nature of ailment. Since the spectrum of the ECG signal lies in the range of 0.05Hz to 130Hz (approximately), the ECG equipment should have the specified bandwidth for diagnostic purposes. A more detailed introduction to the electrocardiography can be found in [75, 138].

1.2 Artifacts in ECG

The ECG signal includes numerous artifacts. The origin and nature of these artifacts are of considerable interest, particularly for long term monitoring applications. Some of the artifacts are caused due to physiological reasons like electromyograph (EMG or muscular activity) noise and slow baseline wandering due to respiration. There are some artifacts which are due to non-physiological reasons, for example, 50 or 60Hz powerline interference and motion artifacts in ECG. The presence of the artifacts will make any morphology based diagnosis problematic. The main sources of ECG artifacts are discussed next.

1.2.1 EMG Noise

Any muscular activity in the body produces a bio-potential signal which is also known as the electromyograph (EMG) signal. The peak amplitude of the EMG signal on the surface of the body is in the range from 0.1 to 1mV and the spectrum is concentrated on the frequency range from 5 to 500Hz. Since the EMG and ECG signals have partly overlapping spectra, the muscular activity may cause interference in the ECG signal. This type of noise is known as EMG noise. During clinical testing, the patient is usually in a rest condition and hence the chances of EMG noise occurring are rare. Moreover, both the patient activity and ECG trace are monitored so that such a noisy episode in ECG trace can be recognized as an EMG interference. For short time monitoring purposes only a few cycles of ECG signals are required. However, for long term monitoring under ambulatory conditions the presence of high frequency EMG noise is problematic.

1.2.2 Baseline Wandering

We have seen in the previous section that the baseline of the ECG should ideally be at a constant level referred to as the isoelectric level. However, variations in lung volume (diaphragm) due to respiration alter the path impedance between the ECG electrodes which results in a slowly varying potential difference for a constant current. Slow motion of the electrodes can also cause a non-steady baseline. The artifact produced by motion of electrodes is known as motion artifact which is discussed in Section 1.2.4. During the rest ECG for short time monitoring in clinics the motion of the patient is restricted and hence the motion artifact is not expected. However, the baseline wandering and EMG noise explained above are quite common in long term ECG monitoring. The slow wandering of the baseline can be eliminated by selecting a frequency value greater than 1Hz as the lower cutoff frequency of the ECG amplifier. However, the low frequency contents of the ECG signal (from 0.05 to 2Hz) like P and T waves are distorted due to this type of filtering.

1.2.3 Powerline Interference

The powerlines and the lead wires of the ECG recorder are coupled through capacitive paths. Hence a 50/60Hz current flows in each of the lead wires depending on the amount of coupling. The currents take path from the corresponding lead wires through the body to the common ground. Assuming the distance between any two leads to be very small, the powerline currents in both the leads would be the same. This common mode powerline interference can be rejected by a front end difference amplifier with a very high common mode rejection ratio (CMRR). However, due to the impedance difference (ΔZ) in the paths taken through the body for both the currents, there will be an additional voltage difference ($i\Delta Z$) caused by the powerline. This voltage signal is further amplified along with the ECG signal by the difference amplifier which is referred as powerline interference. This type of interference appears as a 50 or 60Hz noise.

1.2.4 Motion Artifacts

As described previously, the artifact caused due to motion of electrodes is known as motion artifact. The electrode used for providing electrical contact between the skin and the lead cable can be modeled as a network of equivalent resistors and capacitors representing electrical parameters of different layers of the skin and the skin electrode interface [138]. The values of these electrical parameters may be altered due to relative motion of the electrodes or skin stretch or contract. This means that the equivalent impedance of the skin and the skin electrode interface gets disturbed due to any such action which results in an artifact known as motion artifact. Unfortunately, the motion artifact has a significant overlap with the spectrum of the ECG signal in the frequency range 1-10Hz and hence it is very difficult to handle this type of artifact. It is noted that the motion artifact is more abrupt and distinct in nature as opposed to the slow baseline wander caused due to respiration. The motion artifact poses a major challenge in the long term (ambulatory) cardiac monitoring using a wearable ECG equipment.

1.3 Ambulatory Monitoring

Long term monitoring of ECG is recommended for people who have been diagnosed with mild versions of a cardiac disorder but who still lead an active lifestyle. Currently, this situation applies to a substantial body of people all over the world. Long term monitoring is also a necessity for an improved, post operative life span of a cardiac patient. However, such monitoring has not been given due importance in practice. It is mostly avoided because of the time and resource constraints, and due to the fact that protocols for remote

monitoring of cardiac patients are not yet in place. An ambulatory ECG monitor is a practical solution to prevent this situation. With the miniaturization of electrical circuits and components, very small size, light weight, wearable ECG recorders (W-ECG) are now available for ambulatory cardiac monitoring. One such W-ECG has been developed by Baghini *et al.* [117, 134] at the Department of Electrical Engineering at IIT Bombay, and the corresponding wearable recorder is called *locket*. A prototype of the *locket* which can record ECG from any one of the primary leads continuously for 48 hours into an inbuilt flash memory cell is depicted in Fig. 1.3.



Fig. 1.3. A single-lead wearable ECG recorder called *locket*, developed by Baghini *et al.* [117] at IIT Bombay, placed by the side of a 15cm ruler. (©2007 IEEE)

W-ECG is a variant of the standard ECG in the sense that the electrode placements are on frontal trunk approximating the positions on the limb sites in the standard ECG [12]. Some W-ECG may have fewer leads in order to reduce the number of electrodes and complexity. A commonly used lead II configuration for W-ECG is shown in Fig. 1.4. The purpose of W-ECG is long term monitoring of the heart while the patient is allowed to perform his/her routine activities. Infrequent or irregular symptoms of heart disorders that may not be detected during brief clinical check-ups may be detected through long term monitoring. However, a major difficulty with any skin electrode based physiological monitoring is that motion of electrodes induces artifacts in the recorded signal. This type of artifact arising due to a non-physiological reason and at a superficial level of the skin is called motion artifact.

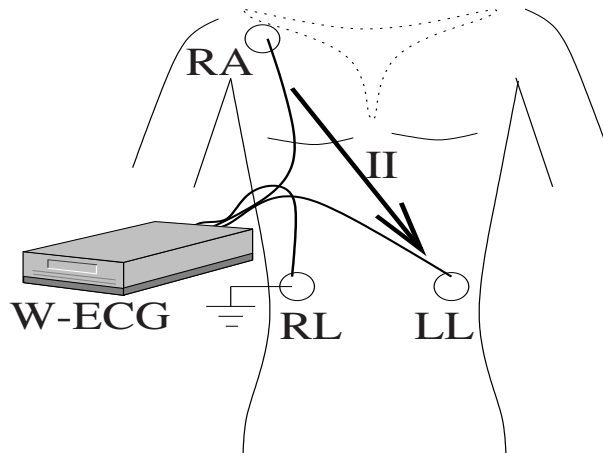


Fig. 1.4. A wearable ECG worn in lead II configuration. The electrodes are placed on trunk proximate to the positions for standard lead II ECG indicated by RA, RL and LL. RA, RL and LL stand for right arm, right leg and left leg positions of the electrodes, respectively.

1.4 Challenges in Ambulatory ECG Processing

The problem of elimination of motion artifacts is non-trivial since the energy contents of both the motion artifact and ECG signals share a common spectral band of 1-10Hz and hence it cannot be removed using a linear filter without distorting the ECG features like P and T waves. Moreover, motion artifacts can mimic a cardiac event in the ECG such as elevation or depression in P or T wave and ST segment, etc. This will be clear from an example of an ECG waveform depicted in Fig. 1.5, which is recorded while the wearer is involved in twisting of body from the waist upwards. Here, the R peaks are clearly seen indicating five heart beats, yet it is difficult to determine correct locations and amplitudes of P and T waves because of the interference due to the motion artifact signal. Accordingly, interpretation of the raw ECG signal will be prone to error and some techniques should be adopted that can characterize and isolate the motion artifact signal.

The quality of the recorded ECG signal is affected by the motion artifact. If the signal power of motion artifact is high then the cardiac signal gets suppressed under the motion artifact, making interpretation of the ECG signal very difficult. Similarly, the recorded signal in absence of any motion artifact, genuinely represents the cardiac signal and is considered suitable for diagnosis purposes. Unfortunately, there is no authenticity measure of the absence of motion artifacts in the ECG signal hence the ECG signals only during sedentary (rest) condition that ensures absence of motion artifact, are considered useful for clinical interpretations. Even filtered signal after the artifact removal

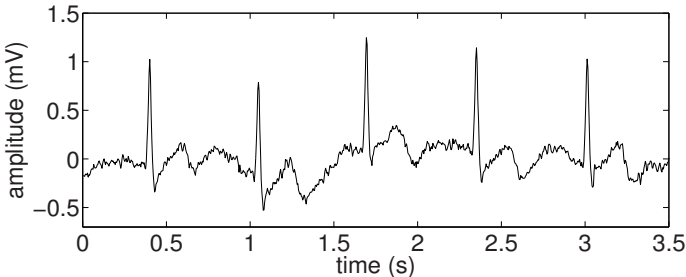


Fig. 1.5. An example of ECG signal captured while the wearer is twisting the upper trunk from waist. The R peaks are visible indicating the presence of heart beats but the other ECG features like P and T waves are contaminated severely due to the motion artifact.

is not considered adequate due to possible distortion of cardiac features like P, T waves and ST segment.

In long term monitoring a huge volume of ECG data is generated and hence it is ideally suited for computer aided analysis (CAA). However, most of the CAA algorithms are suitable only for artifact-free ECG taken under rest conditions and are not adequate to handle the motion artifact generated in ambulatory monitoring. Therefore, during ambulatory monitoring, it is a practice to maintain the account of all physical activities for post event analysis of the recorded ECG signal for quality assurance. The useful parts of the ECG signal can thus be segmented from the noted time of start and end of every body movement performed by the user. This requires a human expert (interpreter) which is not a practical solution to analyze the voluminous ECG data.

If the extent of the motion artifact in the ECG signal is known automatically then it can help in the cardiac interpretation. For example, the physician can decide whether the elevation in T wave is due to ischemia or due to the motion artifact provided the information regarding the motion of the patient is available. However, it may not be so easy to know the exact level of motion artifact from the recording of the patient activities either by motion sensors or video.

1.5 Mathematical Model of Ambulatory ECG Signal

The purpose of ambulatory monitoring is to capture the cardiac activity of the heart taking place while the user (subject) is performing all kinds of routine physical activities. However, during the ambulatory monitoring the induced motion artifact in the recorded ECG signal due to body movements poses a great challenge as we have seen in the previous section. Thus the recorded ECG signal is not just the cardiac signal but a composite ECG signal containing

motion artifacts. Since the generation of the motion artifact is at a superficial level, it is safe to assume that the cardiac cycle itself is not affected by the motion artifact for moderate physical activities. In other words, the composite ECG signal is superposition of two independent events: the cardiac signal and the motion artifact signal induced due to the body movement activity (BMA). Since the W-ECG recorder performs amplification, filtering and digitization of the acquired electrical signal from the electrodes, an additive random noise arising out of the device electronics may be present in the digitized ECG signal. This signal is referred as sensor noise. Therefore, the ambulatory ECG signal $r(n)$ in digital form can be modeled as sample wise addition of three different signal components

$$r(n) = q(n) + s(n) + \eta(n), \quad (1.1)$$

where $q(n)$, $s(n)$ and $\eta(n)$ are cardiac signal, motion artifact signal and sensor noise, respectively. Since the recorder (called *locket*) is calibrated for the dc bias in the output, the sensor noise $\eta(n)$ has zero mean. It is also ensured by selection of suitable design and reliable circuit components, that the sensor noise $\eta(n)$ is very low ($< \text{rms } 6 \mu\text{V}$) compared to the other two components in the model. The mathematical model in Eq. (1.1) represents the composite signal in a single lead of ECG in general and can be extended for ECG signals from multiple leads. The main aim here is to analyze the single lead ECG signal for better interpretations for long term cardiac monitoring in presence of motion artifact. The model in Eq. (1.1) has been adopted to represent the ECG signal recorded by the *locket*. It is further noted that such an additive model is widely used in generating composite ECG signals artificially for testing the performance of various filtering and analysis algorithms [5, 110, 120]. However, here we extract the motion artifact signal from the composite ECG signal available from subjects in real life, involved in physical activities. We use the motion artifact signal to recognize the physical activities. We will present in this monograph some of our experimental results based on the ECG signals captured from the subjects in real life.

1.6 Tour of the Book

Since the cause of generation of the motion artifact is stretching or contraction of skin due to body movement, the induced motion artifact contains information regarding the body movement. Moreover, different body movements are performed in different manners, therefore, the generated motion artifacts due to different body movements are different in nature. It has been observed that different pace levels of the BMA have different impact on the generation of motion artifact in ECG. With this rationale we want to show that the body movement activity (BMA) can be recognized from the motion artifact itself. However, the motion artifact signal is not available separately but contained in

the composite ECG signal as we have explained in Section 1.5. Therefore, we have to devise suitable methods that can separate the motion artifact signal from the composite ECG signal and extract the BMA information contained in the motion artifact signal. The focus here is on deriving some useful information regarding BMA from a single lead ECG itself without requiring any additional sensors. Moreover, it is interesting to quantify the impact of BMA on motion artifact generation. In this monograph some useful techniques for BMA recognition from ECG and impact analysis of BMA on ECG signal are discussed. The accuracy of these techniques have been tested based on real life ambulatory ECG data. Our work shows quite satisfactory results but leaves room for further improvement. Here we briefly highlight the main topics of the monograph.

- The *locket* (W-ECG) used to acquire ECG data is a very compact and sophisticated device. It has been designed in-house by a few colleagues of ours and a brief exposure to the actual design of the hardware is provided. Various specifications which are crucial to the design of portable ECG recorder are also provided. Since the human heart beat follows a very regular cyclic rhythm, it is necessary that such a recorder is calibrated in terms of the sampling rate so that the acquired data can actually be related to the cardiac cycle. A simple method of calibration using power-line signal interference is suggested in the monograph. This would allow the practitioners to repeat all experimentations performed in their study, when the corresponding data is acquired by their own recorder. Finally, we also discuss in details the experimental protocol used throughout in this monograph. Such a protocol is a must if any technology is envisaged to be of any practical use in health sciences.
- As stated previously, the motion artifacts induced due to different types of BMA are different in nature. This hypothesis has been tested successfully on the ECG signals collected from subjects in real life while performing various types of BMA with transitions among different types of BMA. The corresponding ECG signal is analyzed beat by beat using a recursive principal component analysis (RPCA) [72] based method. The proposed RPCA based method can follow the slowly time varying changes in cardiac cycle as well as changes in motion artifact signal due to the same type of BMA, while detecting abrupt changes in motion artifact signal due to the transition to a different type of BMA. This demonstrates that the motion artifact signals induced due to different types of BMA are distinct. The detection of BMA transitions is useful for temporal segmentation of ECG beats with respect to the type of BMA.
- Next, the separability of motion artifacts due to different types of BMA is tested by posing a problem of BMA recognition from the ECG signal itself using the separation between the different motion artifact signals. ECG signals, while subjects performing certain specific types of commonplace BMA encountered in routine daily activities, e.g., hand movements, walk-

ing, climbing stairs, etc., are collected such that each ECG signal contains just one of the specified BMAs. The cardiac cycle in the ECG signal is estimated by arithmetic mean of collected and appropriately time warped ECG beats. The cardiac component is suppressed by subtracting the estimated mean of the cardiac cycle from each of the beats in the recorded ECG signal. The residual signal after mean subtraction mostly contains the motion artifact component. These residual motion artifact signals in each of the BMA classes are analyzed using a principal component analysis (PCA) based method which computes the eigenvectors of the covariance matrix of the motion artifact signal for each of the BMA classes. A set of top few eigenvectors is used for representing the artifact subspace of the particular BMA class. The BMA class of a test ECG beat is recognized using the criterion of minimum error in reconstruction by the corresponding sets of eigenvectors. Here we also discuss a scheme of motion artifact removal from ECG using a class specific PCA based filtering technique. In this class specific filtering, the BMA class of the ECG beat is recognized using the PCA based technique and then the motion artifact components are removed using the corresponding set of eigenvectors for that particular BMA class. The usefulness of this scheme is shown in terms of improvements in detection of P and T waves using some standard methods, since the motion artifact contaminates these two ECG waves severely due to the spectral overlap with the P and T waves.

- Thus far, we have shown that it is possible to detect the changes in different types of BMA and to recognize them as individual classes from the ECG itself using the separability of the motion artifact signals induced due to different types of BMA. Next, we explore the possibility of BMA recognition by taking a very different approach of classification. Likewise the PCA based method, we use a supervised learning technique for the classification. However, instead of using a nonparametric classifier we consider parametric classifiers based on a hidden Markov model (HMM). HMM is a well-known technique for modeling of processes having inherent temporal dependence [24, 106]. First, we separate the motion artifact signal from the recorded ECG by using an adaptive filter. Then the derived motion artifact signals are modeled through an HMM using their temporally localized energy contents in different frequency bands. Since the energy of motion artifact signal is concentrated in a low frequency band of 1-10Hz, we analyze this band using Gabor filter banks of 10 different, equally spaced local frequency components at any given instant of time. Based on this Gabor filter we compute the energy features in each of the spectral bands. The spectral energy features of the motion artifact signal are used for modeling the corresponding BMA class. After having modeled each BMA class with a single HMM based on the derived energy features, the BMA class of a test sequence is recognized based on the maximum likelihood criterion.
- Till now the ECG signals are analyzed from the point of view of separability of the induced motion artifacts due to different types of BMA,

performed at a nearly constant, normal pace for each individual subject. The ECG signal under the impact of body movement is now further analyzed to study and quantize the impact of different pace levels involved in performing the same BMA. The ECG signal is collected while performing a particular BMA at three different pace levels: slow, medium and fast, in order to quantify the difference in the generated motion artifact due these levels. The pace levels are measured quantitatively in terms of the acceleration signals captured by the motion sensors placed at suitable positions on the body. The goal of this work is to find how the different pace levels of the same type of BMA affect the ECG signal differently and their impact on generation of motion artifacts. The RPCA error signal is derived from the resulting ECG signal as a measure of impact of different pace levels on ECG signal, simply referred to as an impact signal. The impact signal and acceleration signals are analyzed in synchronization to demonstrate that the impact signal alone can correctly represent the different pace levels in most of the BMAs considered in this work. We found a very high correlation between the impact signal and the acceleration signals, suggesting that the level of BMA can be determined from the ECG signal itself without requiring any motion sensors.

In this chapter we have provided a basic introduction to ECG, common artifacts in the ECG signal, motion artifact in ambulatory ECG, the challenges in processing ambulatory ECG and a mathematical model of ambulatory ECG signal which is adopted in this monograph for analyses in the forthcoming chapters. The main topics of the monograph are also briefly listed.

The organization of the subsequent chapters in the monograph is as follows. First we discuss some of the relevant works in the literature regarding processing of the ECG signal starting from QRS detection to analysis of physical activities in ECG in Chapter 2. In Chapter 3 we provide hardware design details for the *locket*. We have invited our peers who are experts in the hardware design to write the chapter for completeness of the treatment and for the benefit of all readers. In Chapter 4 we discuss a simple procedure for calibration of the sampling rate of the *locket* which can be used for any electronic ECG recorder in general. We describe the protocols followed for collecting the experimental data in Chapter 5. We discuss a technique for detection of transitions of BMA in Chapter 6. In Chapter 7 we show that BMA can be recognized from ECG signals based on classification of motion artifact signals. We discuss here both nonparametric and parametric classification techniques for BMA recognition. In Chapter 8 we study impact of BMA in ECG from two different types of experiments, one using a treadmill and the other using motion sensors. Finally, we note our conclusions in Chapter 9.

Review of ECG Analysis

In 1887, Augustus D. Waller published the first human electrocardiogram (ECG) recorded with a capillary electrometer. Subsequently, Willem Einthoven invented a more sensitive galvanometer for producing ECG using a fine quartz string coated in silver. He invented the lead system for ECG recording and identified the five deflection points in the cardiac cycle by naming them P, Q, R, S and T which are still being used in the present standards (see Fig. 1.2). Einthoven also started transmission of ECG from hospital to his laboratory on telephone lines [33]. Since then a huge knowledge base has been generated covering clinical and engineering aspects of electrocardiography. Since last few decades electronic recorders have been developed for digital recording of the ECG signal. In recent years the ECG recorders are available in a much compact form so that the user can wear it for ECG recording without much of obstruction in the routine activities. Recently, the wearable ECG recorders (W-ECG) are becoming very popular because of their low cost, long term recording capability and ease of use.

Since a huge volume of ECG data is generated by the W-ECG, automated methods are preferred for analysis of the ECG signal. The ECG data may be composed of single-lead or multiple-lead ECG signals depending upon the type and configuration of the ECG recorder. Accordingly, the method of analysis is also different. Single-lead ECG waveform analysis includes wave shapes (morphologies), spectra and repeatability of the cardiac cycle. On the other hand, multi-lead ECG processing algorithms can utilize additional information like simultaneous features from other leads. This may lead to a greater immunity against interference signals. The disadvantage of multiple leads lie in increased patient discomfort and stress, especially for ambulatory testing. For the purpose of basic cardiac monitoring during ambulatory testing, it is desirable to have fewer leads and hence single-lead algorithms are more suitable for W-ECG applications. In this chapter we will review some of the existing techniques developed for analysis of single-lead ECG signals.

2.1 QRS Detection Methods

As we have seen in Chapter 1, ECG is a pseudo-periodic signal in the sense that the cardiac cycle repeats according to heart rate. However, the heart rate may not remain constant. The components of cardiac cycles appear in a regular sequence P-QRS-T. The variations in the heart rate may affect the durations of PQ and ST segments while the durations of P wave, QRS complex and T wave may still remain the same for a normal heart. The R peak in the QRS complex is the dominant feature of the cardiac cycle, which can be distinctly recognized from the sharp edges and a high amplitude as we have seen in Fig 1.2. Therefore, it is relatively easy to locate the QRS complex in the ECG even in the presence of low frequency noise (like baseline wandering due to respiration) and hence this is used for determining the current heart beat. The QRS detection forms the basis of most ECG analysis algorithms, particularly those used for arrhythmia monitoring [19, 77, 127]. The current heart rate may be determined by calculating the time period between the two consecutive R peaks. Moreover, specific ECG parameters can be derived using the R peak locations. For example, ST segment is measured at a certain predefined time interval from the end of the QRS complex [121] and the corrected QT interval is derived by well known Bazzet's formula using the current QT and RR intervals [14]. This explains the importance of QRS detection in cardiac monitoring using ECG.

QRS detection algorithms, in general, use the relatively high energy contents of the QRS complex that lie in 5-25Hz band [63, 96, 128]. The more complex QRS detection algorithms involve application of neural network, hidden Markov model (HMM), syntactic methods, etc. [22, 48, 124, 133], but they are rarely used in low cost W-ECG applications. Further details of the QRS detection methods and the comparisons of their performances in presence of noise and their computational complexities can be found in [35, 63, 95]. Most of the simple QRS detection algorithms are based on one of the following methods: derivatives, filter-banks, wavelets, mathematical morphology and correlation [35, 63]. Here a few of the approaches in literature for QRS complex detection are discussed in brief.

The characteristic of higher slopes of the QRS complex inspires one to use temporal derivatives for its detection. In the derivative based methods, the ECG signal is first smoothed with an appropriate moving average filter for suppressing any high frequency noise outside the 5-25Hz band. The smoothed signal is differentiated to emphasize the high slopes and to suppress smooth ECG waves and baseline wanders. The overall response of these two simple arithmetic operations results in a bandpass filter to match the spectral band of the QRS while suppressing the relatively low frequencies in P and T waves. The squared magnitude of the derivative signal is used to enhance further the high derivatives of the QRS complex. A moving average integration filter with the window length matching the duration of QRS complex is applied after the squaring operation. The integrated signal is then searched for the

local maxima exceeding an appropriate threshold value. The search is further refined by eliminating the points which occur within the refractory period of a ventricular activity [41, 94, 96].

Wavelet based methods for QRS detection use the principle of singularity detection in the wavelet coefficients [74]. Wavelet coefficients of the ECG signal at several scales are analyzed [11, 59, 70, 71, 111] to find the local maxima and positions of matching in two consecutive scales to locate QRS positions. This is based on the assumption that the energy of the QRS complex is continuously spread over the spectral bands as well as the temporal scales. The noise in the signal may not have this kind of property and hence false alarms due to such noise can be reduced using this multiscale approach.

In a filter bank approach of QRS detection, subbands at different scales are combined to confirm the positions of the local maxima [4]. The filter bank approach is based on the fact that the QRS complex has simultaneous presence in the subbands, whereas other ECG waves and noise may not exhibit this characteristic behavior. This is similar to the wavelet based approach of QRS detection. In [15, 123], a generalized class of filter with a transform having two factors, $(1 - z^{-K})(1 + z^{-1})^L$ is given: the first implements a difference with integer delay K and the other is for a lowpass filter with band width controlled by an integer parameter L . The integer parameters (K, L) are determined depending upon the sampling rate. At a sampling rate of 100Hz, $(K, L) = (1, 2)$ is found to be most suitable choice in [123]. In [25], $(K, L) = (5, 4)$ is used at the sampling rate of 250Hz.

In morphology based QRS detection approach, morphological operators like opening and closing are used to enhance the particular shape of the QRS complex. The QRS complex contains abrupt positive and negative peaks, therefore, using a peak-valley extractor [76], the QRS complexes are enhanced and the other parts of the signal such as P and T waves as well as noise are suppressed [132]. Peak-valley (PV) extractor is a morphological operation used for mapping smooth parts of a signal to corresponding zero amplitude flat segments to extract peaks and valleys in the signal. In PV extractor, a smoothed signal is derived from the opening followed by closing of the input signal by a horizontal structuring element. The structuring element, which is a horizontal line segment of unit amplitude, does not form the basis for the peak and valley and hence, the peaks and valleys of the input signal are mapped to zeros in the smoothed signal. Next, the smoothed signal is subtracted from the input signal itself to yield a PV extracted signal containing only peaks and valleys of the input signal. This approach has previously, been used in [21] for suppression of impulsive noise and baseline correction in ECG signals.

In [146], a curve length transform is used for the detection of QRS complex. The curve length is defined as the sum of distances (Euclidean) between pairs of consecutive sample points in the ECG signal. The curve length of the ECG signal depends on the increments in the sample values and the sampling time of the ECG. For uniform sampling in time the curve length is a measure of the increments in sample values. For QRS detection the curve length of the ECG

signal is evaluated in a window with the length matching with the widest possible QRS complex. When the window is in perfect alignment with the onset of QRS complex it produces the local maximum in the curve length feature and that is utilized for locating the onsets of the QRS complex. A lowpass filter with 3dB cut-off at 16Hz is used as a preprocessing step to suppress noise.

In [110], a real time, microprocessor based QRS detection method is given. An analog filter with a pass band of 0.5-35Hz, and automatic gain derived from the signal envelope is used as a pre-processing stage. The signal is digitized at a sampling rate of 500Hz and further processed through a 0.5-40Hz band-pass filter and a 50Hz notch filter for suppressing the baseline wander, high frequency noise and the power line noise. A 128 tap matched filter is derived from a noise free, bandpass filtered QRS complex, which is used for detection of QRS complexes in the ECG signal. We found the method to be suitable for the analysis of ambulatory ECG also.

2.2 Delineation of Wave Boundaries

In the previous section we have reviewed some of the QRS detection techniques in the literature. For automated analysis of the ECG, detections of P and T waves are also important as the P wave represents atrial activity and the T wave is related to repolarization of ventricles. In a cardiac cycle the sequence of occurrence of these waves is P-QRS-T. Therefore, we can search for P and T waves in appropriate time windows after the QRS complex is located. However, it is recommended in [66] that any fibrillation condition should be detected before proceeding with waveform analysis using procedures proposed in [129].

The T wave is the wave with the next highest level of energy in cardiac cycle. The location of T wave from the R peak depends on the current beat period, measured as the time interval between two consecutive R peaks which is simply called RR interval. In [67], the search window for T wave is defined from the R peak position in the interval from 140 to 500ms if $\text{mean(RR interval)} > 700 \text{ ms}$ and for smaller RR intervals the search window is defined in the range 100ms to $0.7 * \text{RR interval}$ (in ms). The ECG deflection points Q, R, S and T are located using a lowpass filter from the differentiated ECG. In [78, 79], a quadratic spline wavelet is used at four dyadic scales starting from the scale of 2 at a sampling rate of 250Hz. The first two scales are used for detecting QRS and the next two scales are used for detecting P and T waves in appropriately chosen time windows with respect to the location of R peak in the QRS complex.

In [34], assuming that P wave occurs in a specified time window of 240 to 400ms preceding the R wave of the QRS complex in each cardiac cycle, three different P wave detection algorithms are discussed. These techniques are based on the derivatives of the ECG signal in a specified window. First

method in [34] is called the amplitude and first derivative based algorithm. This technique subjects the first derivative of the ECG signal in a specified time window to a predefined threshold value. The criterion applied for P wave detection is: the positive derivative at three consecutive points in the window should exceed the threshold followed by two consecutive points having the negative derivative crossing the threshold within 48ms, and all the sample values in the signal in between these two crossing points must exceed a predefined amplitude threshold. The second technique just searches for a point in the time window at which the negative derivative exceeds the threshold value and in the third method a combination of second derivative and a smoothed first derivative signal is subjected to a threshold value for detection of P wave.

There are model based approaches for analysis of different segments of the cardiac cycle, i.e., P, QRS and T waves. In [55], P, QRS, ST and T are expressed as linear combinations of Hermite functions. This modeling required 2, 7, 2 and 4 Hermite coefficients to represent P, QRS, ST and T, respectively. In [88], a discrete cosine transform based modeling is proposed for delineation of P, QRS and T waves. The biphasic functions given by pole-zero model of order (2,2) are used in this representation. It is shown in [88] that P and T each has a single biphasic function whereas QRS can be represented as two or three biphasic functions. These segmentations of ECG waves are useful for further analysis and compression of ECG signals.

The level and slope of the ST segment are sensitive to levels of physical activity. The ST level is measured with respect to the baseline or isoelectric level of the ECG which can be detected by searching for the flattest line segment between P and Q waves [46, 140]. A method for determining the measurement point for the ST level in terms of current heart rate is given in [46]. In [140], the ST level is measured at $J + 80\text{ms}$ where J is the first inflection point after the S wave. In order to provide immunity against motion artifacts, the ST levels are measured after taking average from several consecutive beats with similar morphology and perfect alignment. A few methods for ECG beat alignment from the literature are described in the next section.

A different approach of ECG segmentation uses a fixed number of functions where the middle and end points of the functions are matched with the wave shapes in ECG signal [98]. This kind of segmentation is used for recognition of ST segments in [119]. A similar approach using a piecewise linear approximation is given in [135]. Here a line segment is initiated from the start of the cardiac cycle and is extended up to the point for which the error in approximation of the ECG segment is less than a fixed empirical value. A new segment is started from the end point of the previous segment. The advantage of this method is that the cardiac cycle can be described in terms of fewer parameters like slopes and lengths of the line segments.

2.3 Beat Alignment

Certain measurements like levels of ST and T waves and morphology of P-QRS-T complex in the cardiac cycle are important for diagnosis of any abnormality. However, the presence of noise can hamper the readability of the ECG and hence can produce errors in estimating these cardiac parameters. In order to reduce the impact of noise, the cardiac cycle should be derived as an average of several epochs of ECG beats. Such estimates using mean composite, median composite, etc., are presented in [5]. This kind of estimation of the cardiac cycle requires correct alignment of corresponding cardiac features like P, QRS and T waves in the ECG beats.

There are various methods for alignment of ECG beats in the literature namely, the double level method, normalized integral method and matched filtering method, etc. These techniques are reviewed in [56, 58]. In the double level method, crossings of a fixed threshold level by the signal in upward and downward directions are measured as time t_1 and t_2 , respectively. The mean of these two, $t_a = (t_1 + t_2)/2$ is used as the temporal point of alignment. In the normalized integral method proposed in [58], a measure called normalized integral of a non-negative function is defined. The integral of a non-negative function is always monotonically increasing and hence it can uniquely represent the time corresponding to a particular amplitude. If we consider a finite delay between two non-negative functions with the same shape and amplitude, then the area under the difference signal between the corresponding integral signals represents the amount of delay. The normalized integral is defined as the running integral divided by the final value of the integral of the function. Therefore, irrespective of the amplitude scales of the function, the normalized integral monotonically increases from 0 to 1 for a non-negative function. Thus, as explained above, the delay can be determined even though the waveforms may have different amplitude scales. The only requirement is that the waveforms should be non-negative to maintain the unique relation of time and amplitude. Since the ECG signal may go below the isoelectric level it may have negative valued samples which are to be replaced by zeros for applying this technique. In the matched filter based technique a noise-free ECG beat forms an impulse response of the matched filter. The local maxima in the output of the matched filter signal indicate positions of the alignment of the beat in the input ECG signal. This is similar to finding cross-correlation of the new beat with the reference beat for their alignment. In [64], a multiscale cross-correlation based approach is proposed for beat alignment. The cross-correlation between a template beat and the current ECG beat is calculated at five different scales and the median of the locations of the maxima, at all the scales is used as the fiducial point for alignment.

In [27], the beat alignment is performed after searching for R peak. The first zero crossing after the R peak is marked as a fiducial point for alignment. Any dc bias and slow baseline wanders are to be removed to ensure that the zero crossing takes place as desired. Therefore, the signal is preprocessed

through a highpass filter with a cut-off at 3Hz. Respiration causes a significant beat to beat variation in amplitude of QRS complex. Hence normalization of the QRS amplitudes is used in [114] for minimizing errors in alignment. A multiple loop alignment approach is proposed in [122] using vectorcardiographic leads which is not applicable to ambulatory cardiac monitoring. A similar approach of multiple loop alignment is used in [10] for studying beat to beat variability.

2.4 Noise Reduction in ECG

It has been noted previously that noise from various sources like muscular activities, 50/60Hz powerline, skin stretching and electrode motion, movement of heart due to respiration, etc. can contaminate the ECG signal and hence affect the interpretation of ECG signal. In particular, an automated analysis requires noise free ECG signal for correct interpretation. However, it is difficult to control the environment and prevent the interference due to some physiological events like breathing. Reduction of noise due to most common sources is addressed in [137].

Thakor *et al.* have presented several adaptive filtering approaches in [130] for noise cancellation in ECG signals. An adaptive filter with a single weight has been proposed here for reducing slow wandering of baseline. A constant is used as the reference signal and the composite ECG signal with baseline wandering is the primary input. At every sample of the ECG signal, the error produced by the difference between the constant reference and the filter weight multiplied by the previous input sample (since it is a single weight filter) is used for updating the filter weight according to the least mean squares (LMS) algorithm as $w[n + 1] = w[n] + 2\mu e[n]$, where $e[n]$ is error signal, $w[n]$ is the filter weight at n^{th} sample and μ is the adaptation parameter. The output of the filter is the error signal $e[n]$. If we consider the relation between the input ECG and the output error signal, the filter acts as a notch at zero frequency. The transfer function of this filter in s domain can be derived as $\frac{s/(\mu f_s/\pi)}{1+s/(\mu f_s/\pi)}$, where f_s is the sampling frequency. The bandwidth of the notch is given as $(\mu/\pi)f_s$, which should not exceed the fundamental frequency of the heart rate ($\approx 0.8\text{Hz}$) as indicated in [7, 54]. Due to this limit the adaptive filter can track the slow baseline wander but cannot remove abrupt motion artifact signal due to physical movement.

Powerline is another most usual source of interference in the ECG recording. This kind of interference is caused due to powerline cords nearby and its effect can be minimized by moving away from such sources of this noise. However, there must be provision in the wearable ECG equipment to minimize the interference. As we know that the powerlines have a specific frequency of either 50 or 60Hz. Therefore, the interference can be removed by using a narrow stopband filter centered at the powerline frequency in the frequency response of the ECG equipment, which is usually from 0.05-100Hz. The notch

filter for powerline is acceptable by the guidelines provided in [28] for exercise monitoring ECG equipment. In [7], authors proposed a technique for removing the powerline interference using a non-recursive finite impulse response. A design of infinite impulse response notch filter is proposed in [104] which can be useful for filtering of ECG signals. Adaptive filtering techniques are applied for cancellation of powerline and the electromyograph (EMG) interference in [130]. The powerline interference appears as the common mode signal to the ECG amplifier and available from the right leg electrode. Hence the signal from the right leg electrode is used as the reference input signal to the adaptive filter for cancellation of powerline noise. Here it should be noted that in many places the powerline frequency may often deviate from the specified value (either 50 or 60Hz) in the range of $\pm 2\text{Hz}$. In this case, the adaptive filtering technique can be more effective [69]. Moreover, it has been shown in [39], the adaptive implementation introduces less noise in measurement of the ST segment in comparison to that by a non-adaptive notch filter.

As we have seen in Section 1.2, the EMG signal due to muscular activity may interfere with the ECG signal. The EMG signal seen on the skin surface is quite localized in nature. Due to this property, the EMG interference in different ECG leads may be uncorrelated because the different leads are placed at different locations on the body. With this rationale an adaptive filtering technique has been proposed in [130]. It suggests that for removal of the EMG from one particular lead of the ECG signal which acts as the primary input, the signals from the orthogonal ECG leads can be used as the reference input of the adaptive filter. Thus by using multiple leads of ECG, the EMG interference can be suppressed using this adaptive cancellation technique.

The motion artifact induced due to relative motion of electrodes is more prevalent during ambulatory conditions. It is still a challenging problem to remove motion artifact reliably without affecting the cardiac components of the ECG signal. For reduction of motion artifact, an adaptive recurrent filter (ARF) [130] is suggested that uses the repetitions of the cardiac cycle. Here a cardiac cycle of a fixed length is estimated by the proposed ARF. The ARF coefficients are adapted once in every cycle of ECG so that the impulse response of the filter represents the P-QRS-T complex of the fixed length. Here the estimate of the fixed length of the P-QRS-T complex may leave some temporal gap between the two cycles which can be filled in by using a linear interpolation of the two end points of the gap. The ARF is modified in [105], to have a variable length filter according to the current RR interval so that the filter itself can handle variable heart rates without leaving any gaps. In another approach for removal of motion artifact, in [73], a signal across two extra electrodes placed near right biceps muscle with a separation of 5mm, is used as the reference input whereas the composite ECG signal is the primary input of the adaptive filter. In [73], a recursive least squares (RLS) adaptation is considered to be more suitable than the least mean squares (LMS) algorithm for faster convergence. In [40], it is shown that an impedance variation due to electrode deformation, measured across two electrodes using an ac current,

can be used as a reference signal for an adaptive filter for the removal of the motion artifact. It is also reported that the variations in the impedance due to skin/electrode stretching are captured better when the reference signal frequency is 120Hz. The sensitivity of the impedance signal toward electrode deformation drops with increasing frequency of the supplied current. In [40], it has also been shown that the signal acquired from an optical sensor placed at the electrode site can represent the deformation in shape of electrode due to motion and hence can be used for removal of motion artifact. A method of deriving a reference signal using a magneto-resistive sensor and a 3-axes accelerometer for adaptive filtering of motion artifact are proposed in [131].

Apart from adaptive filtering, there are several other techniques used for calculating an estimate of the cardiac cycle by suppressing the noise. In [5], several ECG beat epochs are used in alignment to find an estimate of ECG beat using arithmetic mean, median, a hybrid of both mean and median, trimmed mean, and fixed incremental based methods. In [5], a filter bank approach is also proposed for processing of ECG signal in subbands, utilizing the spectral and temporal properties of the cardiac cycle.

2.5 Detection of Body Posture Changes

Body position changes (BPC) cause angular shifts in the axis of the heart which may result in suppression or elevation of ST segment of the cardiac cycle [53]. These changes in the level of the ST segments due to BPC might be falsely interpreted as ischemia, a cardiac disorder which is characterized by transient changes in ST segment. In order to prevent this kind of false alarms in ischemia monitoring, researchers have tried to detect the BPC from the ECG signal itself. In [49], a method for detecting BPC is proposed based on the fact that BPCs are abrupt and cause step like changes in the ST level. In order to detect a step like change in ST signal three measures are defined for the flatness at a given point: average of a fixed number of samples prior to the given point, called backward region, average of a fixed number of samples after the given point, called forward region and difference between the averages of the forward and backward regions. A step like behavior is determined by appropriate thresholds on these three measures.

In [50, 51, 52], the BPCs are detected by showing that BPC affects both the QRS and ST segments abruptly whereas during ischemia episodes mainly the ST segment is affected gradually. Karhunen-Loeve transform (KLT) coefficients are used to demonstrate this and for detecting this characteristic difference between ischemic and BPC related changes in ST segment. The area under QRS [57] and the width of R wave [115] have also been used to characterize BPC.

In [37], BPC is detected using a Bayesian approach with two conditional probability density functions for the observations in three orthogonal vector-

cardiographic leads. The observations can be KLT coefficients for QRS and ST segments or rotation angles derived from the vectorcardiographic leads.

2.6 Overview of Wearable ECG Recorders

Ambulatory ECG recording technology has continuously evolved and matured over time. Originally, Holter had proposed a wearable system that would record the ECG signal in analog form and transmit the recorded ECG signal using a wireless link. This type of system was proposed for ambulatory applications [26, 44, 45].

The state-of-the-art W-ECG recorders are very light weight (< 80gms) and portable, can record long term ECG signal in digital form with a variety of (or programmable) sampling rates as high as 1kHz. Many of them are equipped with wireless transceivers, microprocessors with on board analysis algorithms for calculating cardiac parameters and displaying them on LCD displays and also generating warnings for clinical attention, if necessary. This is made possible due to miniaturization of electronics components, customized chip design for specific analog processing, availability of high speed microcomputers and ECG analysis algorithms [47, 113, 117, 134]. We provide the hardware details of one such W-ECG in the next chapter.

W-ECG uses pre-defined ECG leads which are to be connected to the ECG electrodes appropriately placed on the body. In the standard 12-lead ECG the primary leads are connected to the limbs and hence also referred as limb leads. However, in ambulatory applications the limb leads may obstruct the usual activities of the user (wearer) and hence a modified placement of electrodes is used, called proximal limb leads. In the proximal limb leads the electrode placements are on frontal trunk approximating the positions on the limb sites in the standard ECG [12].

For wearable applications the type of ECG electrodes should be easy to use, compact in size and be able to provide reliable connection for a long duration. Disposable foam-pad adhesive Ag/AgCl electrodes fulfill all such requirements of W-ECG and hence they are preferred in W-ECG. Previously, a large number of studies have focused on electrodes and impact of their placement on ECG applications. In order to reduce the number of electrodes, feasibility of ground-free ECG recording with two electrodes has been investigated in [125].

Skin preparation prior to ECG recording is a standard practice in hospitals in order to reduce the artifacts. This involves removal of hair from the electrode sites, scrubbing of the sites with alcohol (spirit) wipes, and abrasion with abrasive pads. This can help for a short term (for a few minutes) monitoring. However, it has been concluded from the studies carried out on effect of skin preparations on generation of motion artifacts in [126] that the skin preparations are not very helpful for reducing the motion artifact in long term monitoring. Thus the motion artifact cannot be easily prevented and it is a serious problem in a long term monitoring using W-ECG.

2.7 Analysis of Ambulation in ECG

In Section 2.5, we have noted how BPC during sleep may affect the ECG signal. In ambulatory conditions the ECG signal manifests many abnormal and abrupt changes due to motion artifact caused by body movement activities (BMA) of the subject. To interpret the ECG signal correctly in ambulatory conditions, efforts are made to characterize and eliminate the motion artifact signal from ECG.

In [86], a wearable system that can simultaneously record the ECG signal and 2-axes acceleration is developed. The heart rate and the activity levels are compared. The system could not detect the heart rate correctly due to motion artifacts at activity levels which exhibited high acceleration values. From this work it can be concluded that the level of activity in terms of acceleration determines the quality of the ECG captured.

Another such system for recording ECG and 2-axes acceleration signal has been developed in [145]. The heart rate, respiratory rhythm, postural behavior and activity of the subject are computed from the recorded signals. The study reveals that the RR interval, respiration, posture, behavior and activity are very much inter-dependent. Therefore, the information regarding various activities undertaken by the subject must also be used in the ambulatory cardiovascular analysis.

A prototype for wearable ECG monitoring system capable of recording and transmitting continuous ECG and accelerometer data is presented in [43]. Here it is reported that the algorithm used for computing the heart rate from the captured ECG becomes inaccurate at high activity levels as measured by the accelerometer. Thus the measurement of acceleration should be considered while considering the reliability of the estimate of heart rate reported by the automated algorithm.

In [17], a study is performed on the use of wearable devices for monitoring the patient movement. From analysis of simultaneous traces of ECG and acceleration signals shown in [17], we conclude that the motion artifacts are generated in the ECG signal when there is an abrupt and significant change in the acceleration signal due to patient ambulation.

Though the above studies have not quantitatively reported the impact of the levels of the body movement on the generation of motion artifacts in the ECG signal in ambulatory conditions, a reasonable conclusion is that the amount of motion artifact should be proportional to the level of the BMA in terms of body accelerations. We discuss this issue as one of the main topics in this monograph.

Apart from the above works related to the ambulation studies in ECG, a BMA specific characterization of motion artifacts has been proposed using a wavelet transform and a neural network [92, 93]. The signatures of three typical movement patterns are extracted by characterizing the low frequency artifacts from the ECG signal itself. However, the reported performance is

not very satisfactory as the wavelet based representation does not separate the in-band BMA signal from the ECG.

We have seen in this review that many useful and accurate algorithms are available in the literature for automated analysis of ECG signal. However, they fail under subject ambulation due to the contamination of the ambulatory ECG signal by the motion artifacts. The context of ambulation can be useful in interpretation of automated analysis of the signal in W-ECG. However, there is no standard reference database of ECG with ambulation information available for carrying out the studies on impact of BMA on the ambulatory ECG signals. In the remaining chapters of the monograph we will focus on the W-ECG and the analysis of the ambulatory ECG signal. We will perform some experiments on using motion artifacts in ambulatory ECG signal as a source of information, while encountering the real life situation, when the wearer is performing all kinds of daily activities like walking, climbing stairs, etc. In the next chapter we provide some of the hardware details and useful specifications of the W-ECG used for this work.

Hardware Development of Wearable ECG Devices*

Maryam Shojaei Baghini, Dinesh K. Sharma and Rakesh K. Lal,

*Department of Electrical Engineering, IIT Bombay,
India.*

Email: mshojaei@ee.iitb.ac.in

3.1 Introduction

Personal healthcare devices find many applications where noninvasive monitoring of biopotential signals is required. Among physiological parameters ECG (Electrocardiogram) is one of the most important vital signals because it directly reflects the heart condition. Wearable devices used for recording ECG related information may continuously record heart rate and/or ECG for several hours or days and store it on the system memory. The stored ECG can then be used by cardiologists for subsequent analysis and diagnosis. Holter monitors, developed for the first time by N. J. Holter [44], are commonly used for this purpose. Event monitors record ECG for short periods which are set by the user control [87]. More functionality may be incorporated into the monitoring device by providing interface to PC (Personal Computer), mobile phone and PDA (Personal Data Assistant) through USB (serial Bus Interface) or other standards. In advanced monitors short range transceivers send stored ECG to the control center in the hospital.

Meeting medical standards, size, weight, power dissipation and cost are important factors in battery-operated personal or portable ECG monitoring devices. These specifications imply special care in the design and implementation of the internal hardware. In this chapter common functional modules of the signal conditioning Electronics in these devices are introduced. In general, system may be implemented using commercially available chips or special purpose integrated circuits. In either case the device may be a single lead or multi-lead depending on the requirements. Detailed circuits will be given for each module based on the prototypes developed by a design team in IIT (Indian Institute of Technology) Bombay.

*An invited chapter.

3.2 Basics of Personal ECG Instruments

3.2.1 System Modules and Operation

A personal ECG monitoring system, called **Silicon Locket**, has been developed in IIT Bombay. Block diagram of **Silicon Locket** is shown in Fig. 3.1.

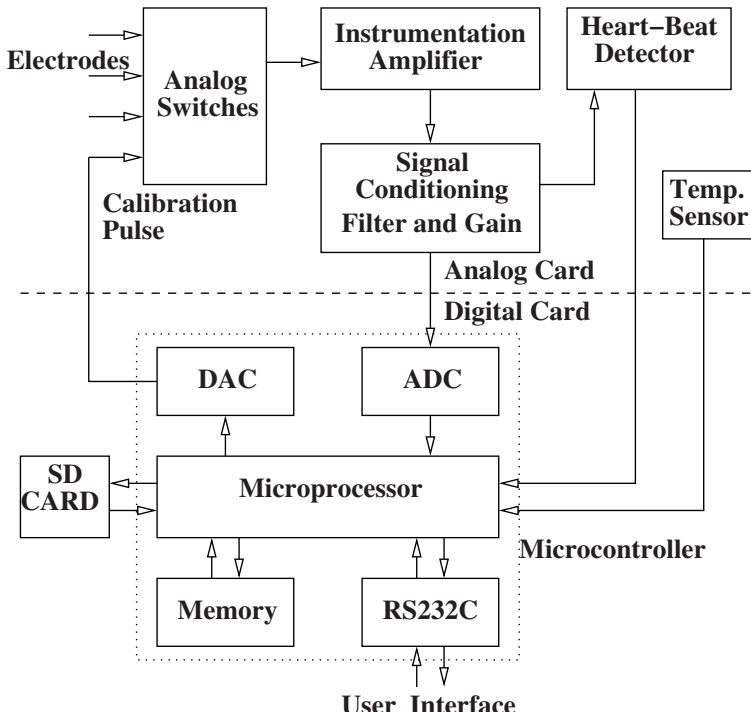


Fig. 3.1. Block diagram of **Silicon Locket**, a personal ECG monitoring device. Interfacing modules may be different among different products.

To be able to understand the requirements of the hardware we should start from ECG itself. ECG signals from electrodes are inherently low voltage analog potentials, ranging from 0.1mV to 4mV [142]. These signals are more often mixed with common mode noise which naturally exist on the human body. An example of such common mode noise is mains supply interference which is induced on the body due to coupling capacitances between the body and AC power boards. Amplitude of the common mode noise is normally large compared to the amplitude of ECG signal. Therefore an INA (instrumentation amplifier) is required at the input stage of the ECG acquisition system to attenuate the common mode noise and amplify the ECG signal which is a differential mode signal, without adding additional noise. Number of ECG

channels, varying from one to twelve channels, determines the number of required instrumentation amplifiers if simultaneous acquisition of ECG through all channels is required. Otherwise a multiplexing scheme at the input may be used.

Typical bandwidth of ECG signal is from 0.05Hz to 150Hz and maximum up to 200Hz [142, 91]. Therefore it should pass through a bandpass filter. However it is possible to highpass filter the signal before or inside INA itself [116, 117]. INA is then followed by an active bandpass/lowpass filter, as shown in Fig. 3.1. In case of heart beat detection cut-off frequency of the lowpass filter can be as low as 40Hz [42].

To store the ECG signal for further processing it is digitized. High resolution ADCs (analog to digital converter) with sampling frequencies not more than few KHz are used for this purpose. Usually a low power microcontroller provides all control signals for multiplexing, sampling and digitization, interfacing with memory and heart beat detection. Nowadays ADCs are also integrated on the microcontroller chips. Limited ECG processing for detection of abnormalities may be also implemented by the microcontroller. Recorded ECG can be sent through a wireless link to a base station or through a data transmission link to PC (personal computer) and/or mobile phone or it can be easily stored on a memory card.

3.2.2 System Requirements

Summary of main performance requirements for electrocardiographs is given in [139]. However all of them are not applicable to wearable ECG recorders because these devices are battery operated. For these devices some important performance requirements are given in table 3.1.

Table 3.1. Some of the main performance requirements for wearable ECG recorders

Parameter	Value
Minimum range of input signal	$\pm 5\text{mV}$
Minimum tolerable input DC offset voltage	$\pm 300\text{mV}$
Maximum Gain error	5%
Minimum upper cut-off frequency (-3dB)	150Hz
Maximum DC current flowing through each patient electrode	$1\mu\text{A}$
Minimum input impedance at 10Hz (each lead)	$2.5\text{M}\Omega$
Minimum CMRR (common mode rejection ratio) at 60Hz	86dB

3.3 Electrodes

As it was explained in the introduction chapter, Ag/AgCl electrodes are common type of electrodes used for sensing ECG signals. A picture of a single

disposable foam-pad adhesive ECG electrode has been shown in Fig. 1.1. Generally electrolyte gel is used to maintain a good contact between the electrode and the skin. A biopotential electrode in contact with the gel and skin can be represented by an equivalent circuit. The equivalent circuit, briefly is a parallel RC impedance in series with a dc voltage source, called half-cell potential [139]. To reduce the magnitude of the impedance, electrodes should have proper contact with the gel and hence with the skin. Since ECG signals are recorded in differential-mode half-cell potential appears as a dc input offset voltage. Value of this offset voltage can be as high as $\pm 300\text{mV}$ [139]. Therefore ECG signal conditioning circuit should tolerate such a high value of input DC offset voltage.

3.4 Signal Conditioning

Performance of any personal biomedical system depends on the performance of analog signal conditioning. Signal conditioning includes extraction and amplification of differential signals from sensors, with maximum amplitude of a few mV, from a noisy environment. These tasks are mainly achieved by INAs (instrumentation amplifiers) followed by gain and filter stages. Often conditioned signals will be converted into digital form for further digital processing. In the context of ECG main analog signal conditioning modules for a multi-lead ECG acquisition system are shown in Fig. 3.2 [89]. In Fig. 3.2 each

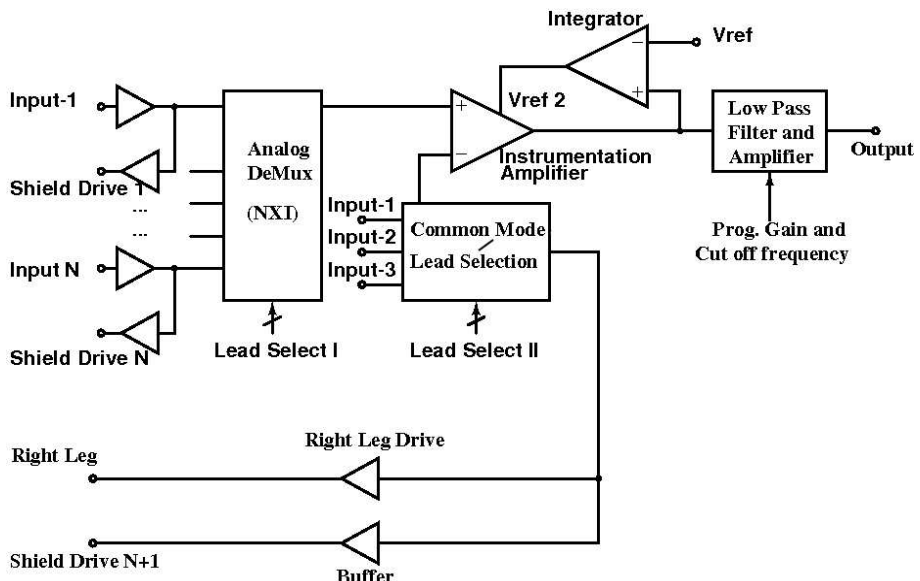


Fig. 3.2. Basic ECG signal conditioning modules.

input i ($1 \leq i \leq N$) comes from a single ECG electrode on the body. An analog demultiplexer (**DeMux** module in Fig. 3.2) selects the electrode of which ECG signal should be applied to the input of INA. Another input of INA either receives ECG signal from another electrode (in the case of limb leads) or receives average of two/three ECG signals (for example Wilson central terminal).

3.4.1 Implementation Using General-Purpose ICs

It is always possible to implement a signal conditioning circuit using available general-purpose ICs. INA as the main module of signal conditioning may be implemented using opamps (operational amplifiers) and resistors. Fig. 3.3 shows a commonly used three-opamp configuration for implementing an INA [139].

The INA, shown in Fig. 3.3, constitutes three operational amplifiers and seven resistors comprising three matched pairs and one single resistor R_1 . Direct connection of input differential voltage to the opamp terminals provides an effective high input impedance for INA. Therefore loading of INA on the sensor will be almost negligible. However sometimes bias resistors at the input of INA are provided to establish a DC bias voltage at the input of INA. In this case value of resistors should be high enough to provide a high input resistance, e.g. at least $2.2\text{M}\Omega$.

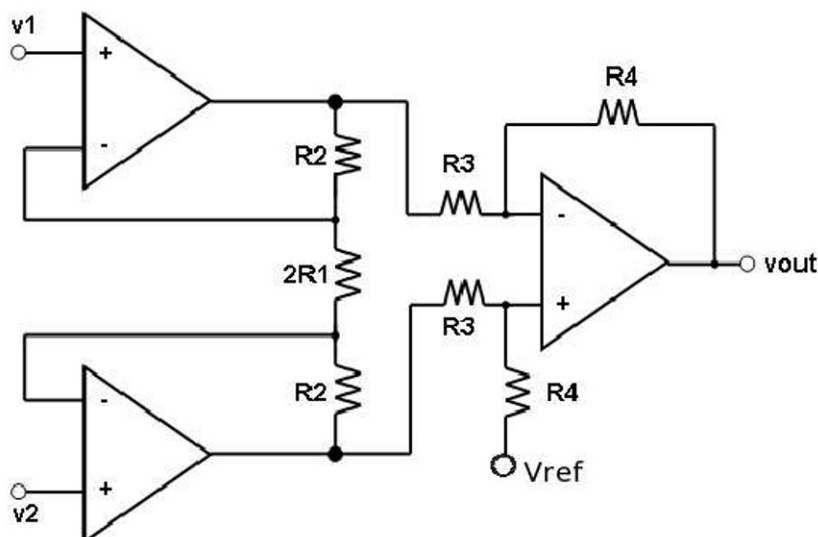


Fig. 3.3. Three-opamp configuration for INA implementation.

It is straightforward to derive the input-output characteristics of the INA, shown in Fig. 3.3. Considering ideal opamps the input-output voltage relationship is given by Eq. (3.1).

$$\frac{V_{out} - V_{ref}}{V_{in+} - V_{in-}} = \frac{2R_2 + R_1}{R_1} \frac{R_4}{R_3} \quad (3.1)$$

Eq. (3.1) is in fact input-output equation for a differential amplifier. As shown in table 3.1 high CMRR (common mode rejection ratio) is one of the main specifications of INAs. The value of CMRR often should be more than 90dB for wearable ECG recorders. Opamps used in three-opamp should have high CMRR. Still three-opamp INA needs accurate matching of the resistor pairs that implement the feedback networks (Fig. 3.3). CMRR degrades by the amount of 6dB for every 2% mismatch between resistor values. For a discrete implementation resistors with accuracy matching better than 1% and opamps with CMRR better than 90dB are required. Since equivalent input noise voltage of two input opamps appears directly at the input of instrumentation amplifier these opamps must be low noise. For a proper design RMS (root mean square) value of the input noise voltage of each opamp over ECG frequency band should not exceed 5 μ V.

General-purpose INA ICs overcome the matching requirements of three-opamp configuration by integrating the entire circuit in one IC. Therefore system developers may use these available INA ICs directly on the ECG signal conditioning board.

Mains power supplies cause interference currents flow through the human body [85]. The interference current is induced due to coupling capacitances between the human body and power lines as well as between human body and ground. There are different paths for this interference current to flow. Some part of the current flows through the body, which generates a common mode signal, at frequency of 50Hz (or 60Hz), on the body. Some part of the current may flow through the input impedance of INA if INA is AC-coupled. AC-coupled INA is desired because INA should tolerate at least ± 300 mV input DC offset voltage.

If all components between the body and input terminals of the instrumentation amplifier are matched still CMRR of the signal conditioner module is a finite value and hence a small portion of the induced common mode signal appears as 50Hz (or 60Hz) noise in the recorded ECG. This noise disturbs the ECG, specifically P-Wave and T-Wave part of it. Using a sharp notch filter with center frequency of 50Hz (or 60Hz) seems to be a solution for reducing the interference. However care should be taken to avoid ECG distortion. Therefore interference reduction is an important practical implementation issue even for portable ECG monitoring devices which are operated by batteries. One of the common ways of attenuating the common mode noise is to drive the right leg using a common mode negative feedback circuit as shown in Fig. 3.4. Right leg drive circuit is also used in bedside electrocardiograph systems [139].

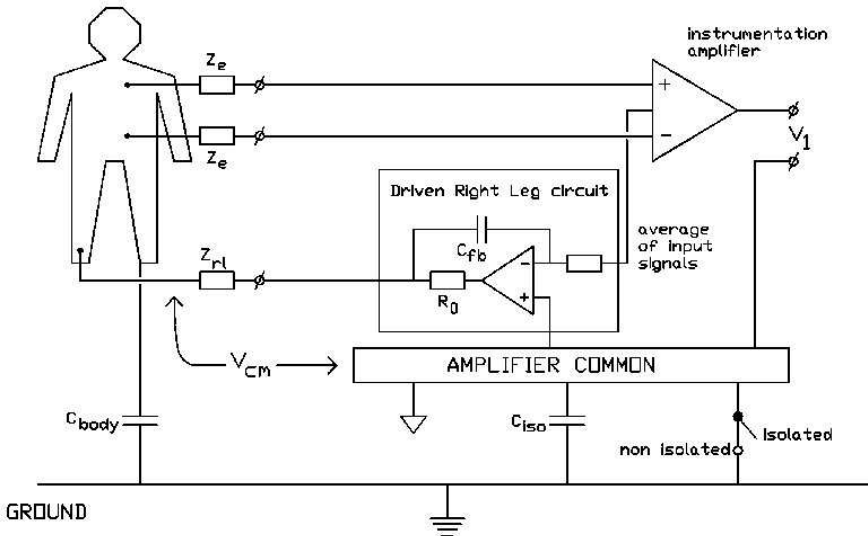


Fig. 3.4. Right leg drive circuit(Used with permission from Biosemi Inc. [85])

For further amplification and filtering of ECG signals more often INA is followed by a LPF (lowpass filter). This lowpass filter is an active filter made by on-chip opamps or OTAs (operational transconductance amplifiers) and discrete resistors and capacitors. The cut-off frequency of the filter is set around 150Hz as specified in table 3.1. However it can be programmable. The overall gain of the analog ECG signal conditioning module is also programmable, usually in the range of 200 to 1000.

Wearable ECG recorders are often interfaced with personal computers, mobile phones or removable memory cards through USB (universal serial bus), IrDA (Infrared interface) or RS232 ports [136]. Therefore digitization of captured ECG signal is required. A low power microcontroller with on-chip ADC (analog to digital converter) is a good choice for digitization of conditioned ECG signal.

3.4.2 ASIC (Application-Specific Integrated Circuit) Design for Signal Conditioning

To reduce the cost, weight and power compact design of personal medical instruments is desired. These requirements motivate development of custom signal conditioning chips. The ultimate goal is the ASIC design as per the recommended specifications for personal health care devices, integration of more functionalities into the chip and compact design of the final monitoring device.

ASIC development for medical instruments is not recent. In fact in 80s research had already started for the development of micropower personal monitoring devices. For example a comprehensive test chip was reported in 1988 for the acquisition of physiological signals [84]. An integrated micropower heart rate indicator with power supply voltage of 10V, developed in 3μ CMOS process, was reported in 1989 [109]. This heart rate monitor was designed for the continuous monitoring of the heart rate. In heartbeat detectors exact retrieval of ECG waveform is not a concern. The detector must only precisely detect QRS peaks to provide a base for counting heart beats. Therefore bandpass filter of analog front end is designed in such a way to attenuate frequencies below 10Hz or above 60Hz. In 1996 a CMOS nine channel ECG measurement IC with complete data acquisition was published [23]. The ASIC was developed in 2μ m CMOS process for general measurement purpose, operating at 10V power supply with power consumption of 270mW. Hayes-Gill et al. reported a generic ASIC again comprising analog modules and ADC in [42]. As CMOS technology advanced more functionalities were incorporated in the integrated circuits aimed for biomedical instruments. An example of such test chips was published by Chih-jen, et al. in 1999 [143]. The test chip included analog signal processing unit, transmitter, receiver and digital processing unit. Analog processing unit constituted instrumentation amplifiers implemented using opamps and analog filters. Transmitter included amplitude modulators, analog adder, frequency modulator and RF transmitter. In the continuation of that work an analog processor IC for wireless bio-signal monitor was reported in 2003 [144].

The research has continued in different directions, for example reducing power dissipation or covering more number of physiological signals or improving noise performance and finally making the chip specifications quite robust using programmable gain, filtering and base line drift compensation [68, 91, 117, 142, 144]. High-performance CMOS biomedical signal conditioning ASICs are not usually developed in nano regime technologies due to low frequency operation, stringent noise and offset requirements, and cost. In this regard 0.35μ m and 0.5μ m CMOS technologies are attractive technologies.

Instrumentation Amplifiers

Instrumentation amplifier (INA) is a key module among all signal conditioning modules. In low power personal health monitoring devices, biopotential INAs with high common mode rejection ratio (CMRR), low input-referred noise voltage and low offset voltage as well as very low power consumption are required. As it was discussed in Section 3.4.1 monolithic implementation of INA using traditional three opamp configuration needs accurate matching of the resistors used in its feedback network to achieve high CMRR. Also this structure is not a proper solution for very low power design. Another approach for the design of integrated ECG INAs is to use current balancing technique [80, 108]. Fig. 3.5 shows the basics of current-balancing technique.

At the transconductance stage, the input difference voltage is converted into a differential current i_g , flowing through resistor R_g . Current i_g is mirrored to the transimpedance section with the unity gain. The mirror current, called i_s , is converted into the voltage by flowing through a resistor R_s . Referring to Fig. 3.5, expression (3.2) applies.

$$i_g = i_s \Rightarrow \frac{V_{out} - V_{ref,internal}}{V_{in+} - V_{in-}} = \frac{R_s}{R_g} \quad (3.2)$$

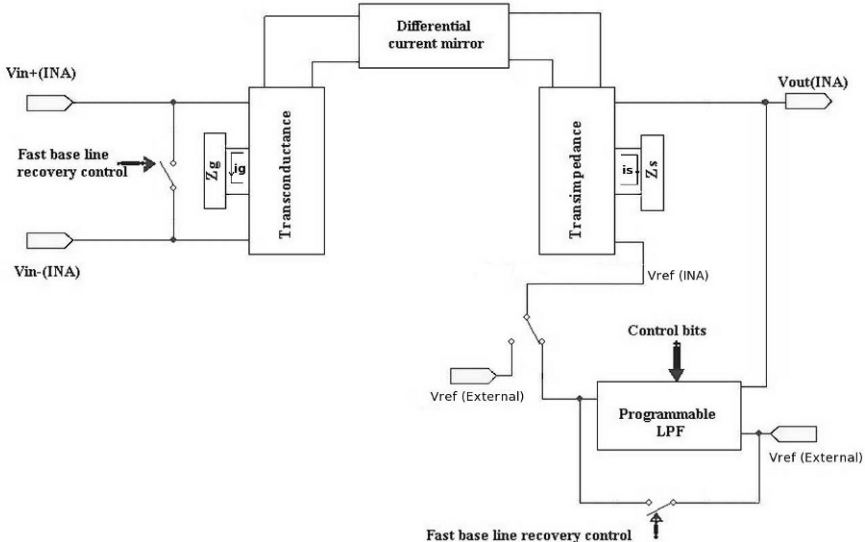


Fig. 3.5. Basics of current balancing technique. (Reprinted with permission from M. Shojaei Baghini, S. Nag, R. K. Lal, D. K. Sharma, "An Ultra Low-Power Current-Mode Integrated CMOS Instrumentation Amplifier for Personal ECG Recorders", Journal of Circuits, Systems, and Computers (JCSC) Vol: 17, Issue: 6, ©2008 World Scientific Publishing Co. Pte. Ltd, Singapore.)

Although current balancing technique is a known method, suitability of this technique for achieving ultra low power ECG signal conditioning chips was reported for the first time in [116]. Integrated INA reported in [116, 118] consumes only $9\mu A$. The circuit has been implemented in a test chip and fabricated in $0.35\mu m$ CMOS technology with supply voltage range of $2.8V$ to $4V$. The circuit schematic of the implemented INA is shown in Fig. 3.6. In Fig. 3.6 transistors ML1 and ML2 act as active loads for input transistors M1 and M2. Transistors MGm1 and MGm2 make an internal transconductance amplifier with feedback path to the input stage through cascode current mirrors. This feedback path keeps drain currents of M1 and M2 almost constant. When a differential voltage is applied, output currents of the transconductance ampli-

fier become unbalanced in order to maintain the drain currents of M1 and M2 equal. Therefore input voltage will drop across R_g . At the transimpedance stage transistors M7 and M8, linearized by the internal opamp, convert the input current into a voltage across resistor R_s . Thus input voltage is amplified at the output by the amount of R_s/R_g . Cascode current mirror is used to obtain high CMRR [29].

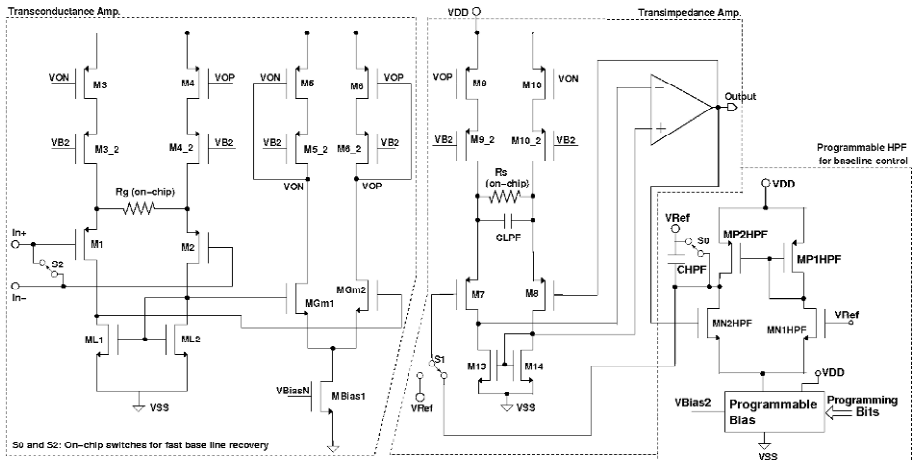


Fig. 3.6. The circuit schematic of ultra low power CMOS INA reported in [116, 117, 118]. (©2004, 2005 IEEE)

Amplifiers and Filters

With current balancing technique it is possible to implement main analog signal conditioning functions by the instrumentation amplifier (INA) itself and so complexity, power and cost of the whole analog circuit reduces. For example, in Fig. 3.6 two external capacitors CHPF and CLPF determine the lower and higher cutoff frequency of the amplifier, respectively [117]. Typical range for corner frequency of lowpass filtering is 150Hz to 200Hz. Typical range for corner frequency of highpass filtering is from 0.05Hz to 0.5Hz. For heart beat detection applications corner frequency of lowpass filtering can be reduced to 40Hz. Programmability of both lowpass and highpass filtering is desired. For example in [118] two control bits program frequency response of HPF. Also by setting both control bits to zero HPF will be disabled and reference voltage of the transimpedance stage will be connected to Vref. It should be noted that highpass filtering also remove out-of-band slow motion artifacts. However for very fast motion artifacts it will take a long time for the base line to recover. In this case to restore the base line to the normal level, on-chip internal switches across input transistors M1 and M2 (switch

S2 in Fig. 3.6) and across CHPF (switch S0 in Fig. 3.6) are used to rapidly discharge external capacitors of INA.

Ultra low power INAs with bandpass frequency response are the main modules for compact integrated analog signal conditioning [116, 117]. In addition to that since amplitude of ECG QRS complex changes from person to person adjustable gain for each channel of ECG signal conditioning is always desired. One simple programmable gain stage after instrumentation amplifiers provides the desired range of channel gains. Typical values of channel gain is from 200 to 1000. The signal conditioning circuit reported in [117] draws DC current of $22\mu\text{A}$ from 3.3V battery supply voltage for each ECG channel. The front-end differential stage is AC coupled to the body through $1\mu\text{F}$ capacitors.

Block diagram of one channel of the compact and low power CMOS signal conditioning chip, called **SLAC1.1**, which is designed in IIT Bombay, is shown in Fig. 3.7(a) [117]. Off-chip components are also shown in the figure. In Fig. 3.7(a) INA, bias generator module and each operational amplifier of the chip draw $9\mu\text{A}$, $10.5\mu\text{A}$ and $8\mu\text{A}$ dc current from 3.3V battery supply voltage, respectively. Operational amplifiers have phase margin of 70 degree while driving 40pF load capacitor. Unity gain frequency of the opamps was measured 130kHz suited for low frequency biopotential signals. Fig. 3.7(b) shows the chip photo. Table 3.2 shows measured specifications of each channel on the chip [117].

Table 3.2. Performance specifications of each ECG channel achieved by custom ECG signal conditioning chip reported in [117].

Parameter	Value
Vdd	$3\text{V} \leq \text{Vdd} \leq 4\text{V}$
Voltage gain of the channel	200
Input voltage range for high linearity	$\pm 6\text{mV}$
Tolerable input DC offset voltage	Any value due to AC-coupling
Input referred noise voltage (RMS) (INA noise plus thermal noise of bias resistors)	$6\ \mu\text{V}$ (BW=200Hz)
CMRR	100dB (at 60Hz)
Input impedance of each channel at 10Hz	Very high due to AC-coupling
HPF cut off frequency	0 to 0.07Hz (programmable)
LPF cut off frequency	170Hz (adjustable by external capacitors)

Interference Issues

Recording of bioelectric signals is always liable to electrically induced and magnetically induced interference. Mains power supply is a common cause of

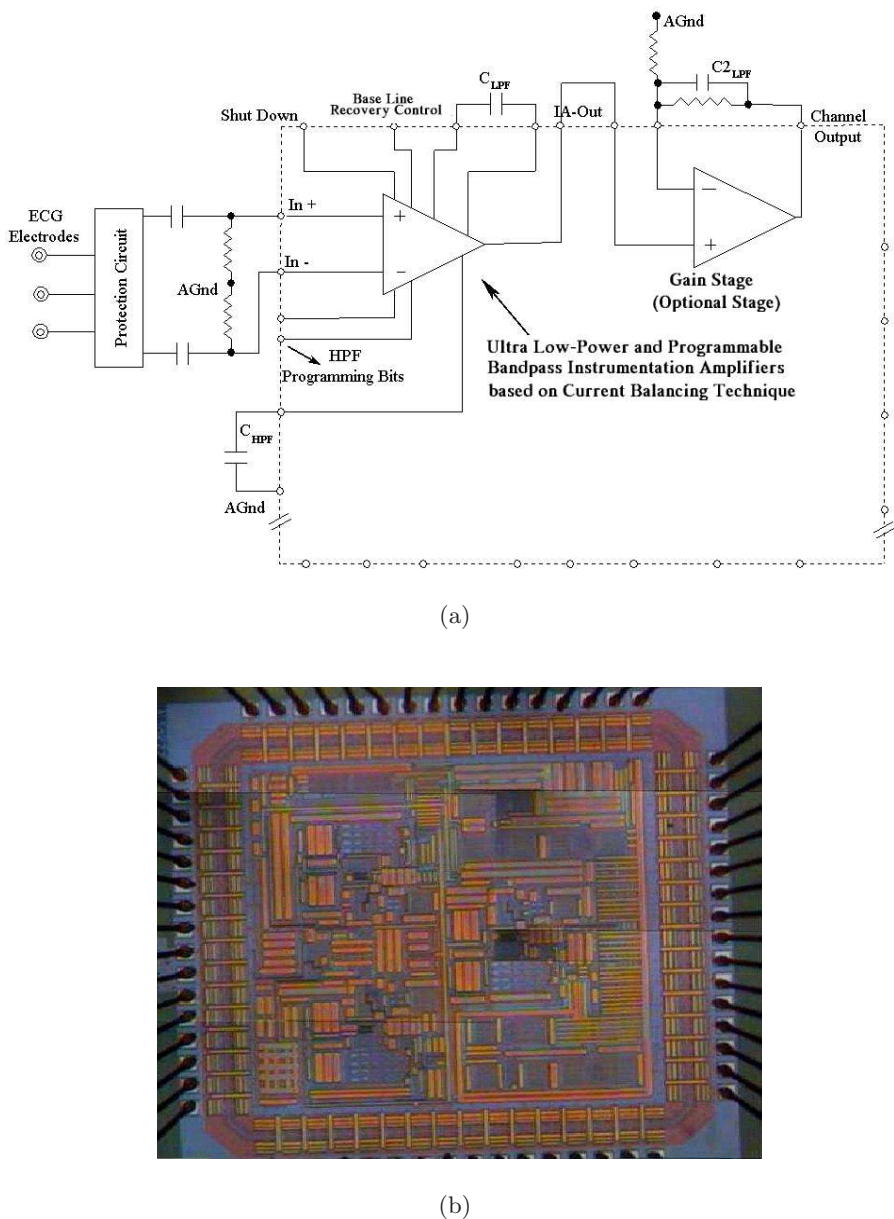


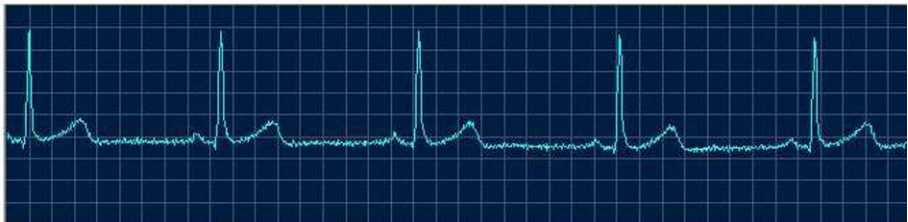
Fig. 3.7. One channel of SLAC1.1 reported in [117], (a) ultra low power CMOS ECG signal conditioning chip and (b) chip photo of SLAC1.1. (©2005 IEEE)

interference for both bedside and personal monitoring devices. The capacitances between the patient and mains power supply cables (or boards) cause an interference current, typically in the range of few μA , to flow through the body [85]. This interference current exists even in personal battery operated ECG monitoring instruments. A part of the interference current flows through right leg drive electrode and enters into the ECG recording device. In return common mode voltage of the ECG instrument changes with frequency of 50Hz (or 60Hz), which appears as common mode noise on the reference level of ECG signal. Therefore INAs with high CMRR (more than 90dB) are required. In addition to common mode noise there is possibility of differential mode noise as well. This is due to the inherent mismatch between impedance of ECG electrode skin interface for every two electrodes. 50/60Hz interference signal on the body is converted into a small differential voltage due to this mismatch. This differential voltage appears at the input of ECG lead, which in turn is amplified and appears as noise on the ECG signal at the output of ECG channel. Fig. 3.8(a) shows recorded Limb lead I ECG using **SLAC1.1** under strong 50Hz interference but with proper shielding. Similar ECG was then recorded without shielding considerations to demonstrate the effect of mains supply interference on the ECG signal as shown in Fig. 3.8(b).

Mains supply interference cannot be easily filtered from ECG because its frequency is in the band of ECG signal. Therefore cables and the entire Electronics of ECG device should be shielded to reduce this noise. Shields should be driven by appropriate signals. The best way is to drive a shield with the signal at the inner wire [85]. However for each input signal an extra shield drive amplifier is required. For example for a simultaneous three lead ECG recording device, three shield drives are required. For higher number of leads, analog demultiplexing reduces the required number of shield drives. For example for a 12 lead arrangement, shown in Fig. 3.2, eight additional op-amps are required for buffering and shield drive purposes. Fig. 3.9 shows the schematic of Wilson Central Terminal generation, guarding and right leg drive circuits for a 64 channel ECG amplifier [85].

3.5 Analog to Digital Converter

ECG is a common non-invasive diagnostic tool for monitoring and detecting cardiac diseases. Main motivation for continuous monitoring of the patients' ECG is to detect transient arrhythmias or transient distortion in ECG waveform, which may not be present during short-time ECG tests in the hospital. ECG is not only analyzed by the cardiologist but also in automatic post-processing ECG analysis systems which act as an assistant to the cardiologist. For example, heart rate variability and ST segment deviations can be automatically detected by post processing of ECG data [18, 61, 110]. This is specially crucial in ambulatory situations. Signal conditioned ECG should be digitized for the purpose of post processing.



(a)



(b)

Fig. 3.8. ECG signal traces from lead-I, using custom ASIC **SLAC1.1**, designed in IIT Bombay, (a) clean ECG signal (b) effect of strong 50Hz interference on ECG signal

Post processing of ECG data is not only used for detection of abnormalities but also sometimes for further noise and artifact removal, specifically in portable and personal health care devices. For example, mains supply interference or motion artifacts can be savior when the patient prefers more freedom in mobility and movements.

Resolution of ADC (Analog to digital converter) in personal ECG monitoring devices depends on the amount of information which will be extracted from recorded ECG or accuracy the cardiologist requires. Resolutions up to 16 bits and sampling rates up to 2k samples/s are used when sophisticated post processing like ST-T micro-variabilities need to be detected [61]. It has been shown that beat-to-beat micro-variations of the T wave, are related to arrhythmia [61]. However these micro-variations are not visually apparent from ECG. On the other hand if sophisticated analysis is not required and noise removals like removal of motion artifacts are concerned resolutions maximum to 12 bits with sampling frequencies as low as 256 samples/s are usually enough [40, 100, 103].

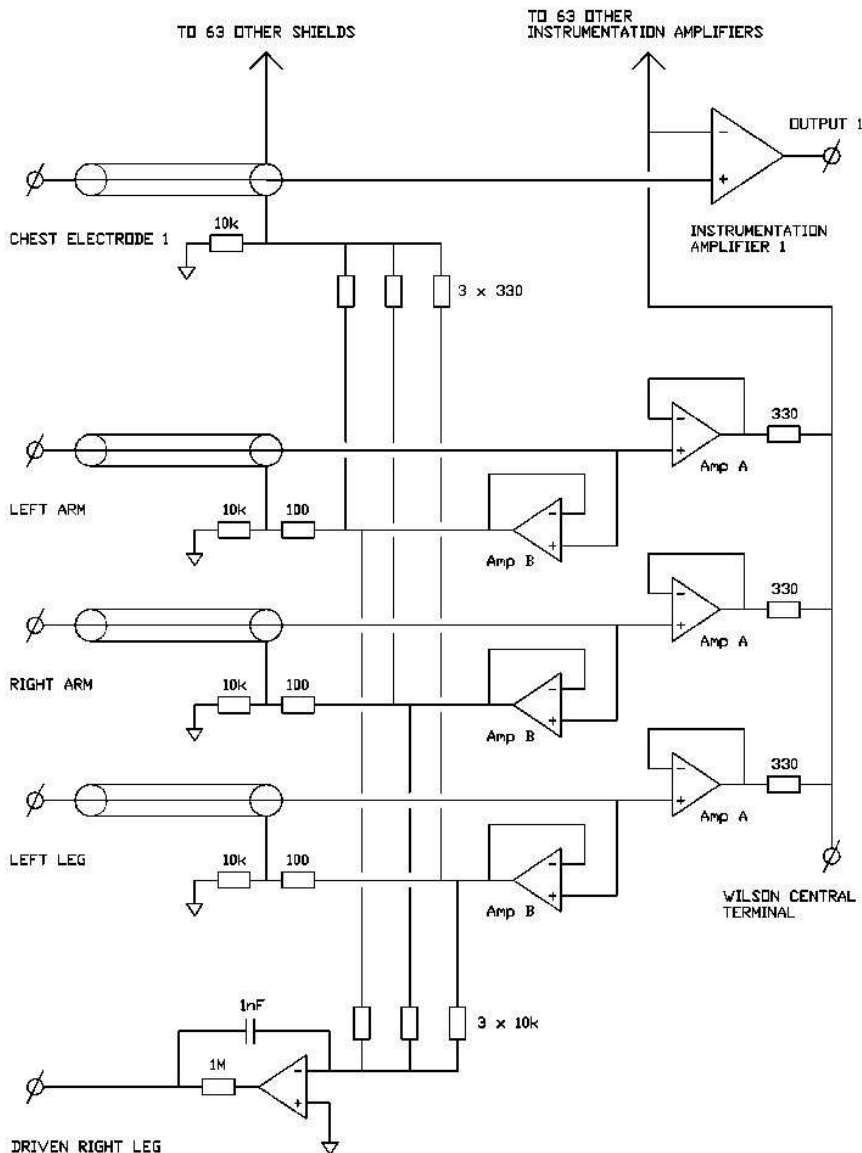


Fig. 3.9. A typical Wilson Central Terminal generation, guarding and driven right leg circuits in front end of a multi-channel ECG signal conditioning circuit (Used with permission from Biosemi Inc. [85])

3.6 Digital Modules

In standard monitoring sophisticated signal processing is not necessary. Therefore the device may display the heart rate or provide crucial but limited functionalities like continuous recording and storage of ECG with or without wireless link and detecting vital abnormalities like arrhythmia. As far as standard monitoring is concerned the entire control and processing tasks can be handled by a low power microcontroller. However diagnostic monitoring needs advanced and highly-accurate DSP algorithms to be embedded into the device. This will drastically increase the power consumption of the medical gadget much beyond the rate at which a battery-operated instrument can work continuously at least for 24 hours. As a result diagnostic monitoring is handled by the base station or central processing unit in the medical control center.

Main digital modules in a personal ECG monitoring device are as follows.

1. Microcontroller (more often with built in data converters)
2. Clock generator
3. Memory modules for storing application software (usually compiled in assembly code), patient data and digitized ECG
4. Display driver (some ECG monitoring devices do not have display)
5. Data transfer interface like USB interface or serial link
6. Data transmission interface like interface with short range ECG wireless transmitter like infrared and Bluetooth.

3.6.1 Microcontroller

Main digital modules of **Silicon Locket** are shown in Fig. 3.1. Low power microcontroller MSP430F149 from TI (Texas Instrument) was used in the first prototype of **Silicon Locket** [90]. This microcontroller has an internal 12 bit ADC with reference voltage of 2.5V. MSP430F149 consumes $280\mu\text{A}$ current at 1 MHz operational frequency with standby current of $1.6\mu\text{A}$ [2]. On-chip 60KB flash memory is used for temporary storage of digital data as ECG is acquired and digitized in **Silicon Locket** [90].

3.6.2 Data Storage

In many cases real time transmission of ECG data is not required. Instead cardiologist needs latest ECG data from the patient recorded, say for 24 hours. One of the best ways of storing ECG data is SD (secure digital) card [3]. SD card is a non-volatile memory card which can be easily plugged into portable electronic devices such as cameras, mobile phones, etc. Capacity of the card may change from few Mega bytes to tens of Giga bytes. As shown in Fig. 3.1 **Silicon Locket** uses a removable SD card interface. Patient can easily carry the stored data any time she/he visits the doctor.

3.6.3 Data Retrieval

Data storage, transmission and retrieval are crucial in wearable healthcare instruments. In the context of ECG, data retrieval methods depend on the storage media. For example ECG retrieval from SD card can be addressed in two ways. One way is to provide a removable SD card interface to the instrument and then use a media-card reader. Another way is to provide a reader based on one of the commonly used connectivity standards, such as USB or Bluetooth [60]. In latter case additional conversion chips are required to interface the microcontroller to the peripheral devices. In case monitoring should be real time or acquired ECG should be sent to a base station with minimum delay low power wireless transceivers supporting short range connectivity standards such as IEEE 802.15.4 may be used.

3.7 Discussion

Personal health monitoring technologies provide medical facilities in small devices. The device can be like a mobile phone so that a person can easily carry it or will be inserted in proper textiles so that the person can wear it. Low cost wearable or mobile personal healthcare devices record vital physiological signals or provide standard measures of health. Many of these devices are already available in the market. However to make these devices reliable and affordable for every body research is going on to provide solutions with more functionalities, better performance, less energy consumption, less size and lower price. In this chapter an example of a low cost power efficient custom IC for signal conditioning of simultaneously three channel ECG was presented. From hardware side integration of sensor, signal conditioning, data conversion, control and processing modules all in one chip will significantly improve the performance, cost, size, price and energy consumption of the device. Development of special microcontrollers and processors for wearable healthcare devices plays a vital role in embedding more algorithms for annotation and post processing of recorded or measured signals.

Calibration of Locket

In Chapter 3 we have seen the hardware details and specifications of the *locket* which we have used for acquisition of ECG signals. Here we reproduce some of the important features and measured performance parameters of the analog processing part of the *locket* in Table 4.1 (from [117]) for convenience.

Table 4.1. Specifications of the analog processing part of the *locket*. Reproduced from [117].

Feature/Parameter	Value
ECG-lead	Single, primary lead
Battery Voltage	3.7V
Supply current for a single-channel	22 μ A
Voltage gain	600
Input voltage dynamic range	6mV
Input referred noise voltage (rms)	6 μ V ($0 < \text{BW} < 200\text{Hz}$)
Common mode rejection ratio	100dB (at 60Hz)
Output signal slew rate	50mV/ μ s
Input impedance	3.2M Ω
High-pass cut-off frequency	0.05Hz
Low-pass cut-off frequency	106Hz
Quantization	12 bits/sample in the range 0-2.5V
Memory	32MB SD card
File formats	binary, ASCII
Computer interface	serial port data transfer, on-line and off-line

The battery voltage 3.7V matches with the commercially available Li-ion rechargeable, BL-5C battery. The supply current specification gives an idea how frequently the battery needs to be recharged. For example, the BL-5C battery permits the *locket* to record single channel ECG data continuously for more than 10 hours. The voltage gain is set to amplify the analog signal captured by the electrodes sufficiently for analog to digital conversion. For the

specified operating voltage and gain the amplifier is able to cover the dynamic range of 6mV, which is considered suitable for surface ECG. Typically, the ECG signal has an amplitude of 1mV at the skin surface but it can be as high as 3mV for some subjects. The rms level of noise is as low as $6\mu\text{V}$ as indicated in Table 4.1, which accounts for the thermal noise of resistors at the input of the amplifier. The common mode rejection ratio indicates capability of the amplifier to reject the common mode input signal such as powerline noise. The slew rate represents the highest rate of change in the input signal and hence the maximum amplitude of the signal at a specified frequency that the amplifier can handle. The input impedance of the amplifier matches with the skin electrode impedance for optimal capture of the ECG signal from the skin surface. The highpass and lowpass cut-off frequencies determine the frequency range of the amplifier and the selected bandwidth is considered suitable for the ECG signal for clinical applications.

The detailed specifications of the *locket* related to the analog part such as frequency response, noise level, common mode rejection ratio, slew rate, etc., have been characterized and reported in [117]. However, the sampling rate which is determined from the crystal frequency and the multiplier set in the firmware, is adjustable. This is preferred over a fixed sampling rate to suit the needs of different applications and limitations imposed by the number of channels and the available memory storage, particularly at the development stage of the recorder. For the prototype used in this work the sampling rate is pre-set and kept the same for all data recorded for the same purpose.

In this chapter we discuss a simple calibration procedure performed to confirm the pre-set sampling rate of the *locket* with respect to a standard analog to digital converter (ADC). The sampling rate is useful when the ECG signal is required to be analyzed with respect to other signals such as accelerometer data.

4.1 Calibration Requirements

It is important to know the sampling rate for physical understanding and interpretation of the signals recorded in digital form. The sampling rate can provide the exact time instance of a particular event in the digital signal and also allows us to compare the signals from several different sensors working at different sampling rates. For example, in Chapter 8 we use body acceleration signals recorded using a stand-alone motion sensor system with a sampling rate different from that of the *locket*. Thus the collected acceleration and ECG signals are at different sampling rates. To analyze the ambulation activities in time we must have a common time reference for both the signals which is possible only if the sampling rates for both the systems are known.

A pulse with a very stable amplitude, frequency and duty cycle is required as the input for the calibration of the sampling rate of the *locket*. The number of samples during ON time of the pulse can be counted to know the exact

sampling rate. There are, however, some limitations on the calibration pulse: the amplitude of the pulse should be less than 1mV in order to prevent the device from going into saturation due to high amplifier gain and the ON time of the pulse should be integer multiple of sampling period to avoid the error in counting of number of samples per second. Considering the difficulties in generating the calibration pulse with the strict specifications for the method given above, we instead show here a practical approach to estimate or confirm the exact sampling rate of the *locket* with an analog to digital converter (ADC). In this method we require an analog ECG processor (amplifier) and an ADC with known sampling rate. We use the powerline interference as a reference signal for both the systems, the *locket* and the ADC.

4.2 Experimental Set-up

Since we wish to use the powerline signal as a common reference signal for the ADC as well as the recorder to be calibrated, we allow the powerline interference to occur in both the channels. It is known that there is increased powerline interference if the lead cables of the ECG amplifiers are not shielded [137]. Therefore, for the signal acquisition process during the calibration, we use unshielded cables and choose an environment like an electronics laboratory, where significant powerline interference is known to occur. Care has to be taken that the level of the interference signal does not saturate the ECG amplifier. This is practically achieved by keeping an appropriate distance from the source of the interference like a switch or a power supply regulator. This method is different from the impedance measurement using a current supplied across the electrode at a specified frequency, since there is no active source connected to the electrode itself. Since the skin electrode impedance is sensitive to the skin stretch at the lower frequencies (below 200Hz) [40], we restrict any body movements activity (BMA) during the ECG acquisition to prevent undesired artifacts. Thus according to the model given in Eq. (1.1) of the recorded ECG signal, $r(n) = q(n) + s(n) + \eta(n)$, we try to enhance the sensor noise $\eta(n)$ with the characteristic of a very narrow spectrum, centered at $\approx 50\text{Hz}$ in this experiment, while minimizing the motion artifact signal $s(n)$. Ideally, $s(n) = 0$ in absence of any BMA. A set-up of the experiment is given in Fig. 4.1, in which two parallel channels of the lead-II ECG acquisition are depicted. The two channels for the lead-II configuration are obtained by placing a pair of electrodes side-by-side with a separation of 1.5cm, for each of the paired locations as shown in Fig. 4.1. The upper channel is connected to an ECG amplifier followed by an ADC, *NI-USB-6009* from *National Instruments (NI)*. The *NI-USB-6009* is configured to sample the analog signal in the single ended mode with a common ground (the same as the amplifier ground), unity gain and quantization of 12 bits/sample. Further details about connections and configuration of *NI-USB-6009* are provided in [1]. The digitized data is transferred to the computer through a universal serial bus (USB) in real-time

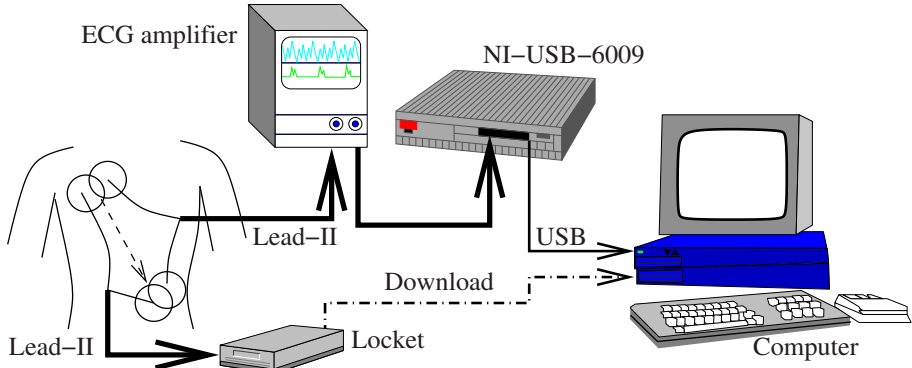


Fig. 4.1. Experimental set up for the calibration of the sampling frequency of the wearable ECG recorder.

using a software interface. The sampling frequency of the device was software controlled using the *NI-DAQmx Base 1.4* driver programmed through the *NI Labwindows CVI 7.1* interface. The other channel in Fig. 4.1, is connected to the *locket*. Since the data in both the channels are being recorded separately without any time synchronization, the recordings in both the channels are started with a minimum possible delay between the two channels.

4.3 Calibration Technique

From the experimental set-up described in the previous section, we have seen that there are two ECG signals recorded separately but from the same location configured for the lead-II: one using the *locket* and the other using the ADC (*NI-USB-6009*). Let us denote the recorded signal in *locket* as x_1 and that recorded in the ADC as x_2 . Let the sampling rates of the signals x_1 and x_2 be f_1 and f_2 , respectively. Here f_1 is unknown and f_2 is pre-programmed in the ADC using the software.

It is known that the powerline interference is dominant in both the recorded signals, which is centered at a frequency $\approx 50\text{Hz}$. However, the exact value of the frequency f_p may deviate by $\pm 2\text{Hz}$. Moreover, the value of f_p may not remain steady over a long period of time. Thus we cannot adopt the method of counting the number of samples per cycle of the interference wave for calculating the sampling rate. Instead, we acquire a reference signal using an ADC for which the sampling rate is known. Here, we use the fact that both the ADC and the *locket* signals are being recorded simultaneously, hence the line frequency f_p remains the same for both the signals. A block diagram of the processing steps involved in this method is given in Fig. 4.2. First, in the DFT block the magnitude spectrum of the input signal is computed over a fixed window using discrete Fourier transform (DFT). Since the frequency

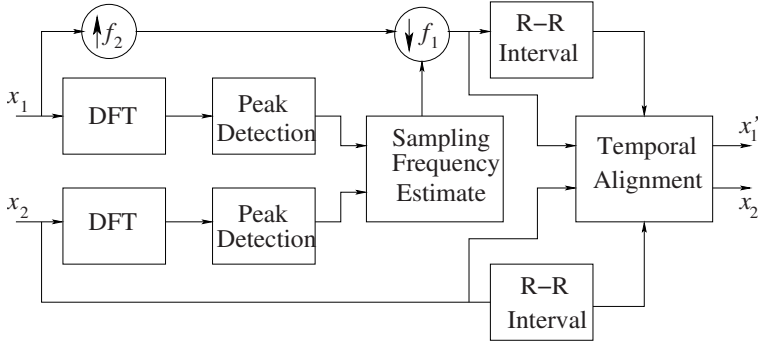


Fig. 4.2. Processing steps in the calibration method.

resolution of the DFT is related to the number of samples in the window as well as the sampling rate, we should choose a reasonably high number of samples. The powerline frequency component is dominant in both the signals x_1 and x_2 and hence it produces corresponding peaks in the computed spectra. Since f_1 is unknown, the locations of the peaks are detected on a normalized frequency axis $2f_O/f_2$, where f_O is frequency observed in the DFT at the sampling rate of f_2 . Therefore, f_O is the actual frequency for x_2 , whereas the actual frequency for x_1 is given by $(f_O f_1)/f_2$. The unknown sampling frequency f_1 is estimated in Fig. 4.2 as follows.

Let us denote the locations of the peaks on a normalized frequency axis $2f_O/f_2$ as p_1 and p_2 for the signals x_1 and x_2 , respectively. The actual powerline frequency f_p corresponding to both the peaks is the same. However, the observed frequency f_O is related to the actual frequency in each signal in a different way as explained above.

Therefore we have,

$$\begin{aligned} f_p &= \frac{p_1}{2} \cdot \frac{f_1}{f_2} = \frac{p_2}{2} \\ \Rightarrow f_1 &= f_2 \frac{p_2}{p_1}. \end{aligned} \quad (4.1)$$

Since we know the variables in the right hand side of the above equation, we can calculate the sampling frequency of the locket f_1 . We can also calculate the powerline frequency f_p for the given data.

4.4 Results and Discussion

Following the technique given in the above section, the magnitudes of DFT (spectra) of the signals x_1 and x_2 against normalized frequency values $2f_O/f_2$ are plotted in Fig. 4.3(a), where $f_2 = 256\text{Hz}$. A distinct peak in the spectrum of each of the signals is found as shown in Fig. 4.3(a), which is attributed to the powerline interference. However, the locations of the peaks in both the

spectra are shifted because of difference in the frequency scales for both the signals. The shift is more clearly visible in the cross-correlation function of the two spectra, plotted in Fig. 4.3(b). The half-width of the lobe produced in the cross-correlation represents the variance in the frequency estimation, which is $< 0.2\text{Hz}$. We have found the values of $f_1 = 242\text{Hz}$ and $f_p = 48.9\text{Hz}$ using Eq. (4.1) from the recorded data in this experiment.

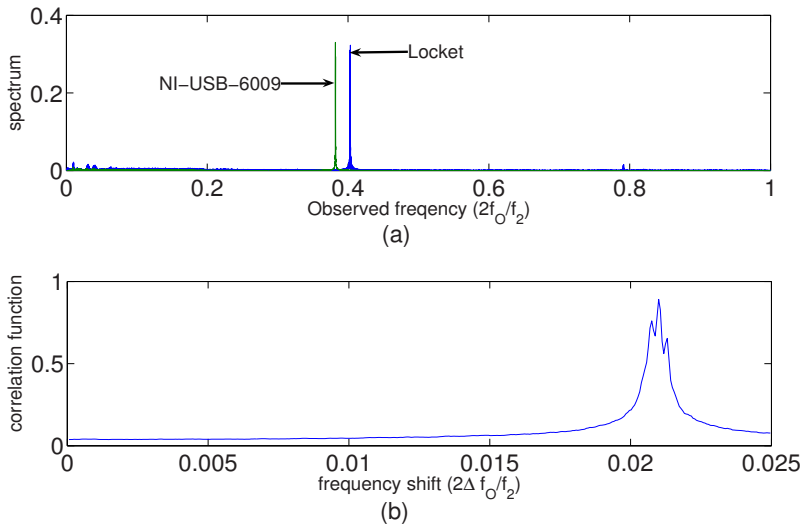


Fig. 4.3. (a) Observed spectra of powerline interference with sampling rate $f_2=256\text{Hz}$ and unknown f_1 . (b) The shift in the observed powerline frequencies using cross-correlation of the two spectra.

It is worth explaining here, why the cross-correlation based technique should work in estimating the sampling frequency of the locket. Ideally, spectra of both the signals x_1 and x_2 are nearly identical as both are acquired from (almost) the same lead-II positions of the ECG electrodes. The difference in peak in Fig. 4.3(a) is due to different choice of sampling frequencies in two channels. Ideally, one would like to dilate or contract one of the power spectral densities (PSD) to estimate the exact frequency. Since we have selected the reference frequency f_2 , very close to the locket frequency f_1 , the expression Eq. (4.1) can be simplified as

$$\begin{aligned} f_1 &= f_2 \frac{p_2}{p_1} \\ &\approx f_2 \frac{p_1 + \delta}{p_1} \\ &\approx f_2 + \frac{\delta}{p_1} f_2 \end{aligned}$$

$$\approx f_2 + \Delta f, \quad (4.2)$$

where Δf is the shift in frequency. Cross-correlation of the PSD of these two signals, thus, gives us the frequency offset required to calculate the sampling frequency of the locket.

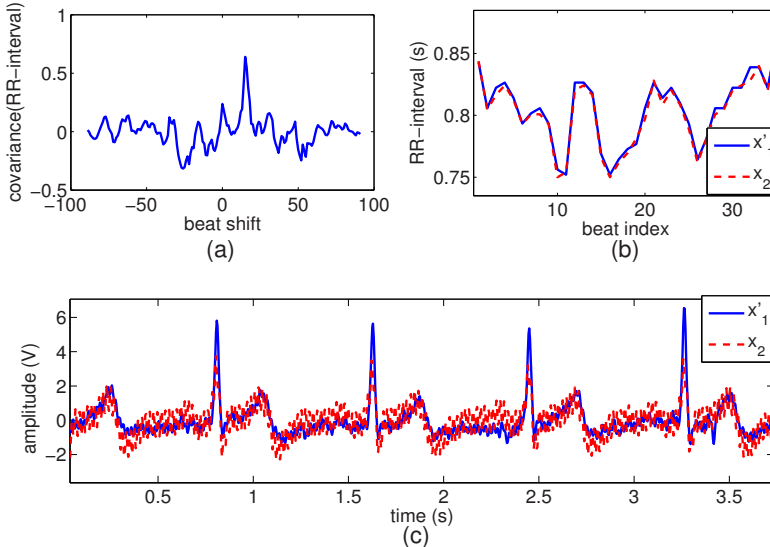


Fig. 4.4. Temporal synchronization of the two signals using the covariance of RR interval sequence. (a) Cross-covariance function of the two RR interval sequences, (b) the two RR interval sequences after alignment and (c) the ECG signals after alignment.

Now, the sampling rate of the *locket* is known, which can be used for resampling of the signal x_1 so as to match it with the sampling rate of x_2 . The signal x_1 is resampled by a rational factor of f_2/f_1 as indicated by $\uparrow f_2$ (upsampling) followed by $\downarrow f_1$ (down sampling) in Fig. 4.2. Let us denote the resampled version of signal x_1 as x'_1 . The resampled signal x'_1 and the signal x_2 have the same sampling rate but they may not be exactly time-synchronized. At this stage we cannot use cross-correlation between these two signals for time-synchronization because the powerline noise as well as ECG signal are both periodic in nature and may produce several peaks in the cross-correlation function creating ambiguity in finding the exact delay between the two signals. Instead, we use the cross-covariance function of RR interval obtained from QRS detection in both x'_1 and x_2 . We also verify that the error between the corresponding pairs of RR interval values for both the signals is very small after time synchronization. The cross-covariance function of the RR interval series is shown in Fig. 4.4(a). A distinct peak at a shift of

16 beats indicates the delay between the two signals. A part of RR intervals for both the signals after the alignment is shown in Fig. 4.4(b), indicating a perfect match. The ECG signals after time-synchronization are shown in Fig. 4.4(c). The spectra of both the signals are shown in Fig. 4.5. At the lower frequency band of 0-25Hz, both the spectra are matching very well, the faster roll-off for spectrum of signal x_2 is due to the 50Hz high frequency cut-off (as opposed to 106Hz for the *locket*) of the ECG amplifier used in the experiment. The peaks of the powerline are produced at $f_p = 48.9\text{Hz}$ in both the spectra.

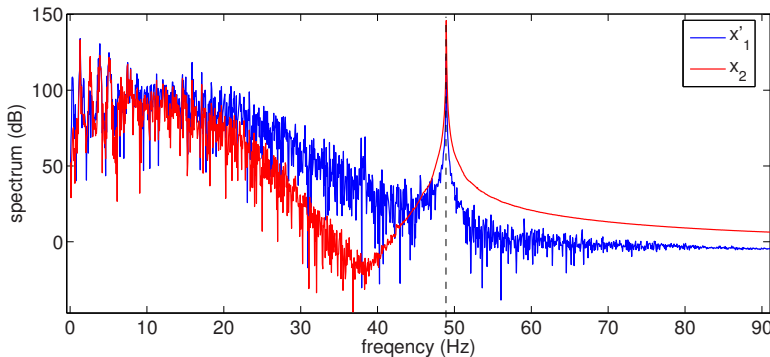


Fig. 4.5. The spectra of two ECG signals after achieving the alignment. The peak at powerline frequency is in perfect alignment for both the signals.

In this chapter, we have presented a simple yet effective method for calibrating the sampling rate of a W-ECG using powerline interference. The experimental set-up for the calibration is very simple to implement in the laboratory. The method is also useful for calculating the exact powerline frequency over a short period of time and hence can be used for generating a reference signal for adaptive noise removal applications. Since the method is based on DFT, peak detection and cross-correlation operations are easy to implement on micro-computers, and hence it can be easily adapted for W-ECG.

Data Acquisition

In previous chapters we have provided some background on ECG and discussed issues such as calibration those are specific to wearable ECG recorders. In the remaining part of the monograph we shall discuss various signal processing techniques for analysis of ambulatory ECG signal. We shall demonstrate their usefulness through a number of experimental results. All experiments have been conducted in real life situations. In this chapter we discuss the various data acquisition procedures. The same experimental protocol is followed everywhere in this monograph.

5.1 Introduction

Motion artifact is a major problem in the analysis of ambulatory ECG signals. Though the motion artifact is undesirable, it cannot be removed completely from the ECG signal using any linear filtering methods because of the spectral overlap. Our aim is to extract information regarding the body movement activities (BMA) from the ambulatory ECG signal itself. Once the motion artifact signal $s(n)$, in Eq. (1.1), has been well characterized, it can be eliminated and the true ECG signal $q(n)$ can be recovered under certain restrictions.

In ECG acquired at rest there is no movement of the subject and hence the motion artifact is not present. However, when we consider the ECG signal recorded by a wearable ECG device (W-ECG) then motion artifact is prevalent whenever the user (wearer) performs any kind of body movement. Since the purpose of the W-ECG is to monitor the cardiac signal of the wearer while the routine activities are being performed unrestrictedly, one may be interested in analyzing the ECG signal from the activity view point.

The various body movement activities (BMA) that have been considered in this study, influence the ECG signal in some ways that are similar, yet in other respects in different and unique manners. For example, consider the following two activities: (i) walking on a level floor and (ii) walking down stairs. Both these activities are different, however, in as much they influence the ECG

signal, there are a lot of similarities and this will be shown in subsequent chapters. Therefore, it is practically very difficult to distinguish all the types of BMA from the ambulatory ECG signal itself. However, in our experiments we find that classifiability improves drastically with training. Our analysis of ambulatory ECG signal involves transition detection, BMA recognition and impact analysis and these are presented in the Chapters 6-8. First of all we consider commonplace BMAs like walking, climbing stairs, etc. and acquire the ECG signal during the specific BMA. The ECG signal itself is qualitatively described by the corresponding BMA label. In the next section, we acquire ECG signals during the transitions among any two BMAs. Finally, we acquire both the ambulatory ECG signal and the motion sensor signals during various BMAs. The motion sensors are attached to different body parts to measure the acceleration signals due to the BMA. Using these data we can study the impact of the variation of the activity levels on the motion artifact signal in ECG. Impact analysis has also been performed on ECG data acquired from subjects undergoing multiple levels of activities on a treadmill. In this chapter we discuss the various data acquisition procedures as well as the protocols for various ambulatory ECG experiments.

5.2 Commonplace Body Movement Activities

The intended use of the *locket* or a W-ECG is that the user should be able to perform all routine activities with not too many constraints. Hence we wish to analyze the ECG signal during such activities in order to detect any unique pattern specific to an activity. We consider some of the most commonplace body movement activities (BMA) like movements of left, right and both hands, walking on level floor, climbing on stairs, etc. The ECG signal is acquired when only one of the specified BMA is being performed continuously. In this sense each of the ECG signal in this data set qualitatively represents a specific BMA and can be recognized by the particular BMA label.

A single-lead W-ECG is used for acquisition of the ECG signals in lead-II configuration at a sampling frequency of 242Hz. The detailed specifications of the W-ECG are summarized in Chapter 4 [117]. The lead-II configuration [12] is chosen for all the recordings in this study for consistency. In this experiment, certain commonplace BMAs such as sitting, walking, movement of arms, and climbing up and down stairs are recorded. Stair climbing is chosen as it is a routine activity in urban life. Also, it is perhaps one of the most demanding activities which will cause strain on the heart at a high activity level and should be carefully monitored. The activities are performed over a short duration followed by sufficient rest so that the effect of a particular BMA subsides before the next activity is initiated. Thus, care has been taken not to unduly stress the heart during the BMA. Since climbing up the stairs may cause stress, this is restricted to only up to three floors and is performed at a relaxed pace. Since we are exploring the feasibility of BMA recognition

from a single-lead ECG signal, thus as a precaution, testing is restricted to subjects with no known cardiac disorders as a precautionary measure. Again, all subjects were intentionally chosen to be right-handed males in order to preclude variations arising out of possible gender and orientation effects. In addition, there were no instances of dextrocardia. The subjects volunteered to perform all of the following defined classes of body movement activities:

1. sitting still on a chair,
2. up and down movement of left arm, at a rate of approximately 25 cycles of the up-down movement per minute,
3. up and down movement of right arm, at a similar pace,
4. similar up and down movement of both arms,
5. walking at a gentle pace with an average speed of about 3 km/hour on a level floor,
6. twisting left-right-left body movement at the waist while standing, at a rate of approximately 25 cycles per minute, as a common body stretching activity,
7. climbing down stairs at an average rate of 100 steps per minute or equivalently coming down at an average speed of 30 cm/s,
8. climbing up stairs at an average rate of 85 steps per minute or equivalently gaining a height at an average speed of 25 cm/s.

A total of 23 healthy subjects were chosen in the age group of 22 to 50 years with an average age of 29 years and a standard deviation of 7 years. A part of the data collected was used for training purposes and the other part was reserved for performance evaluation of the proposed technique. The ground truth with regards to type of BMA is known for the entire dataset.

5.3 Activity Transition

In the previous section ambulatory ECG signals have been acquired which represent certain specific types of BMA. In this section we consider the same set of BMA as above. However, the goal is to detect transitions among any two different types of BMA on the basis of the differences in the induced motion artifact signal due to different types of BMAs. In order to study transition detection we acquired ECG signals while the subject switches from one activity to another. The specific BMA sequence and the exact time of the transition in the ECG signal is recorded by a passive observer to obtain the ground truth.

The specifications of the *locket* [117] used for ECG data acquisition in this study are the same as above. Here in the proposed experiment, activities such as sitting down, standing up, movement of arm(s), walking, climbing on stairs, twisting motion at waist, and some transitions among some common body postures during sleep such as left lateral, supine and right lateral are performed. We also included a few examples of yawning during data collection as this involves a significant expansion of chest, introducing its own form of

motion artifact in the ECG data. Care has been taken not to unduly stress the heart during the BMA and hence all the BMAs are performed at a normal relaxed pace. The ECG signals are collected from normal subjects with no known cardiac disorders, containing different types of BMA transitions given in Table 5.1. The total number of each type of BMA transitions is indicated in the next column in Table 5.1.

Table 5.1. Summary of the dataset acquired from various subjects for the purpose of detecting the activity transitions.

BMA Transition	Number of Transitions
Still→Twisting	21
Twisting→Still	10
Still→Walking	50
Walking→Still	5
Still→Climb up	23
Climb up→Still	9
Still→Climb down	18
Climb down→Still	8
Still→Arm movement	73
Arm movement→Still	18
Arm movement→Walking	6
Walking→Arm movement	13
Turning while walking	62
Sit→Stand	22
Stand→Sit	22
Supine→Left-lateral	6
Left-lateral→Supine	7
Supine→Right-lateral	6
Right-lateral→Supine	6
Still→Yawning	5
Total	390

A total of 27 healthy subjects were chosen in the age group of 22 to 40 years with an average age of 28 years and a standard deviation of 6 years. Again, all subjects were intentionally chosen to be right-handed males without any instances of dextrocardia. Apart from these healthy subjects, one 62 years old male cardiac patient with a prosthetic aortic valve and a left bundle branch block (LBBB) has also participated in this experiment. This particular subject has been chosen to verify that the proposed method works satisfactorily even if the QRS morphology is very different. In this example, the positive R peak is smaller as compared to the negative S peak and hence the S peak is dominating in QRS complex instead of the usually dominating R peak.

5.4 Motion Sensing

In the data sets mentioned in the previous two sections, we have described the type of body movement qualitatively with labels. Here, all the BMAs have been performed by maintaining a moderate and almost constant pace. This is because the goal has been recognition of any differences in the motion artifacts due to different types of body movements. Obviously, these kind of experiments do not tell anything about the impact of variations in the pace levels for the same type of body movement.

One way to represent the level of body movement is by measuring the acceleration signals from appropriate locations on the body. This also helps to quantify the activity levels rather than just describing them qualitatively as slow, medium or fast. For determining various pace levels of the physical activities, we have recorded both the ECG and acceleration signals. The acceleration signals are acquired to establish/verify the ground truth. The ECG signals are acquired with the *locket*. The lead-II configuration is chosen in all the experiments. In this section we explain data collection using motion sensors and processing of the collected acceleration data.

5.4.1 Data Collection using Accelerometer

Accelerations of various body parts have been measured using *MTx[®]* motion trackers from *Xsens Motion Technologies[®]* placed at appropriate positions on the body. The *MTx[®]* motion tracker senses linear acceleration along 3 axes. It also senses the 3D rotations of the sensor co-ordinate system in a fixed local co-ordinate system (LCS). The fixed LCS has its positive (+ve) X pointing toward the local magnetic North, +ve Y toward the West and +ve Z pointing up wards. All accelerations and rotations were measured at 32 bit resolution and sampled at 25Hz. A bluetooth wireless interface was used to transmit data. Recently, a similar data acquisition system has been used for ambulation analysis and assessment of human ankle and foot posture [112].

Motion sensors are placed on the upper arm(s), right thigh and the frontal waist of test subject. The sensor at waist measures the local acceleration at the waist while twisting, and the resultant acceleration of the subject's body during other activities. The accelerometers at the arm(s) and on the thigh measure local accelerations in these parts. Motion trackers are tightly strapped on the subject's body to prevent slippage or any relative motion between the sensor and the body. However, it is also ensured that the subject faced minimal discomfiture after wearing the ECG electrodes and the motion sensors, such that the usual body movement of the subject remains unaffected. For better understanding of events recorded by motion sensors as well as for *post facto* verification, all activities of the subjects are time stamped and recorded using a video camera. The start and end times for ECG and motion recordings are noted down. The experimental setup is illustrated in Fig. 5.1, with the motion

sensor apparatus and electrodes of the W-EKG firmly secured at appropriate locations on the body of a subject.



Fig. 5.1. Illustration of the experimental setup. Motion trackers (small orange objects) are strapped on the upper arms and the waist. The bigger object hanging at the waist where the left hand touches is the bluetooth interface for motion sensors. The single lead ECG recorder is attached to the front right side of the waist. The entire experiment is recorded on video to capture stray events not recorded by the motion sensor.

In the first set of experiments involving motion sensors, each of the following BMA is performed at three different levels of pace: slow, normal and fast.

1. Change in posture from sitting on a chair to standing up, and vice versa.
2. Up-down movement of one of the two arms, left or right, parallel to the sagittal plane, with the other hand at rest.
3. Walking on a level floor.
4. Twisting the torso at the waist while standing, as a common body stretching activity.
5. Climbing up and down the stairs.

A total of 5 healthy male subjects in the age group of 22 to 27 years and 2 cardiac patients of ages 31 and 62 years participated in this experiment. The subjects are requested to avoid undue tightening of muscles to avoid extra EMG noise due to muscle stiffness. It should be noted that though the activities in the list above are apparently similar to those that have been

done in the previous sections, here the experiments and the purpose both are different. Here we introduce different levels of pace of performing the BMA for the purpose of impact analysis. This is in contrast with previous studies where the BMA have been performed at a nearly constant, slow or normal pace without any variations in the levels as the objective was BMA recognition.

5.4.2 Processing of Accelerometer Data

Here we describe the procedure followed for computing local acceleration signals at a given position with reference to the body. The motion sensor system described above records accelerations in sensor axes and rotations of the sensor axes in the fixed local co-ordinate system (LCS). Since the sensor axes are rotating during the body movements, all accelerations are converted to the fixed LCS using the rotation matrix of direction cosines for each individual sensor. Let $R_k(n)$ be the 3×3 rotation matrix in the fixed LCS and $\underline{a}_k(n) = [a_{kx}(n) \ a_{ky}(n) \ a_{kz}(n)]^T$ be the 3-axes acceleration vector recorded at n^{th} sample for the k^{th} accelerometer (at a suitable body position), respectively. The corresponding accelerations $\underline{a}'_k(n) = [a_{kX}(n) \ a_{kY}(n) \ a_{kZ}(n)]^T$ in the LCS can be computed as

$$\underline{a}'_k(n) = R_k(n)\underline{a}_k(n). \quad (5.1)$$

Measured accelerations \underline{a}'_k have static components due to gravity and general translation of the body, as well as dynamic components associated with local limb motion. To account for only the local limb movements, the static components are suppressed by local mean subtraction, calculated over a moving time window of 8 seconds, from each element of the acceleration $\underline{a}'_k(n)$. The acceleration of the k^{th} limb is given by

$$\underline{a}''_k(n) = \underline{a}'_k(n) - \frac{1}{8f_s + 1} \sum_{j=n-4f_s}^{n+4f_s} \underline{a}'_k(j), \quad (5.2)$$

where $f_s=25\text{Hz}$ is the sampling frequency for the motion sensor. The movement of the k^{th} limb (sensor) is quantified in terms of the norm of the acceleration vector $\beta_k(n) = |\underline{a}''_k(n)|$. In this chapter, $k=1$ refers to the sensor at the right arm, $k=2$ is the right leg sensor, $k=3$ is the sensor at the frontal waist and $k=4$ refers to the sensor on the upper left arm. Our objective is to relate the impact signal in the recorded ECG to the limb motion signal $\beta_k(n)$ and show that these are strongly correlated.

To study the behavior of motion artifacts with respect to the extent of movement, the displacements of individual sensors need to be recorded. The extent is defined as the distance between two extreme positions during limb movement. The relative position of the k^{th} sensor at the n^{th} sample, $\underline{p}''_k(n)$ is computed by discrete integration of the corresponding accelerations \underline{a}''_k twice in time using the trapezoidal rule.

The extent of a body movement from the initial position is computed as the norm of vector $\underline{p''}_k(n)$, as $\delta_k(n) = \|\underline{p''}_k(n)\|$. The envelope of $\delta_k(n)$ gives the extent of the body movement. While $\beta_k(n)$ is a measure of the instantaneous motion of a limb, $\delta_k(n)$ could be viewed as a measure of the combined effect of physical stretching of the surrounding skin along with contraction of the associated limb muscles.

5.5 Variation of Activity Levels

In previous sections we discussed about various types of BMA and the data collection process for the specified types of BMA. We have also quantified the activity levels using the acceleration data collected from the body using the motion sensors. We can broadly categorize the levels of the activities as slow, medium and fast. Of course there may be variations in the acceleration values for the specified activity level because very fine control of the movement cannot be expected from the human subjects without any mechanical assistance. However, we observe that the corresponding acceleration values recorded by the motion sensors for the three different levels of the same BMA are quite distinct from one another, as compared to the BMA for the same level. We have already mentioned that the motion artifacts are induced due to BMA. Hence it is interesting to know about the impact of variations in the levels of BMA.

The cause of the motion artifact is relative motion of the skin and the electrode. The skin area under the electrode is stretched or contracted in certain directions due to BMA. The amount of the skin stretch or contraction depends on the level of the BMA. Hence it is likely that any variation in the level of the BMA will be reflected on the amplitude of the motion artifact signal. Thus, the BMA performed at higher levels of pace should induce motion artifacts with higher amplitudes. However, we still need to verify this hypothesis experimentally. Hence we have acquired the ambulatory ECG signals during various BMAs performed at the three different levels. In this experiment we consider certain routine BMAs like movement of arms, walking, twisting at waist, etc. The acceleration data is used as the ground truth.

We have also used treadmill to achieve a controlled variation of the pace of walking. Since the speed of the treadmill is constant for a particular level, the subject synchronizes the walking speed accordingly. We can obtain the ground truth from the treadmill speed settings following a set of protocols which are noted below.

5.6 Protocols for Treadmill Tests

In the previous section we discussed about the experiments related to the variations of the BMA levels. For the same purpose the ECG of a subject is

monitored while walking at controlled speeds for fixed durations on a treadmill (Quinton®). Lead-II ECG signals are acquired from five healthy volunteers in the age group from 22 to 26 years and 9 cardiac patients in the age group from 39 to 63 years. In the case of patients, treadmill testing is done using the Bruce protocol in the clinical setup under strict medical supervision, with simultaneous monitoring of vital parameters such as heart rate and blood pressure, and other stipulations in accordance with the guidelines provided by American Heart Association (AHA) [32]. The Bruce protocol subjects the patients to increasing levels of stress by increasing the speed and gradient (treadmill inclination), as given in Table 5.2. For the cardiac patients, the test is terminated as soon as the target heart rate is reached, or when signs of instability are observed in the ECG or in the other parameters.

Table 5.2. The Bruce protocol

Level	Time(mins)	Speed(kmph)	Gradient(%)
1	0-3	2.74	10
2	3-6	4.02	12
3	6-9	5.47	14
4	9-12	6.76	16
5	12-15	8.05	18
6	15-18	8.85	20
7	18-21	9.65	22

Stress test ECG signals from the healthy volunteers are obtained using a treadmill exercise protocol that is physically less taxing than the conventional Bruce protocol. The protocol is devised taking into consideration patient safety issues in a non-clinical set up. The gradient is set to zero throughout the test, and each stage of the test is limited to two minutes as compared to three minutes in the Bruce protocol. There are 5 stages in all for a total duration of 10 minutes, with treadmill speed ranging from 3 km/hr to 7 km/hr at increments of 1 km/hr in every stage. The heart rate of the subject is monitored continuously, using a pressure sensor attached to the chest, communicating via infrared to a display device. Accelerometers are not connected during the treadmill exercise since the motion of the subject is directly measurable from the treadmill, and to ensure patient comfort.

In this chapter we have provided the details of data acquisition protocols for various ambulatory ECG experiments. We shall present the complete analysis of our results in the subsequent chapters.

Detection of Activity Transition

In an ambulatory cardiac monitoring system using wearable ECG recorders (W-ECG), the motion artifact is generated in the ECG signal due to body movement activity (BMA) of the subject. This is because, as explained earlier, BMA causes the skin to stretch or contract and hence the interface between ECG electrodes and the skin is disturbed. Based on such a dependence of motion artifact on BMA we hypothesize that a specific class of BMA will result in a specific signature of the artifact. As a corollary any abrupt change in the BMA should also be reflected as an abrupt change in the motion artifact signal. To test these hypotheses we analyze the ECG beat-by-beat in temporal continuation and try to detect abrupt changes in the motion artifact signal due to the abrupt changes or transitions in the types of BMA.

The purpose of the monograph is to explain how one can build a wearable system for ambulatory cardiac monitoring. The key signal that the medical practitioners would like to have is the true ECG signal, extricated out of motion artifacts. Since the motion artifacts are spectrally overlapping with the ECG signal, and since different types of BMAs introduce different artifacts, we show in the next section a clean ECG signal can be obtained if the BMA can be recognized from the corrupted ECG signal. However, in order to recognize a particular BMA, we need ECG data from a few cycles of heart beat contiguously (this will be explained in the next chapter) while performing a specific BMA. In our daily life we perform several routine activities (BMA) one after another. Hence it is essential that we temporally segment the various BMA segments automatically. This calls for detection of activity transitions, which is discussed in this chapter.

Here every recorded ECG beat is considered in a vector form. A single ECG beat vector represents a cardiac cycle. However, in our case due to the impact of BMA the cardiac signal has the motion artifact component. Since the motion artifact signal itself is not available separately, it is derived as the residual signal after the subtraction of the estimated mean cardiac cycle from the current ECG beat vector. Thus the motion artifact vectors are computed over all the cardiac cycles for each type of BMA. The details of the

analysis and processing steps are provided in this chapter. The motion artifact vectors are considered to belong to a particular subspace which is different for each type of BMA. We propose to use a recursive principal component analysis (RPCA) based method to learn the BMA subspaces. The principal components are continuously updated to follow the smooth variations in the ECG signal due to the usual physiological reasons such as variability of the heart rate, breathing, etc. Based on the nature of BMA classes that were selected, there appears to exist a significant separation between two different subspaces corresponding to two different types of BMA.

In this chapter, we aim to show that based on the above hypothesis it is possible to detect the transitions among different types of BMA. First, we give a brief introduction to the problem and some of the relevant work for motivation. Next we explain the signal analysis method and processing steps involved in detail. Finally we present the experimental results in terms of accuracies in detecting the BMA transitions from the ECG signal itself.

6.1 Introduction

In Chapter 1, we have introduced a model of composite ECG signal recorded during ambulatory cardiac monitoring. It has also been mentioned that the body movement activity (BMA) of the subject distorts the collected ECG by inducing motion artifacts and hence the ECG signal contains a motion artifact component. All other kinds of noise present in the ECG due to the device itself and the environment, are represented as sensor noise. Thus the ECG signal has three components: cardiac signal, motion artifacts and sensor noise. The motion artifact signal induced in the ECG is due to skin stretching and contracting while performing any physical activity and has a significant spectral overlap with the cardiac signal itself. Therefore, motion artifact is considered as a serious problem in ECG recording, particularly, in ambulatory monitoring where the physical activities of the patient should not be restricted. The focus of most studies to remove the motion artifact component from ECG signal met with a limited success. It is understood that this component cannot be removed completely from the ECG signal due spectral overlap by using any digital filtering method.

In practice, the ECG is visually analyzed by a human expert for diagnosis purposes. The human expert, in most cases, can identify the segments where motion artifacts are dominant visually and discard those parts while deriving cardiac parameters. However, in W-ECG application for long term monitoring a huge volume of the data is collected and therefore the analysis should preferably be automated. Most automated methods perform accurately for ECG under rest conditions but fail miserably while encountering the real, ambulatory situations because of their limitations in detecting the superficial distortions in the ECG that are not related to any cardiac event.

Previously, one such problem of automated analysis for detecting body position changes for ischemia monitoring at rest (while lying in bed) has been addressed in [8, 9, 37, 52]. The changes in body positions cause angular shifts in the axis of heart and hence affect the cardiac cycle such that the changes in ST segment are often detected as ischemia episodes by the automated monitoring system. The methods in [8, 9, 37, 52], are devised in order to reduce the frequency of the false alarms due to body position changes by correctly identifying them from the ECG signal itself. These methods were developed based on the fact that the heart axis will shift with the selected three different body postures at rest: supine, right lateral and left lateral. Multi-lead ECG signal analysis is required for finding these shifts in the axis of the heart. This requires algorithms that are computationally more complex. This is useful when critical monitoring of the hospitalized patient is required.

As an alternate approach, one can consider the problem of detecting body position changes by using the induced motion artifact signal. In this approach, even a single lead ECG is sufficient for detection of the body position change, thus minimizing complexity. We present an example of posture change detection using the motion artifact signal in this chapter, where the subject is performing transitions between sitting and standing postures without any significant shift in the heart axis. However, our work is not limited to detection of posture changes only. We will also demonstrate how to detect transitions among different kinds of physical activities from the motion artifact signal itself using a single-lead ECG. The goal of this work is to facilitate automated analysis of ECG for ambulatory cardiac monitoring with W-ECG by deriving some useful information from the collected ECG itself.

Recently, an approach of movement specific characterization of the motion artifacts in ECG signal using a wavelet transform and a neural network has been discussed in [93]. The ECG signal is analyzed for extracting the motion artifact signal using wavelet transform and the corresponding wavelet coefficients are used for training a neural network for recognition of different types of motion artifacts. In this chapter, we are investigating the feasibility of the detection of changes within the motion artifact signal caused due to abrupt changes of the different kinds of BMAs.

In previous works related to detection of transitions in the signal, Fancourt and Principe [30] have provided a method for segmentation of a nonstationary signal into stationary segments using a learnt time delay neural network. Khalil *et al.* [62] have provided an unsupervised solution to the above problem for the specific case of analyzing uterine electromyograph (EMG) signal. Recently, Assaf [6] has proposed a supervised, multi-resolution based method for detecting transitions in muscular activities from the myoelectric signal. The purpose is to develop intelligent prosthetic aids.

The effect we consider here is the change in skin resistance due to stretching and contraction as opposed to the previous studies which are based on shift in the axis of heart. The disturbance caused in the skin electrode interface due to body movement is very superficial. Moreover, the motion artifact signal

appears to be random in nature because of a huge variety in the types of BMAs and the manner and pace in which they can be performed. However, the direct link between the type of BMA and the skin disturbance provides the basis for characterizing the motion artifact signal in a more systematic manner which we will see in the next chapter. This kind of analysis of motion artifact signal is specific to the particular ECG lead or electrode positions and also to the particular person. However, the person specific analysis is not necessarily problematic in the context of W-ECG as the main objective here is personalized health care.

In this chapter we show how the BMA transitions can be detected automatically from the ECG signal itself without any supervised learning. Since different BMAs will affect the skin electrode interface in a different manner, a transition between any two different BMAs will cause abrupt changes in motion artifacts patterns. We use a recursively updating PCA (RPCA) [72] to detect sudden discontinuities in the motion artifacts. To study the feasibility of BMA transition detection using the RPCA technique, continuous ECG signals are recorded while the wearer performs various physical activities using a W-ECG developed by Baghini *et al.* [117] and discussed in Chapter 5.

6.2 Transition Detection

In Chapter 1, the collected ECG signal $r(n)$ is modeled as an additive mixture of the cardiac signal, the motion artifact signal and the sensor noise. Here we repeat the model of the ECG signal for convenience,

$$r(n) = q(n) + s(n) + \eta(n), \quad (6.1)$$

where $q(n)$, $s(n)$ and $\eta(n)$ are cardiac signal, motion artifact signal and sensor noise, respectively.

We assume that the sensor noise is very small as compared to the other two components of the collected ECG signal and has zero mean. We also assume that the cardiac cycle is stable in the sense that no rhythm disturbances or arrhythmia are present. However, the cardiac cycle may be subjected to smooth usual changes such as those due to normal breathing, etc..

We adopt the signal model given in Eq. (6.1) for representing the recorded signal over one cardiac cycle of the heart. Therefore, the i^{th} ECG beat can be modeled in a vector form as

$$\tilde{r}(i) = \tilde{q}(i) + \tilde{s}(i) + \tilde{\eta}(i), \quad (6.2)$$

where $\tilde{r}(i)$, $\tilde{q}(i)$, $\tilde{s}(i)$ and $\tilde{\eta}(i)$ are the column vectors of the same dimension $RR(i) \times 1$, where $RR(i)$ is the number of samples under the i^{th} cardiac cycle. Since the duration of a cardiac cycle is not fixed but varying according to the heart rate, the dimension $RR(i)$ is not same for all the cardiac cycles (ECG beats). We can compute $RR(i)$ from the value of R to R interval at the i^{th}

ECG beat, defined as the sample interval between the R peak in the i^{th} ECG beat and that in the previous ECG beat.

Here we show that the motion artifact vector $\tilde{s}(i)$ in the present ECG beat $\tilde{r}(i)$ as given in the vector model of the ECG beat in Eq. (6.2), can be represented in terms of a few eigenvectors of the motion artifact subspace determined by the motion artifact vectors in the recent past $\{\dots, \tilde{s}(i-2), \tilde{s}(i-1)\}$, provided that there is no abrupt change in the BMA. An error in reconstruction in this representation is a measure of difference between the motion artifact vector in the present beat and the preceding beats. If the error signal remains below a threshold value then there is no change in BMA and if it crosses the threshold value this will mean that a different activity is being initiated. Thus transition detection in BMA should be possible from the ECG signal itself, even without any person specific training. The bases for the subspaces of currently ongoing BMA are learnt adaptively from the signal itself.

We discuss a recursive principal component analysis (RPCA) based algorithm to detect abrupt changes in motion artifacts due to BMA transition. Since the RPCA algorithm, like any PCA based algorithm is sensitive to feature alignment and since it requires the data vectors to have the same dimension, the ECG beats are time synchronized with respect to R peak in each beat and resampled to equalize each beat to a fix length of M_0 samples. The value of M_0 is chosen based on the normal heart beat duration and the given sampling rate of the ECG recorder. The choice of R peak for the purpose of heart beat alignment is due to the fact that the R peak is the most prominent feature of the ECG signal that can be detected easily even in presence of significant motion artifacts. The R peaks in the ECG signals are detected using the Pan-Tompkins method [96].

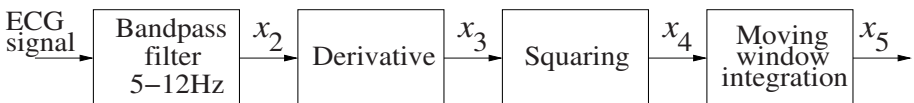


Fig. 6.1. Block diagram of Pan-Tompkins method for QRS detection in ECG [96].

This QRS detection algorithm is implemented through some simple processing steps provided in [96] as shown in Fig. 6.1. Here we describe the processing steps in brief. The rationale for using such steps can be found in [96].

- A bandpass filter with a passband of 5-12Hz is implemented using a low-pass filter with cutoff at about 12Hz followed by a highpass filter with cutoff at about 5Hz. The difference equation used for the lowpass filter is

$$y(n) - 2y(n-1) + y(n-2) = x(n) - 2x(n-6) + x(n-12), \quad (6.3)$$

and the difference equation for the highpass filter is

$$y(n) + y(n - 1) = -x(n) + 32x(n - 16) + x(n - 32). \quad (6.4)$$

The bandpass filtered signal is indicated as x_2 in Fig. 6.1.

- A derivative with nearly a linear frequency response between 0-30Hz is implemented by the difference equation

$$y(n) = \frac{1}{8}[-x(n - 2) - 2x(n - 1) + 2x(n + 1) + x(n + 2)]. \quad (6.5)$$

The derivative signal is indicated as x_3 in Fig. 6.1.

- The derivative signal x_3 is passed through a sample-wise squaring operation

$$x_4(n) = [x_3(n)]^2. \quad (6.6)$$

- A moving window integration signal $x_5(n)$ is derived from $x_4(n)$ using a window length N matching to the widest QRS complex in the ECG as

$$x_5(n) = \frac{1}{N}[x_4(n - (N - 1)) + x_4(n - (N - 2)) + \dots + x_4(n)]. \quad (6.7)$$

- The QRS locations are searched in a specific time interval by applying an initial threshold on the integration signal x_5 . If QRS is not found then a second threshold, which is half of the first threshold is applied in the same time interval. The threshold values are computed adaptively from the previous estimates and current values of detected peaks in the signal due to QRS complex and noise.
- A similar procedure of searching QRS complex using adaptive thresholds, is also applied to the bandpass filter signal x_2 .
- The QRS is claimed to be located where both the procedures recognized it in the given time interval.
- Two different, average RR estimates are maintained. The first one is calculated as a mean of RR intervals of the preceding eight beats. The second one is calculated as the mean of selected preceding eight RR intervals which are within the specified limits of 92% to 116% of the previous, second average RR estimate.
- If the first average RR estimate is within the specified limits of 92% to 116% of the second average RR estimate, then the rhythm is considered regular. The next QRS complex is searched in a time interval of 166% of the second average RR estimate from the most recently detected QRS complex.

The time duration between the current R peak and the preceding one is considered as the current ECG beat interval. In order to account for occasional instances of atrial extra systoles (AES) and missed R peaks, the ECG beat interval is estimated as the median of the five most recent RR intervals. Thus for the i^{th} beat, the length of current beat period $M(i)$ is estimated as median of $RR(i)$, $RR(i - 1)$, $RR(i - 1)$, $RR(i - 2)$, $RR(i - 3)$, $RR(i - 4)$,

where $RR(i)$ is the computed beat period for the i^{th} beat. For length equalization, the i^{th} beat with estimated beat period $M(i)$ is resampled by a factor of $M_0/M(i)$. The dimension $M(i)$ depends on the beat period and the sampling frequency. For example, for a normal heart rate of 72/min and a sampling rate of 256Hz, the dimension $M(i) = 256 \times 60/72 \approx 213$. A small variation in heart rate is quite natural during body movement and hence this requires that the lengths of the ECG beats be resampled so that a PCA based technique can be used. The resampling may generate a certain amount of noise in the QRS complex. The use of dc padding circumvents this problem. However, since our interest lies in studying the motion artifacts prevailing over the entire beat period and not just in the QRS complex and since the effect of distortion in QRS complex due to resampling is small, we have used the resampling technique for length equalization.

The i^{th} length normalized ECG beat $\underline{r}(i)$ is represented as the addition of two components in a column vector format

$$\underline{r}(i) = \underline{q}(i) + \underline{s}(i) + \underline{\eta}(i) = \underline{r}'(i) + \underline{\eta}(i), \quad (6.8)$$

where $\underline{r}'(i)$ is the composite signal component of dimension $M_0 \times 1$, The motion artifact $\underline{s}(i)$ is riding on the cardiac cycle $\underline{q}(i)$ and $\underline{\eta}(i)$ is the noise. As we shall demonstrate, the composite signal for a given BMA can be represented by a few principal components (eigenvectors) only.

In order to estimate the principal components, the covariance matrix C_i is recursively computed as

$$C_i = \sum_{k=1}^i \alpha^{(i-k)} \underline{r}(k) \underline{r}^T(k) = \alpha C_{i-1} + \underline{r}(i) \underline{r}^T(i), \quad (6.9)$$

where α , $0 < \alpha < 1$ is the forgetting factor. A smaller value of α results in a faster forgetting of the past data. The application of the forgetting factor α prevents any possible buffer overflow and hence memory constraints in a hardware implementation of the given technique. A set of top L eigenvectors of the covariance matrix C_i at i^{th} ECG beat is derived using Eq. (6.9). Let $E_i = [\underline{e}_{i1} \ \underline{e}_{i2} \dots \underline{e}_{iL}]_{M_0 \times L}$ be the set of top L eigenvectors arranged in a non-ascending order of magnitudes of the corresponding eigenvalues, $|\lambda_{i1}| \geq |\lambda_{i2}| \geq \dots \geq |\lambda_{iL}|$ till the i^{th} beat, where \underline{e}_{ik} and λ_{ik} are k^{th} eigenvector and eigenvalue, respectively.

To detect changes in motion artifacts present in the next ECG beat $\underline{r}(i+1)$, we obtain the component that lies in the span $\{\underline{e}_{i1}, \underline{e}_{i2}, \dots, \underline{e}_{iL}\}$. The error in approximation

$$\epsilon(i) = |\underline{r}(i+1) - (E_i E_i^T) \underline{r}(i+1)| \quad (6.10)$$

provides a measure of departure from the nearest BMA signal of the same class. If the error is large it corresponds to initiation of different BMA by the user. Hence the BMA transition is detected as a binary signal $T(i)$

$$\begin{aligned} T(i) &= 1, \text{ if } \epsilon(i) \geq \theta \\ &= 0, \text{ if } \epsilon(i) < \theta, \end{aligned} \quad (6.11)$$

where θ is an appropriate threshold, chosen empirically to be 2.5 times the error magnitude $\epsilon(i)$ averaged over a running window of 15 beats. This introduces a delay of 15 beats in detecting the transition which corresponds to about 12s delay in detection which is quite acceptable from the health monitoring point of view. One may instead select a fixed threshold θ when there would be no delay. But the choice of θ would then be subjective as the generated motion artifacts are often person specific, due to the nature of skin in contact with the electrode. It may be noted that the RPCA method is quite different from the two-step adaptive PCA based method [107] as we are not explicitly solving the time series segmentation problem.

6.3 Experimental Results

Continuous single-lead ECG signals are recorded with various types of BMA transitions as described in Section 5.3. The ground truth regarding all BMA transitions are obtained by a passive observer and reinforced through simultaneous video recording. The RPCA algorithm as given in the previous section is applied to all the available ECG signals. The ECG beats are time aligned and length equalized to a uniform length of 160 sample point duration as explained in Section 6.2. The complete ECG signal is marked beat-by-beat for the BMA transitions in terms of the binary transition signal $T(i)$.

Initially, we consider four different types of BMA episodes: movement of right arm, twisting motion at waist, standing up and walking. A rest period of 1.5 min was enforced after each episode so that the artifacts may subside before the next episode is performed. The duration of each of the ECG signals thus collected is around 7.5 min. There are overall 36 (9×4) BMA episodes for a duration of 67.5 (9×7.5) min. Fig. 6.2(a) and 6.2(b) depict RR interval and transition detection of the four BMA episodes in a single ECG signal. A significant correlation between the variation in RR interval and the BMA transition can be seen in Fig. 6.2. However, some deviations are also noted, and hence the RR interval itself cannot be fully indicative of a BMA transition (see Fig. 6.3). The ECG beats near a detected BMA transition are shown in Fig. 6.2(c).

Next, walking transitions are performed as a single step of walking, followed by a rest period of 1-1.5 min. There were 9-12 transitions in each ECG signal of 12 min duration. Three ECG signals were collected under this protocol, thus there are a total of 27 walking transitions over a duration of 36 (3×12) min. Fig. 6.3(a) and 6.3(b) show the corresponding RR interval and detection of the walking transitions. Here the correlation between RR intervals and the BMA transitions is not at all apparent. However, all the transitions are detected correctly by the RPCA method. A marked portion of the ECG signal

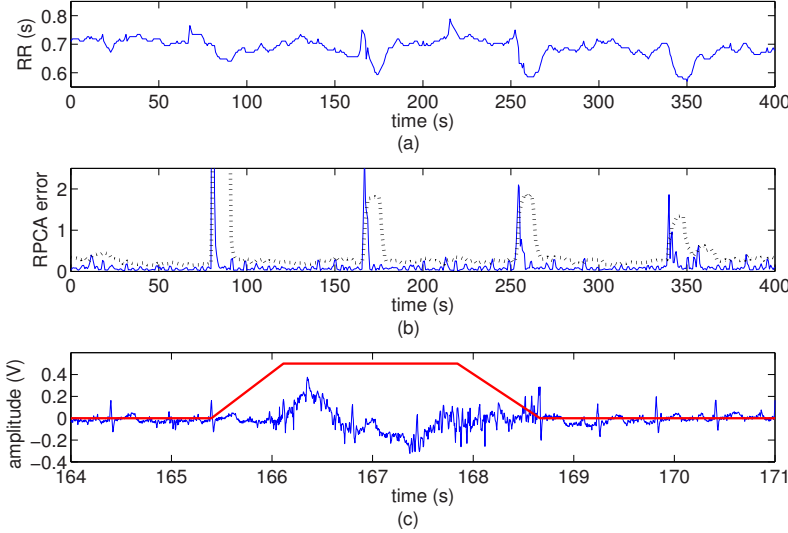


Fig. 6.2. Illustration of transition detection of four different BMAs from an ambulatory ECG recording using the RPCA based method. (a) Estimated RR interval in seconds, (b) RPCA error signal and threshold detection of BMA transitions from the RPCA error signal (dotted line corresponds to threshold θ), and (c) corresponding ECG signal for one of the detected BMA transitions. (©2007 IEEE)

corresponding to one of the walking transitions is depicted in the Fig. 6.3(c). In all our experiments we have chosen the number of eigenvectors $L = 8$ and value of forgetting factor $\alpha = 0.8$. This allows rapid learning of the subspace of the new BMA artifacts (4-8 heart beats).

Next, we have applied this technique to detect BMA transitions when certain commonplace BMAs like, sitting and standing, hand movements, walking, climbing stairs, twisting at waist, etc. are performed in a sequence to verify the BMA transition detection by the RPCA method. There were 10-12 transitions in each ECG signal of 7-8min duration. A total of five ECG signals were collected for this purpose. An example of detection of turning while walking is shown in Fig. 6.4. Except for the case of continuous right arm movement, the method worked satisfactorily for all other BMA transitions. The difficulty with the right arm motion is due to the close proximity of the electrode to the moving limb, where the EMG signal dominates over the ECG signal making the approximation of the BMA subspace of the ECG inaccurate.

We have also applied this method for detection of posture changes. Three common positions during sleep are considered: left lateral, supine and right lateral and the ECG is recorded while the subject is sleeping in bed and alternating among these three positions. Any change in the position induces motion artifact in the ECG and therefore, changes in the sleeping positions are

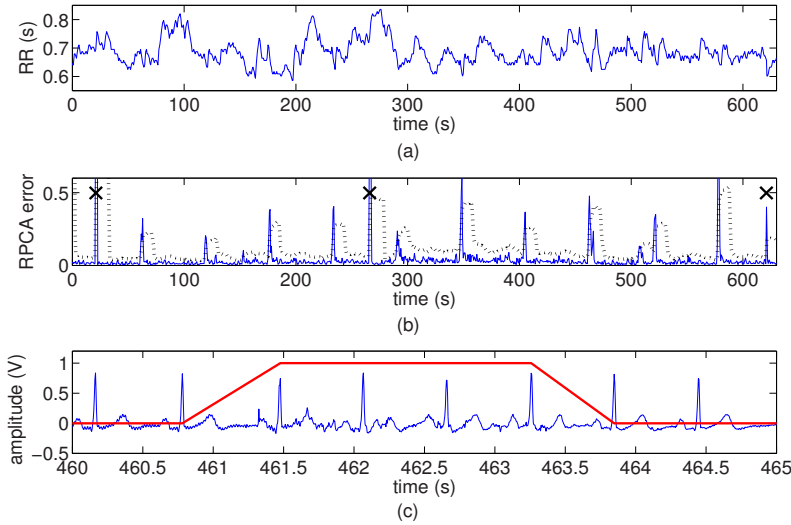


Fig. 6.3. Illustration of transition detection from ambulatory ECG recording during changes in walking stride using the RPCA based method. (a) Estimated RR interval in seconds, (b) RPCA error signal and threshold detection of BMA transitions from the RPCA error signal (dotted line corresponds to threshold θ and ‘ \times ’ sign indicates three detected atrial extra-systoles), and (c) corresponding ECG signal for one of the detected BMA transitions. (©2007 IEEE)

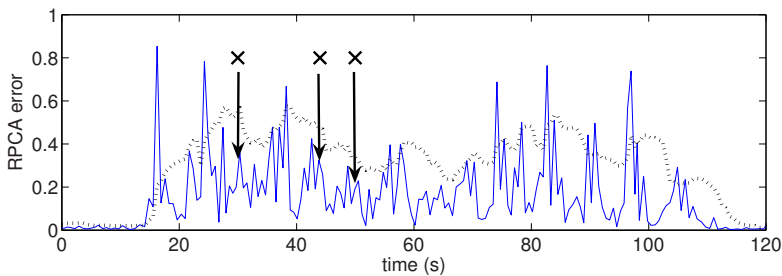


Fig. 6.4. Illustration of detection of turning while walking by plotting RPCA error signal. ‘ \times ’ signs indicate the locations of three missed detections. (©2007 IEEE)

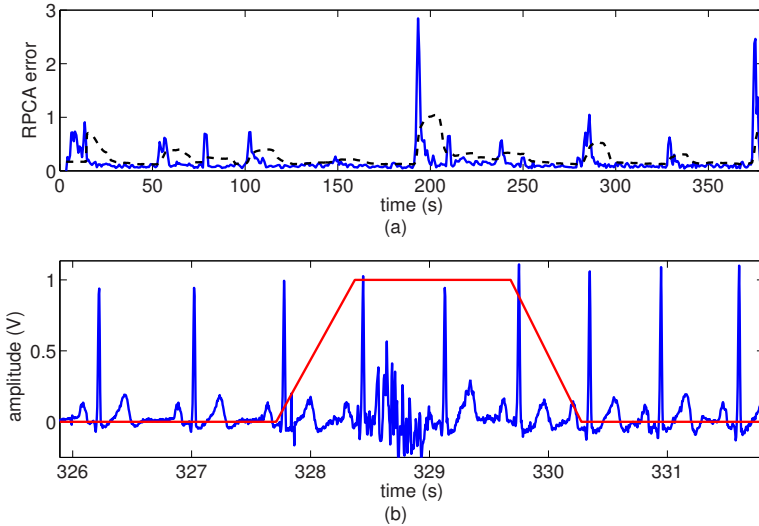


Fig. 6.5. Illustration of transition detection from ambulatory ECG recording during sleep positions: left lateral, supine and right lateral changes. (a) RPCA error signal and threshold detection of BMA transitions from the RPCA error signal, and (b) corresponding ECG signal for one of the detected position change. The rise in the R peak amplitude after this transition is attributed to the shift in heart axis.

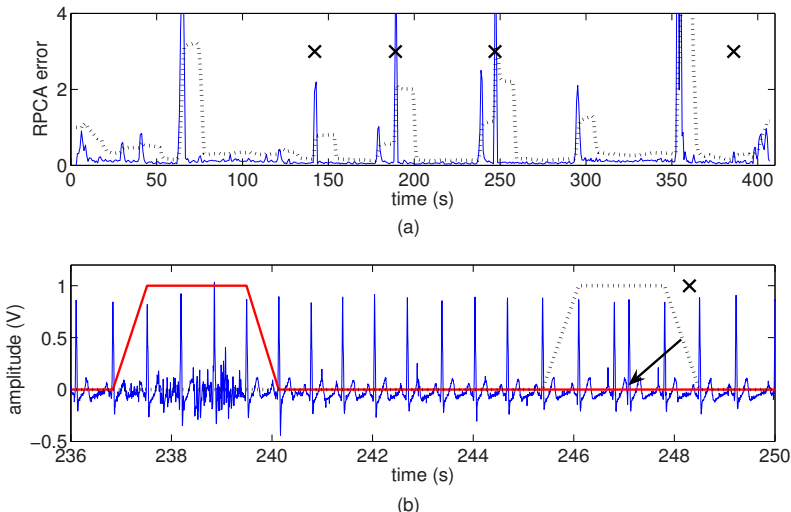


Fig. 6.6. Illustration of transition detection from ambulatory ECG recording during sitting, standing and supine posture changes. (a) RPCA error signal and threshold detection of BMA transitions from the RPCA error signal ('x' sign indicates four detected atrial extra systoles), and (b) corresponding ECG signal for one of the detected BMA transitions and one of the detected AES (indicated by 'x'). (©2007 IEEE)

detected using the RPCA method. One of the examples of this type of position changes during the sleep is presented in Fig. 6.5. An angular shift in the heart axis due to a change of position causes the change in amplitudes of certain cardiac features. An increase in R peak amplitude can be observed clearly in the depicted ECG segment in Fig. 6.5 after a position transition. Another type of postural change occurs when the subject is active (not during sleep). We have recorded the transition between sitting and standing which does not cause a significant shift in heart axis. Next we present the detection of postural changes among standing, sitting and sleeping in supine position in Fig. 6.6. The changes in various body postures like sitting, standing, resting supine, resting left lateral and resting right lateral have also been successfully detected using the RPCA method (Figs. 6.5 and 6.6). The method is also able to detect transitions due to yawning very accurately, as yawning leads to a large movement of the diaphragm. The details of the number of BMA transitions in the available ECG data and true detections by the RPCA method are given in Table 6.1.

Table 6.1. Summary of performance for transition detection.

BMA	True	Missed	False
Still→Twisting	21	0	6
Twisting→Still	10	0	3
Still→Walking	50	0	0
Walking→Still	5	0	0
Still→Climb up	23	0	0
Climb up→Still	9	0	0
Still→Climb down	18	0	0
Climb down→Still	8	0	0
Still→Arm movement	72	1	22
Arm movement→Still	18	0	9
Arm movement→Walking	6	0	2
Walking→Arm movement	11	2	1
Turning while walking	54	8	1
Sit→Stand	20	2	0
Stand→Sit	20	2	1
Supine→Left-lateral	6	0	0
Left-lateral→Supine	6	1	0
Supine→Right-lateral	6	0	0
Right-lateral→Supine	6	0	0
Yawning	5	0	0
Total	374	16	45

The accuracy of the RPCA technique is found to be $100 \times \frac{374}{374+16} = 95.9\%$ with false detection rate of $100 \times \frac{45}{374+45} = 10.7\%$. If we increase the threshold θ in Eq. (6.11), the false detection rate is lowered at the expense of increased missed detections.

In the collected data there are quite a few instances of atrial extra systole (AES). Since the AES represents an abrupt change in the ECG beat pattern, it is also detected by the RPCA method. To identify the AES from the BMA transitions we have applied an autocorrelation based detection technique on the detected ECG beats. We have detected 70 AES episodes in the entire recorded data, using the RPCA technique. All these detections (for example, see Fig. 6.6) match the ground truth. Similarly, ventricular extra systoles (VES), or in general, any ectopic beat patterns also exhibit abrupt changes in the ECG signal and are also detected by the RPCA method. To separate ectopic beats correctly from BMA transitions, suitable detection methods available in the literature [65, 97] can be applied. However, these cases are rare in our data sets. We have detected only two such instances of VES in the processed data. But there are some other factors that affect the performance of the algorithm such as, EMG noise due to muscular activities, 50Hz power noise and changes in diaphragm when the subject is highly vocal.

As we have explained above, the RPCA method may not work well for BMA transition detection for the infrequent and abrupt disturbances in the cardiac rhythm. However, the method works well for the cardiac patients having a very different morphology but still having a regular rhythm in ECG signal and who are also leading an active life. Here we present a case of one such cardiac patient who has a prosthetic aortic valve and a left bundle branch block (LBBB). This particular subject has a larger S peak amplitude and smaller R peak and thus a very different QRS morphology as compared to the QRS complex for healthy subjects. We show an example of detection of BMA transitions from the ECG signal using the RPCA method for this subject in Fig. 6.7. Four different transitions can be seen as the spikes in the derived RPCA signal crossing the dotted threshold line in Fig. 6.7(a). The recorded ECG signal during the second BMA transition in this case is presented in Fig. 6.7(b). It can be seen that the QRS morphology of the ECG for this subject is quite different from the normal QRS morphology in lead II. The R peak is very small and the S wave is dominant. The part of the depicted ECG signal marked with a time window, $t = 115 - 117$ seconds in Fig. 6.7(b) is corresponding to a BMA transition, which appears to be quite noisy. However, this noise does not affect the accuracy of detection.

Next, we discuss another example of transition detection for the same subject in Fig. 6.8. In this experiment we try to detect sleep position changes. In Fig. 6.8, the position changes: left lateral, supine and right lateral during sleep are detected for the same patient. There are four positional transitions during the sleep which are the peaks crossing the dotted threshold in Fig. 6.8(a). The ECG signal during the fourth positional change is depicted in Fig. 6.8(b). Here the position change is marked by the time window, $t = 222 - 224$ seconds. The ECG signal is not much noisy, and the transition is detected accurately. Note the variation in the amplitude of the S waves before and after the position change in Fig. 6.8(b), which is attributed to shift in heart axis.

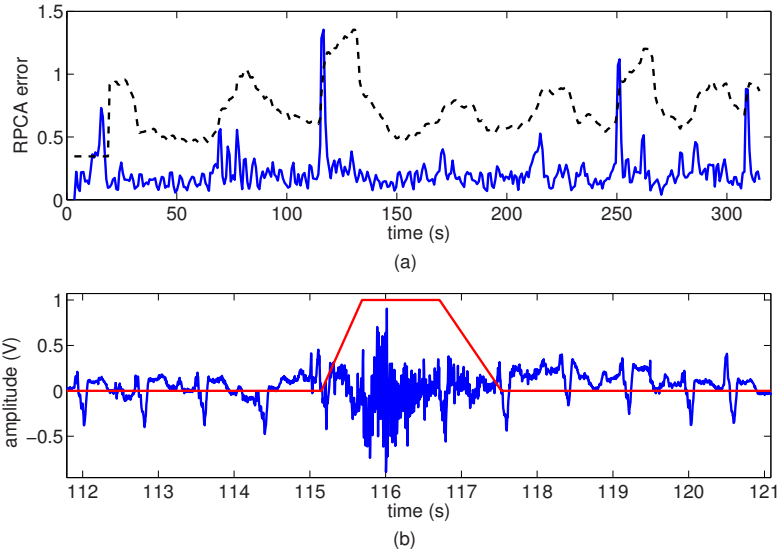


Fig. 6.7. Illustration of transition detection of different BMAs from an ambulatory ECG recording of a cardiac patient having a very different QRS complex morphology using the RPCA based method. (a) RPCA error signal and threshold detection of BMA transitions from the RPCA error signal (dotted line corresponds to threshold), and (b) corresponding ECG signal for one of the detected BMA transitions.

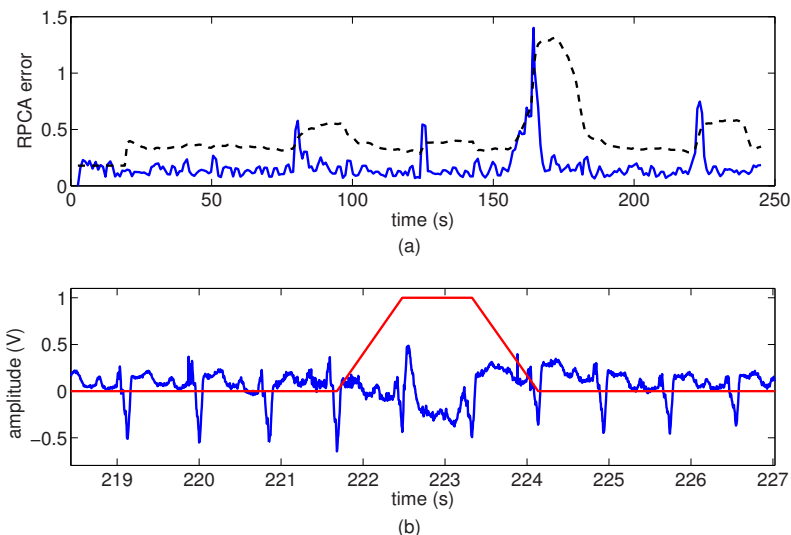


Fig. 6.8. Illustration of transition detection from ambulatory ECG recording for a cardiac patient during sleep positions: left lateral, supine and right lateral changes. (a) RPCA error signal and threshold detection of BMA transitions from the RPCA error signal, and (b) corresponding ECG signal for one of the detected position changes.

6.4 Discussion

In this chapter we have discussed a PCA based technique to detect transitions in various BMAs such as movement of arms, walking, twisting motion at waist and changes in different body postures using the motion artifacts present in ECG signals. The recursive updating of PCA technique was found to be able to adapt to gradual changes in the ECG signal due to sustained activities (resulting in slow variations in respiration and heart rate). In addition, the given method was able to handle an increased heart rate nearly double of the heart rate at rest. However, some spurious ECG beats like AES or ectopicity may cause false detections, which can be rectified using suitable post processing techniques. It is also verified from the ECG data of a cardiac patient that the method is capable of handling the different morphology for the QRS complex.

In the next chapter we will see how the PCA based method can be used for further analysis of ECG signals for recognition of BMA using the induced motion artifact signals. The transition detection discussed in this chapter will be helpful for temporal segmentation of the ECG signal in order to use a particular ECG segment for BMA recognition. The RPCA signal derived in this chapter is an indication of motion artifact and hence it can measure the impact of the BMA on ECG signal. Therefore, we will use this RPCA error signal as an impact signal for quantification of different pace levels of BMA and will validate it by the measured acceleration signal in Chapter 8.

Activity Recognition

Wearable ECG recorders (W-ECG) provide a practical solution for ambulatory cardiac monitoring. W-ECGs are increasingly being used by people suffering from cardiac abnormalities, who also choose to lead an active lifestyle. From the discussions in the previous chapters regarding W-ECG, we can now understand that the challenge presently is that the ambulatory ECG signal is influenced by motion artifacts induced by body movement activity (BMA) of the wearer. The usual practice is to develop effective filtering algorithms which can eliminate the motion artifacts. However, due to spectral overlap between the motion artifact signal and the cardiac signal the complete elimination of the motion artifact from the ambulatory ECG signal is not possible without unduly affecting the cardiac signal component. Therefore, instead of filtering we would like to identify the presence of the motion artifact and the type of body movement from the analysis of the ambulatory ECG signal itself. We have already addressed the issue of detecting BMA transitions from the ECG signal in the previous chapter. The method proposed for the transition detection is an unsupervised learning approach which only looks for any abrupt changes in the nature of the motion artifact signal due to changes in BMA. However, a particular BMA is not yet characterized from the analysis of ECG in the previous chapter. In this chapter we focus on the BMA recognition from the ambulatory ECG signal for which we will use BMA classifiers with certain specific types of BMA classes. The classification approach for BMA recognition requires supervised training of the specified BMA classes using the corresponding ECG data during the specified BMA. For this purpose we have recorded the ECG signals during specified BMA, e.g. sitting still, walking, movements of arms and climbing stairs, etc. with a single-lead W-ECG as described in Section 5.2. The collected ECG signal during the BMA is presumed to be an additive mix of signals due to cardiac activities, motion artifacts and sensor noise as per the mathematical model given in Section 1.5. We have successfully used the mathematical model of the ambulatory ECG in the previous chapter for the transition detection from the ambulatory ECG signal. Here we follow the same model of the ambulatory ECG signal for the

analysis which leads to the recognition of different types of BMA from the ECG itself. According to the mathematical model, the motion artifact signal is one of the components of the ambulatory ECG signal which depends on the type of BMA and hence the BMA recognition should be possible from the analysis of the ECG signal. The motion artifact signal can be derived from the ambulatory ECG by suppressing the cardiac signal and the sensor noise. We hypothesize that a similar type of BMA induces a similar type of motion artifact whereas different types of BMA induce different types of artifact. If this is true then we can train a classifier to detect the type of BMA class using the motion artifact signal. As per the mathematical model in Section 1.5, we first derive the motion artifact signal by estimating the cardiac signal. The derived motion artifact signal can be used for the BMA recognition. We use classifiers trained for different BMA classes in which there are two types of representations: one is a nonparametric representation and the other is a parametric representation. In the nonparametric BMA classifiers each of the BMA classes is represented by a set of vectors derived from the ambulatory ECG data for the specific BMA class during training. Whereas in the parametric BMA classifiers, the individual BMA class is modeled by certain parameters derived from the ambulatory ECG data available for only that particular BMA class. Both kinds of representations obtained by the supervised learning are then used for classification of the ambulatory ECG signals to recognize the BMA class during testing. Here we use the derived motion artifact signal for supervised training of the BMA classifiers and the classification of BMA types, which requires some preprocessing on the ambulatory ECG signals recorded by W-ECG. The details of preprocessing and analysis are presented in this chapter.

7.1 Introduction

The ECG signal collected by the W-ECG is contaminated by BMA induced artifacts owing to disturbances at the skin electrode interface and noise due to muscular activities, collectively known as motion artifacts. For the W-ECG to handle motion artifacts occurring naturally during its intended use is a challenge. The motion artifacts have a significant overlap in frequency with ECG signal, so filtering based on spectral separation is of limited use [5].

In the earlier chapters we have provided a brief introduction to the problem of motion artifact in W-ECG. Any body movement activity (BMA) of the wearer causes motion artifacts and we have shown from the BMA transition detection in the previous chapter that different types of BMA induce different kinds of motion artifact. Using the BMA transition detection method, it is possible to segment the ECG signal temporally in order to separate each of the signal segments containing just one type of BMA. Since BMA influences the ECG output, we propose to determine the BMA from the motion artifacts in the ECG signal. The possibility of recognition of the BMA from ECG data

is yet to be fully studied in the literature. We also show that BMA recognition can help in improving the automated analysis of the ambulatory ECG signal in W-ECG. This will be helpful eventually in pervasive monitoring of cardiac activity of a patient and determining if any BMA is having a deleterious effect. The possibility of such a classification has initially been explored in [93]. Here the ECG signals are analyzed using a wavelet transform and a neural network. However, the reported performance is not very satisfactory as the wavelet based representation does not separate the in-band BMA signal from the ECG. In other works related to BMA analysis from non-ambulatory ECG, body position changes are detected for ischemia monitoring in [9, 37, 52]. In [37, 52], Karhunen-Loeve transform of the ECG beats are analyzed to detect position changes. A synthesized vectorcardiograph based approach has been proposed in [9, 37], where a series of angles for the three orthogonal leads X, Y and Z are derived using a loop alignment method [9, 122]. The sequence of angles is then analyzed to detect the changes in body position. However, this method requires a comprehensive 12-lead ECG signal to be able to synthesize the three vectorcardiograph leads and is currently restricted to a clinical environment. The single-lead system that we have used is less informative but enables long term cardiac monitoring and is also preferable from the standpoint of wearer's comfort and cost.

In this chapter we characterize the motion artifacts induced by the following specific BMAs: sitting still, up and down movement of left, right and both arms, walking on a level floor, and climbing stairs up and down, using two different supervised learning approaches. In the first approach we use a non-parametric classification technique based on principal component analysis (PCA). The second approach is a parametric classification technique based on hidden Markov models (HMM). In both the approaches we test for classifiability of the motion artifacts based on the characterization obtained using the supervised learning. For this purpose we build various BMA classifiers for different BMA classes where each class is either a distinct BMA or a combination of two or more different BMAs as specified above. If two specified BMAs are not quite separable using the proposed characterization of motion artifacts, they are both combined into a single BMA class. Here we demonstrate that it is indeed possible to recognize several BMA classes accurately from the ECG signal itself. Since the proposed non-parametric classification technique is based on the PCA of motion artifacts in the ECG signal, it follows that class specific PCA-based filtering can also be used for removal of motion artifacts. Accordingly, we have demonstrated the usefulness of the PCA-based filtering technique by locating the P and T waves in the ECG signal in the presence of body movement.

Here we have restricted our studies to only people with no known cardiac abnormalities but under multiple settings (laboratory and outdoors). Since the motion artifact is caused at the superficial level at the skin, it is understood that the possibility of the BMA recognition shown here for the healthy subjects should also be applicable for cardiac patients except the fact that the

proposed PCA-based method may not be suited for cardiac patients with frequent rhythmic disturbances. However, for patients with infrequent rhythmic disturbances, it is possible to detect such abrupt episodes using the RPCA method proposed in the previous chapter following a post-processing step of arrhythmia classification using some standard method.

The organization of the chapter is as follows. We discuss a nonparametric, supervised learning-based classifier using PCA in Section 7.2. There we discuss the mathematical model for the ambulatory ECG signal recorded by the W-ECG, required preprocessing steps for implementation of the proposed method on ECG signal, basics of PCA, supervised learning and classification of BMA. We also explain how the BMA classification can be used for removal of the motion artifacts. We explain a parametric, supervised learning-based classifier using hidden Markov models (HMM) in Section 7.3. The results of the BMA classification obtained by the two algorithms are presented in Section 7.4. We discuss about the conclusions of our experiments on BMA recognition from ambulatory ECG signal in Section 7.5.

7.2 Nonparametric Classification

According to the mathematical model of the ambulatory ECG signal given in the earlier chapters, the recorded ECG signal has three components: cardiac signal due to normal heart activity, motion artifacts due to body movement and sensor noise introduced by the W-ECG. Following the BMA transition detection results presented in the previous chapter and some preliminary results regarding BMA recognition using the wavelet based method in [93], we hypothesize that each type of body movement induces a particular type of motion artifacts in the ECG signal. An ECG signal for the i^{th} class of BMA is modeled as

$$r_i(n) = q_i(n) + s_i(n) + \eta(n), \quad (7.1)$$

where r_i is a recorded ECG signal, q_i is a cardiac signal of a normal heart during BMA specified by i^{th} class, s_i is an additive motion artifact due to i^{th} class of BMA and η is the sensor noise present in the ECG signal. It is noted that the cardiac cycle q_i is denoted for the specific BMA to emphasize that the cardiac cycle can be more accurately represented and estimated when considered separately for an individual BMA class.

Here we discuss a nonparametric approach of classification for recognition of BMA from the ambulatory ECG signal based on principle component analysis (PCA) technique. We segment the ambulatory ECG signal contiguously as a sequence of ECG beats. Each of the ECG beats in the sequence will be represented as a vector of a fixed dimension for the PCA-based analysis for BMA recognition.

Let the vector representations of the corresponding signals captured during a single period of heart beat be \underline{r}_i , \underline{q}_i , \underline{s}_i and $\underline{\eta}$, respectively. All vectors used for

the classification are column vectors. As mentioned earlier, the dimension M_0 of these vectors depend on the beat period and the sampling frequency. If one considers N consecutive heart beats together as a signal then the dimension of the signal would be NM_0 . Following are the various assumptions made while developing the nonparametric PCA-based classifiers.

1. The cardiac signal q_i is assumed to be representing normal cardiac activity only and it remains stable in the presence of a specific BMA.
2. Since cardiac activity is by nature involuntary, it is independent of voluntary muscular activities and motion of electrodes. Hence BMA induced motion artifacts s_i are independent of the cardiac signal q_i , i.e., $q_i \perp s_i$.
3. The sensor noise η present in the ECG signal is due to ambient conditions of recording like power line interference, device temperature, skin humidity, etc. and, therefore, it is assumed to be independent of both cardiac signal and the motion artifact, i.e., $\eta \perp q_i$ and $\eta \perp s_i$.
4. In the preprocessing steps described next (Section 7.2.1), the dc bias estimated from the isoelectric level of the ECG signal is set to zero. Therefore, the sensor noise is assumed to be of zero mean, i.e., $E[\underline{\eta}] = 0$.
5. $\text{Rank}(E[\underline{r}_i \underline{r}_i^T]) \approx M_i$, where $M_i \leq M_0$, signifying that the actual information in the recorded ECG signal can be compactly represented by only top M_i eigenvectors.
6. The energy of the motion artifact signal s_i is concentrated into a top few (say K_i where $K_i \ll M_i$) eigenvectors of $E[\underline{s}_i \underline{s}_i^T]$, and that the composite signal \underline{r}_i is sufficiently excitatory.
7. There is greater correlation between signals due to same type of body movement than that for any two different types of body movement. That is, s_i and s_k are highly correlated if $i = k$ (at different time instants) and nearly uncorrelated if $i \neq k$.
8. The signal component due to motion artifacts is smaller compared to the strength of the cardiac signal, but much greater than the sensor noise, i.e., $|\underline{\eta}| \ll |\underline{s}_i| < |\underline{q}_i|, \forall i$.

Based on the mathematical model and the assumptions discussed above, we will extract the signature of a specific BMA (s_i) by eliminating the cardiac signal (q_i) and the sensor noise (η).

The cardiac signal is characterized by a stable rhythm of heart beats. Following assumption (1), the cardiac rhythm stays nearly constant over the heart beats within the observation window. An arithmetic mean of several epochs of heart beats provides an estimate of the constant cardiac rhythm and hence the cardiac signal [5, 49]. For a specific BMA class, this estimate is averaged over the entire training data set for a particular class and is termed as class mean of the BMA. If the class mean is a correct estimate of the cardiac signal then according to Eq. (7.1), the motion artifacts component (also sensor noise) is derived by removing the class mean from the ECG signal.

The sensor noise component is suppressed by elimination of the dc bias during the preprocessing step described next. Accordingly, the motion artifacts component will dominate as per assumption (8).

In the nonparametric classification, an unknown ECG beat is classified into a specific BMA class according to the best reconstruction criterion. A particular BMA class is represented by a set of top few eigenvectors of the training BMA data belonging to that BMA class. The eigenvectors are obtained from eigen decomposition of the correlation matrix of the training BMA data. The test ECG beat is reconstructed using the set of eigenvectors in conjunction with the class mean for each BMA class. The BMA class for which the error between the reconstructed signal and the test ECG beat is minimum is determined as the true BMA class for the unknown ambulatory ECG data.

The eigen decomposition technique described above is optimal for the assumed data representation model because the eigenvectors are orthogonal. Thus, after preprocessing, if the artifact signal (s_i) is corrupted by an uncorrelated noise signal (η) then the top few eigenvectors represent mostly the signal component due to BMA as the signal to noise ratio (SNR) is considered to be high in these components and the remaining eigenvectors mostly represent the noise subspace, thus isolating the BMA signal from noise.

Thus the method applied here is a nonparametric supervised technique for body movement classification. However, in order to be able to use the technique and for suppressing the sensor noise η , certain preprocessing steps are required to handle both intra-personal and inter-personal variations in the cardiac signal (q_i).

7.2.1 Preprocessing

It is assumed that the heart is not stressed during the activities that are being performed in this study. However, certain parameters like the coupling between skin and electrodes, and the variability in the heart rate have multi-parameter dependence. The coupling between skin and electrodes depends mostly on the skin humidity levels and also if the setting is indoors or outdoors. Similarly, a small variation of heart rate during ambulatory activity is present even in healthy subjects. Finally, there are person specific variations in the above two parameters. While the coupling between skin and electrodes affects the amplitude (scale) of the ECG beat data, the heart rate affects the time interval of the ECG beat data.

The arithmetic mean as an estimate of the cardiac signal (q_i) and eigen decomposition for extraction of the motion artifact component (s_i) are both sensitive to translation, variations in amplitude and time scales of the data [52]. Thus it is necessary to perform the following preprocessing steps that involve proper alignment, amplitude scaling and time warping of the data as shown in Fig. 7.1.

The data is processed as a batch of ECG beat epochs collected over about one minute duration after appropriate beat alignment. This implicitly assumes

that the collected beat epochs in this short time duration, may have nearly constant amplitudes and time periods.

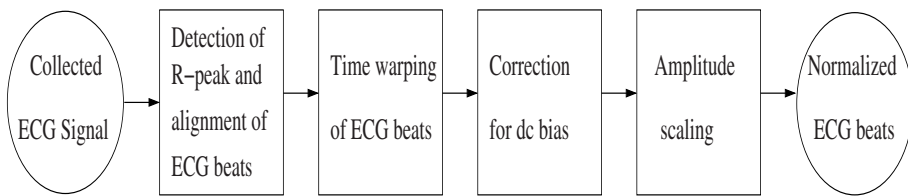


Fig. 7.1. Preprocessing applied to the ECG signal captured by the W-ECG. (©2007 IEEE)

Detection of R peak and alignment of ECG beats

The R peak is the most prominent feature of the ECG signal that can be detected easily even in the presence of motion artifacts, and is used for calculating the heart rate. The R peaks in the ECG signals are detected using the Pan-Tompkins method [96]. The method for detection of R peaks in ECG has been explained in the previous chapter. The duration between the current R peak and the preceding one is considered as the current ECG beat interval, i.e., j^{th} beat interval is given by duration between $(j - 1)^{th}$ and j^{th} R peaks. The average interval of the ECG beats is estimated from the number of R peaks detected over a period of one minute. If there are a total of N ECG beats over the given period then the ECG signal is partitioned into N ECG beat epochs. The R peak in each epoch is aligned to the exact middle position. This strategy ensures the alignment of ECG beats even after time warping is applied to the data.

Time warping of ECG beats

As explained above, the ECG beat intervals may vary due to change in the heart rate. Accordingly, the number of samples recorded for each ECG beat epoch may vary. Since the given PCA-based method is applicable only to vector observations in a space of fixed dimension, it is required to equalize the dimensions (M_0) of all the ECG beats. A simple technique to achieve this is linear time warping and is implemented as follows. The ECG beat is resampled by a rational factor a/b , where a is the fixed number of samples after the time warping, and b is the number of samples in the ECG beat being resampled. This is performed through MATLAB® using a polyphase implementation of resampling and a linear phase anti-aliasing filter with finite impulse response. Following the application of time warping, all the ECG beat observations are of equal length.

Correction for dc bias

The constant voltage level of the flat portion of ECG beat segment that lies between the end of P wave and the beginning of Q wave is termed as the isoelectric level of the ECG beat [49]. Ideally, the isoelectric level should be at ground potential. The dc bias is estimated by calculating the arithmetic mean of isoelectric levels of all ECG beat observations collected during a one minute interval. This dc bias is then subtracted from the ECG signal. Thus any dc bias introduced due to sensor noise or otherwise is removed during this step. The shape of the recorded ECG signal remains unchanged at this point of time and the sensor noise in ECG signal has now zero mean as per assumption (4).

Amplitude scaling

This is the last stage of preprocessing. As discussed earlier, the coupling between skin and electrodes can affect the amplitude of the signal. Since the proposed method calculates the arithmetic mean of the ECG beats for estimating the cardiac signal component, all the ECG beats should represent the cardiac activity with the same amplitude. The R wave peak with respect to the isoelectric level is considered here to represent the full signal strength. A normalization factor is estimated by averaging of R wave amplitudes with respect to the corresponding isoelectric levels from all ECG beats over a period of one minute. Thus the amplitude of the ECG data over the period is normalized and the estimate of average R wave amplitude with respect to the corresponding isoelectric level becomes unity.

7.2.2 Principal Component Analysis (PCA)

We propose to use a nonparametric classification technique for recognition of BMA from the ECG signal. Since we focus in this work on W-ECG devices which may provide only a single lead ECG signal at a time, we choose a technique for a suitable nonparametric representation of the signals. The technique we consider here is known as PCA. Here the data set is organized in such a way that each point in the data lies in a fixed dimensional space and each element of the data is along a specific orientation (axis) in the space. That is to say that each data can be represented as a vector in the fixed dimensional space. In this representation let M be the fixed dimension of the space and the data be represented in a column vector form of dimension $M \times 1$. Thus the complete vector space can be defined by a basis which is a set of independent vectors in \mathbb{R}^M . Since the dimension of the vector space is M , there must be at most M such independent vectors in the basis. Each of the elements in the column vector is the projection corresponding to a basis vector in an ordered manner.

The PCA is a technique used for finding the most suitable bases to represent the given data. This is because there may be some redundancy in the data and therefore, the dimension can be reduced. In this case the bases would be such that even a few of the vectors from the bases can represent the data satisfactorily without much loss in terms of the errors in reconstruction. Using PCA the vectors forming such bases can be found in an ordered manner. Here the vectors found by the PCA are called eigenvectors which are orthogonal to one another and also normalized to yield the signal power of each vector to be unity. Therefore, one can say the derived bases form an orthonormal set of bases. There is no redundancy in this representation due to the orthogonality of the basis. Moreover, the eigenvectors are found in such a manner that the first eigenvector captures the maximum signal power in the data along any direction. The next eigenvector will be in an orthogonal direction to the previously found eigenvector(s) that captures the next highest amount of signal power from data along all other possible (orthogonal) directions. According to the signal power captured by each of the eigenvectors, it is assigned an eigenvalue which represents the weight of the particular eigenvector for the given data. Thus the eigenvectors are arranged in a non-ascending order of eigenvalues. In most practical applications the first few eigenvectors are able to capture most of the signal power in the data and the remaining eigenvectors only represent a small residual which is either considered as noise or can be neglected without much loss in data reconstruction. Thus a graceful trade-off between the number of eigenvectors and the loss in data reconstruction is achieved using the PCA.

Let a set of data contain a total of N observation points from a fixed dimensional space, $\underline{r}_i(n)$, $i = 1, 2, \dots, N$ observations where $\forall \underline{r}_i(n) \in \Re^M$. Here M is the fixed dimension of the space under consideration. We want to apply PCA to the given data set.

First, the data set is centered to zero by subtracting the arithmetic mean of the data. The arithmetic mean of the original data is computed as

$$\bar{\underline{r}} = \frac{1}{N} \sum_{i=1}^N \underline{r}_i. \quad (7.2)$$

The corresponding vector after mean subtraction is denoted by \underline{r}' where

$$\underline{r}'_i = \underline{r}_i - \bar{\underline{r}}, \quad i = 1, 2, \dots, N. \quad (7.3)$$

The covariance matrix is computed from the mean subtracted data as

$$C = \frac{1}{N} \sum_{i=1}^N (\underline{r}'_i)(\underline{r}'_i)^T, \quad (7.4)$$

where C is the covariance matrix for the given data and $(\cdot)^T$ is matrix transpose. Here C is an $M \times M$ matrix and its eigen decomposition gives a total of

M eigenvectors $[e_1, e_2, \dots, e_M]$, arranged in a non-ascending order of the corresponding eigenvalues, denoted by $\lambda_1 \geq \lambda_2 \geq \dots \geq \lambda_M$. For details of eigen decomposition the interested reader may refer to [38]. Let $E = [e_1, e_2, \dots, e_K]$, $K \ll M$ be a set of first K eigenvectors with the largest eigenvalues that represents a smaller K dimensional subspace in the M dimensional space of the given data. In many practical applications a suitable choice of K will yield an almost perfect reconstruction with a very small residual error. Hence the PCA technique is used for reducing the dimensionality of the given problem. Moreover, in most cases the residual errors are from the noise subspace which one would like to suppress from the data. Therefore, the PCA is also used for noise removal.

The dimensionality reduction helps to shrink certain useful subspaces in the data which characterize the conditions under which the observations are recorded. We may expect that the corresponding subspaces derived from different data sets recorded under different conditions will be quite separate. This separation of subspaces for different conditions may help to solve the classification problem. One can first derive the corresponding subspace from the training data given for each specific pre-defined condition and then try to find the distance of a test data from the derived subspace. The point may be allocated the condition (or class) represented by the nearest subspace. However, the PCA itself does not guarantee the separability of the subspaces and hence it is not necessarily always the preferred technique for solving the problem of classification. For details of various techniques of classification, the interested reader may refer to [24]. For certain types of data the PCA can indeed be applied successfully for classification purposes. We discuss a technique based on PCA for BMA recognition from the ECG signal in this chapter.

7.2.3 Supervised Learning of Body Movement

Following the mathematical model of the ambulatory ECG signal adopted for the analysis, the ECG signal comprises of the cardiac signal (q_i), motion artifacts (s_i) and sensor noise (η). The ECG beats segmented after the preprocessing will be considered for training and subsequent classification of BMA. As explained above, the vector representation of the j^{th} ECG beat observation in the training data of i^{th} BMA class is \underline{r}_{ij} and the vector representations of the corresponding cardiac signal, motion artifact and sensor noise components are \underline{q}_{ij} , \underline{s}_{ij} and $\underline{\eta}_{ij}$, respectively.

We plan to use a supervised approach of training a BMA classifier using the processed ECG beat, \underline{r}_{ij} , $i = 1, 2, \dots, c$ and $j = 1, 2, \dots, N_i$, where c is the number of BMA classes in a classifier and N_i is the number of ECG beats used for training of i^{th} BMA class. In this nonparametric classification approach each BMA class is represented by a class mean and a set of eigenvectors computed using the PCA of all training observations. The class mean is computed from the arithmetic mean of the training data \underline{r}_{ij} , $j = 1, 2, \dots, N_i$

of the i^{th} BMA class. The eigenvectors for the BMA class are obtained from the corresponding data after subtracting the class mean.

The class mean of i^{th} BMA class is calculated as follows

$$\tilde{\underline{q}}_i = \frac{1}{N_i} \sum_{j=1}^{N_i} (\underline{r}_{ij}), \quad (7.5)$$

which approximates the average cardiac signal for the given BMA class [49]. The average cardiac component $\tilde{\underline{q}}_i$ is subtracted from the signal \underline{r}_{ij} to derive mean subtracted BMA vectors (residual signal) for the i^{th} BMA class

$$\underline{r}'_{ij} = \underline{r}_{ij} - \tilde{\underline{q}}_i \simeq \underline{s}_{ij} + \underline{\eta}'_{ij}, \quad (7.6)$$

where $\underline{\eta}'_{ij}$ is comprised of the sensor noise plus the noise arising in the estimation of the cardiac component due to inter-personal variation (refer to multi-subject testing, classifiers VI-X in Section 7.4.1). The BMA vectors with regards to signal power, contain predominantly the motion artifact \underline{s}_{ij} , along with the noise $\underline{\eta}'_{ij}$.

Next, PCA is applied on the BMA vectors \underline{r}'_{ij} to compute the significant eigenvectors of the training data for each BMA class. An eigenvalue corresponding to an eigenvector is a measure of signal strength in the data in the direction of the eigenvector. As per assumption (8), the motion artifact component dominates the residual signal. Thus, if the eigenvectors of this data are arranged in a non-ascending order of the respective eigenvalues, the first few eigenvectors will represent the motion artifacts by neglecting the noise components. For the i^{th} BMA class, the eigenvectors and eigenvalues are computed by eigen decomposition of the covariance matrix of the training residual signal \underline{r}'_{ij} , given by

$$C_i = \frac{1}{N_i} \sum_{j=1}^{N_i} (\underline{r}'_{ij})(\underline{r}'_{ij})^T, \quad (7.7)$$

where C_i is the covariance matrix for the i^{th} BMA class. If the data occupies an M dimensional space then C_i is a $M \times M$ matrix and its eigen decomposition gives a total of M eigenvectors $[e_{i1}, e_{i2}, \dots, e_{iM}]$, arranged in the non-ascending order of the corresponding eigenvalues, denoted by $\lambda_{i1} \geq \lambda_{i2} \geq \dots \geq \lambda_{iM}$ for the i^{th} BMA class. Let $E_i = [e_{i1}, e_{i2}, \dots, e_{iK_i}]$, $K_i \ll M$ be a set of first K_i eigenvectors with the largest eigenvalues that represent the motion artifacts. Here E_i forms a basis for a small K_i dimensional motion artifact subspace in the M dimensional space of the data for the i^{th} class. As per assumption (7) the motion artifacts due to any two different types of BMA are nearly uncorrelated, eigen functions for any two different motion artifacts are also expected to be nearly uncorrelated.

For each BMA class, a class mean and a set of eigenvectors are computed from the training observations, which represent the characteristics of motion artifacts for the particular BMA and is used as the basis of the BMA classifier. Thus we have obtained a non-parametric representation of each BMA class.

7.2.4 Activity Classification

Based on the nonparametric representation obtained in the previous section for each of the specified BMA classes in a classifier, we discuss a BMA classification procedure in this section. Let \underline{p}_u be a test ECG beat extracted after the preprocessing steps given in Section 7.2.1, where u is the label of the BMA class of \underline{p}_u which is unknown to the BMA classifier but can be any one of BMA class labels $i = 1, 2, \dots, c$; where c is the total number of BMA classes in the classifier. To classify \underline{p}_u , i.e., to recognize the class label u , the following procedure is applied. First, the corresponding class mean $\tilde{\underline{q}}_i$ is subtracted from \underline{p}_u for all the BMA classes $i = 1, 2, \dots, c$ to get

$$\underline{p}'_i = \underline{p}_u - \tilde{\underline{q}}_i, \quad (7.8)$$

where \underline{p}'_i is a mean subtracted residual BMA vector for the candidate i^{th} BMA class. The BMA vector \underline{p}'_i is reconstructed from projections on the computed set of eigenvectors E_i to capture its contents in the i^{th} motion artifact subspace defined by E_i in the prior training as

$$\tilde{\underline{p}}'_i = (E_i E_i^T) \underline{p}'_i, \quad (7.9)$$

where $\tilde{\underline{p}}'_i$ is the reconstructed i^{th} motion artifact.

A measure of error in reconstruction in i^{th} motion artifact is denoted by $error(i)$ and defined as

$$error(i) = |\tilde{\underline{p}}'_i - \underline{p}'_i|^2. \quad (7.10)$$

To recognize the BMA class of the ECG beat, u is assigned the class label from $i = 1, 2, \dots, c$ for which the error in reconstruction is the minimum

$$u = \arg \min_i error(i). \quad (7.11)$$

The above derivation is valid when one is trying to classify motion artifacts using the ECG signal for a single beat duration. However, one can have l number of consecutive ECG beats during a particular BMA. The use of l beats instead of a single beat can lead to a better classification accuracy. Hence, for the BMA classifier, the given method of classification can be generalized for a test sequence of l ECG beats $\{\underline{p}\}_u = \{\underline{p}_{u1}, \underline{p}_{u2}, \dots, \underline{p}_{ul}\}$, where \underline{p}_{uj} is j^{th} test ECG beat and u is the single label for all the test ECG beats in the sequence. The error in reconstruction given in Eq. (7.10) for the test ECG beats \underline{p}_{uj} , is denoted by $error_j(i)$ for $j = 1, 2, \dots, l$ in the given sequence. Finally, the following measure of error is computed

$$error(i) = \sum_{j=1}^l error_j(i). \quad (7.12)$$

The class label corresponds to i for which $error(i)$ is minimum.

7.2.5 Removal of Motion Artifacts

The classification procedure as derived above can also be applied to eliminate motion artifacts in ECG due to body movements. The BMA class for an ECG beat under test is recognized by the BMA classifier and the corresponding artifact components are removed. Let \underline{p}_i be an ECG beat where i is the recognized BMA class, and the set of eigenvectors E_i represents the artifacts in \underline{p}_i due to the recognized BMA. For artifact removal, the ECG beat is reconstructed by removing the components of the corresponding mean subtracted observation $\underline{p}'_i = \underline{p}_i - \tilde{\underline{q}}_i$, in the artifact subspace spanned by E_i as

$$\tilde{\underline{p}}_i = \underline{p}_i - (E_i E_i^T) \underline{p}'_i, \quad (7.13)$$

where $\tilde{\underline{q}}_i$ is the class mean of the recognized BMA class as defined in Eq. (7.5) and $\tilde{\underline{p}}_i$ is the reconstructed ECG beat. We expect such a signal to be more useful to clinicians. We demonstrate this by analyzing this signal to obtain more accurate results in the detection of P and T waves. This is given in Section 7.4.1.

7.3 Parametric classification

In the previous section we have discussed nonparametric classification of BMA from the ambulatory ECG signal. In this section we provide a very different approach of BMA classification. The parametric, supervised classification technique is based on hidden Markov models (HMM). Here we overcome some of the limitations in using the PCA-based technique discussed in the previous section. The ECG beat alignment procedure required in the PCA-based technique can distort the motion artifact signal if there is a significant variation in the heart rate. Here we prevent this situation by proposing an adaptive filter as a preprocessing step for separating the motion artifact signal from the ECG signal. The derived motion artifact signal is then processed further for classification of various types of BMA. The classification of BMA is performed using different HMMs for different BMA classes. Like the previously proposed PCA-based technique, this method is also a supervised learning based classification method. However, since the parameters of the HMM model are estimated from the training signals, the method is a parametric classification technique as opposed to the PCA-based method which is a non-parametric classification technique. At the end of this chapter we compare the BMA classification results obtained using both the methods. It is noted that the HMM-based method, though computationally a bit more expensive, outperforms the PCA-based method. However, this is predominantly a classification scheme as opposed to the PCA-based method which is a subspace based reconstruction scheme where artifact removal is obtained as a by-product. For the HMM-based method, once a BMA is recognized, the corresponding PCA for the class should be used if noise removal is required.

In the PCA-based method different sets of principal components and the mean cardiac cycle are computed from the training data to represent the corresponding BMA classes. The PCA-based method provides a good dimensionality reduction and can be applied even when only a single-lead ECG signal is available. However, the PCA-based method requires alignment of cardiac features for separation of cardiac and motion artifact signal subspaces. The problem of alignment is partially solved by resampling of the ECG beats in accordance with the heart rate. However, the resampling process introduces artifacts in the QRS complex and distortion in the spectra of the motion artifact signal. Since the cardiac cycle in PCA is computed from the average of time-warped ECG beats, the artifacts caused due to resampling of the QRS complexes, also affect this estimate. The severity of the distortion is proportional to the amount of resampling, which is determined by the variability of the heart rate. Due to this reason the method is restricted to the cases where the heart rate variability in the individual BMA class is not significant. Therefore, it is necessary to devise a new method for BMA recognition, in which this kind of distortion can be prevented.

To circumvent the problems due to resampling, we separate the motion artifact signal from the ECG initially using an adaptive filter. This is done in order to suppress any cardiac signal components which are common in all types of BMA and which may overwhelm the modeling effort by the HMM, and hence may not help in the BMA classification. We assume that since each BMA is performed in a different manner the spectral features of the motion artifact signal will exhibit some specific kind of temporal behavior. If this assumption is true then the specific temporal characteristic can be modeled using an HMM for each individual BMA class. The time-localized features derived from spectral energy of the motion artifact signals can be computed for each specific BMA class using Gabor filters and they will be simply referred to as Gabor features from here on. The details of computing the Gabor features from the motion artifact signals will be explained later in this chapter.

We explore the feasibility of BMA recognition using HMM, which is considered here also due to its inherent temporality [24, 106]. For this purpose, parameters of an HMM for each BMA class will be determined by using a supervised learning approach, from the Gabor features of the corresponding motion artifact signals reserved for training. The parameters of an individual HMM are initialized by random choice and then updated for maximizing the likelihood of the data from the corresponding BMA class during this training. After the training, all the HMMs with known parameters will be used for calculating likelihood of each of the data provided for testing. The BMA class of the test data is recognized based on the maximum likelihood criterion over all the trained HMMs. The details of the implementation of the adaptive filter, Gabor feature extraction and the HMM-based classification method are provided in the following subsections.

7.3.1 Pre-processing

The ECG signal acquired during a specific BMA is contaminated by the induced motion artifact signals. Preprocessing is required to separate the motion artifact signals from the composite ECG recordings. This is required so that the HMM can be trained on the artifact signal alone and the training is not overwhelmed by the dominant cardiac signal. We use an adaptive filter that is conceptually similar to the adaptive recurrent filter (ARF) given in [130] for cancellation of motion artifacts.

In [130], an ARF is provided to obtain the impulse response \underline{w} of the desired signal spanning over a fixed length M_0 . In this case the desired signal is the recurring cardiac cycle (P-QRS-T complex) in the ECG signal which should be estimated by the filter impulse response $\underline{w} = [w_1 \ w_2 \ \dots \ w_{M_0}]^T$. An impulse train is used as an input to the ARF, in which an impulse (unit sample) occurs at a specified point of each cardiac cycle (ECG beat). This specific point should preferably be at the starting of the ECG beat. This can be determined from the location of the R peak in the particular ECG beat. The length of the filter should be the same as the length of the ECG beat in order to estimate the complete cardiac cycle. The k^{th} filter coefficient w_k is adaptively modified by a least mean squares (LMS) algorithm at the incidence of the k^{th} sample of the current cardiac cycle based on the error between the k^{th} sample and the filter output.

Though the ARF, given in [130] is able to capture the cardiac cycle effectively, it is sensitive to the time synchronization of the impulses at the specified starting points of the cardiac cycles. Since the starting point is determined with respect to the R peak of the cardiac cycle the method is very sensitive to any error in locating the R peaks, which is likely to occur in presence of noise.

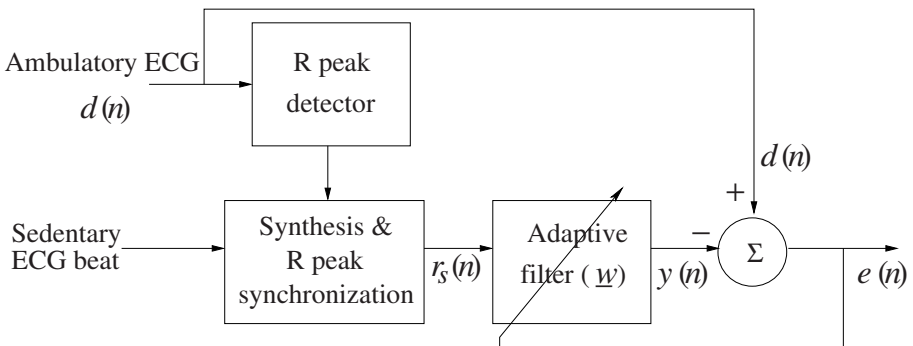


Fig. 7.2. A block diagram of the adaptive filter inspired by the ARF, given in [130].

Here in order to estimate the cardiac cycle more robustly we use a conventional adaptive filter [141] in which, as opposed to the ARF, all the filter

coefficients $\underline{w} = [w_1 \ w_2 \ \cdots \ w_N]^T$ are adaptively modified simultaneously at every sample. A block diagram of the adaptive filter is given in Fig. 7.2. A reference signal $r_s(n)$ is synthesized from a noise free ECG beat. This noise free ECG beat is acquired while the subject is in a sedentary condition. Next, the reference beat length is equalized with the current ECG beat length $r(n)$ such that the R peak positions of both the beats are perfectly aligned. This time synchronization of the R peaks of both the signals is performed by the synthesis block based on the R peak locations detected in the ambulatory ECG signal $r(n)$ using the R peak detector block. Thus the synthesized reference signal $r_s(n)$ exhibits the same heart rate as that of the ambulatory ECG signal $r(n)$ and the R peaks of both the signals are aligned. The coefficients of adaptive filter $\underline{w} = [w_1 \ w_2 \ \cdots \ w_N]^T$ are updated by the LMS algorithm given in [141] using the error signal $e(n)$ computed as the difference between the desired signal $r(n)$ and the filtered signal $y(n)$. The weights at n^{th} instant are updated using the error $e(n) = r(n) - y(n)$ as

$$\underline{w}_{n+1} = \underline{w}_n + \mu e(n) \underline{x}_n, \quad (7.14)$$

where $\underline{x}_n = [r_s(n - N + 1) \ r_s(n - N + 2) \ \cdots \ r_s(n)]^T$ is an input vector to the filter at n^{th} instant, μ is a parameter controlling the adaptation and convergence rate of the LMS algorithm, and N is the length of the filter. After the convergence, the adaptively filtered signal $y(n)$ estimates the desired cardiac signal component of the acquired ambulatory ECG signal $r(n)$ and the error signal $e(n)$ approximates the motion artifact signal $s(n)$.

It may be noted that for all the BMAs considered in this experiment, the quality of the acquired ECG signals from lead-II, despite the presence of motion artifacts, was such that it allowed a reliable detection of the R peak using the Pan-Tompkins algorithm [96]. Fig. 7.3 illustrates the cleaning of ECG signal acquired during a twisting at waist activity performed by a subject. The acquired ECG signal is depicted in Fig. 7.3(a). The cleaned ECG signals by the given adaptive filter and the ARF discussed in [130] are shown in Fig. 7.3(b) and Fig. 7.3(c), respectively. The filtered ECG signals are representatives of the cardiac signal component of the acquired ECG signal which is contaminated by the motion artifact. The P-QRS-T complex is clean and clearly visible in both the filtered ECG signal. The signal obtained by the adaptive filter has the P-QRS-T complex similar to that obtained by the ARF method [130]. Moreover, the length of the P-QRS-T complex is not required to be fixed in the given adaptive filter. Therefore, it can handle variation in the heart rate in an automated manner. Thus we obtain a good estimate of the cardiac signal component from an ambulatory ECG signal contaminated by motion artifact. However, the quality of the signal has not yet been examined for its use in clinical purposes. The filtering is performed just for obtaining the motion artifact signal $s(n)$ for further analysis of ambulation in this study.

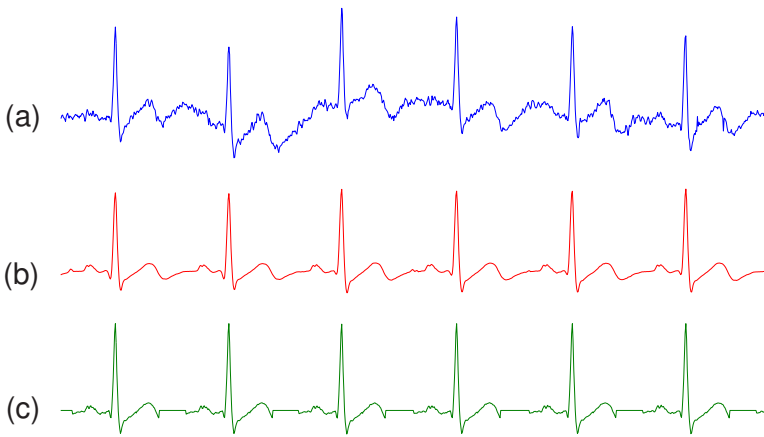


Fig. 7.3. Illustration of cleaning of ECG signal. (a) Original ECG signal while twisting at waist, computed ECG signal obtained with (b) the scheme of using noise free ECG beat reference, and (c) the ARF method in [130].

7.3.2 Feature Extraction

While preprocessing, an adaptive filter for obtaining the motion artifact signal $s(n)$ from the acquired ECG during a BMA is discussed. Since we are planning to use temporal relations among time localized frequency features for the modeling, the motion artifact signal $s(n)$ is analyzed into various subbands using Gabor filters. Gabor transform is known to have good time-frequency localization properties [36]. The different, equally spaced frequency components of the motion artifact signal $s(n)$ are computed by

$$\hat{s}_l(n) = e^{-\alpha^2(n/f_s)^2} e^{(j2\pi nl f_0/f_s)} * s(n), \quad (7.15)$$

where $*$ is convolution operator, f_s is sampling frequency, α , and f_0 are constant “sharpness” and “frequency” parameters [36], respectively, $\hat{s}_l(n)$ is a component of the motion artifact signal $s(n)$ and l is the index of a frequency component or subband. The envelopes of the impulse responses of the Gabor filters used for first three subbands are depicted in Fig. 7.4. The impulse responses span over 2 seconds and the center frequency $l f_0$ of the l^{th} subband filter increases proportionately to the value of index l , i.e., 1Hz, 2Hz and 3Hz, respectively for $l= 1, 2$ and 3 and $f_0 = 1\text{Hz}$.

Since the energies of the motion artifact signal are concentrated in 1-10Hz band, the number of subbands is selected through a suitable choice L to cover this frequency band, i. e., $l = 1, 2, \dots, L$. An estimate of the energy in each of

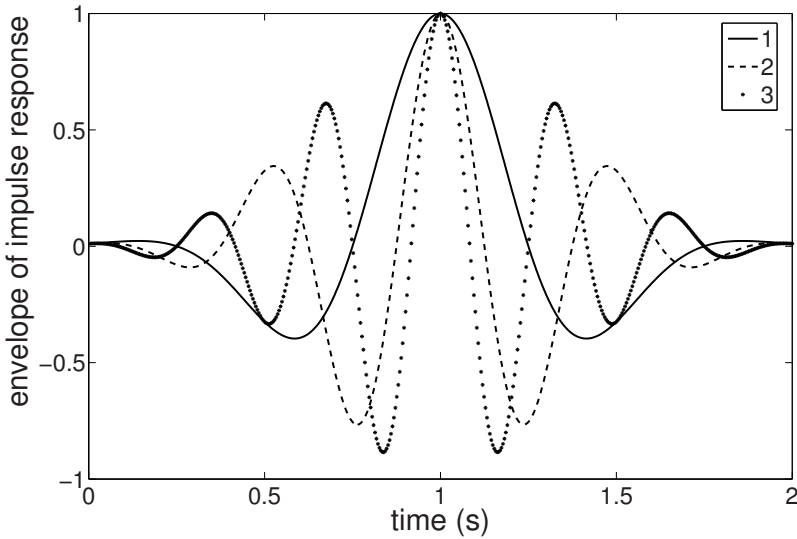


Fig. 7.4. Envelopes of the impulse responses of the Gabor filters used for first three subbands, $l=1, 2$ and 3 .

these L frequency components $\hat{s}_l(n)$ is computed by a moving average of the windowed function as

$$g_l(n) = \frac{1}{W+1} \sum_{k=n-W/2}^{n+W/2} |\hat{s}_l(k)|^2, \quad (7.16)$$

where W is the width of the moving window. An example of the energy features for the analyzed signals in first four subbands is depicted in Fig. 7.5. It is noted that the signal power drops down with the increasing number of the subband.

For activity recognition, the feature vector $G(n) = [g_1(n) \ g_2(n) \ \dots \ g_L(n)]^T$ is formed by L frequency components. This feature corresponds to the properties of the artifact signal at a given time instant. In order to consider the properties over a duration of N_0 consecutive samples, we put them as subsequent columns and construct the corresponding feature matrix

$$F(n, N_0) = [G(n - N_0 + 1) \ G(n - N_0 + 2) \ \dots \ G(n)], \quad (7.17)$$

computed over N_0 contiguous samples of the motion artifact signal $s(n)$. This is used for the training and classification of BMA classes using an HMM-based technique. The dimension of the feature matrix $F(n, N_0)$ is $L \times N_0$.

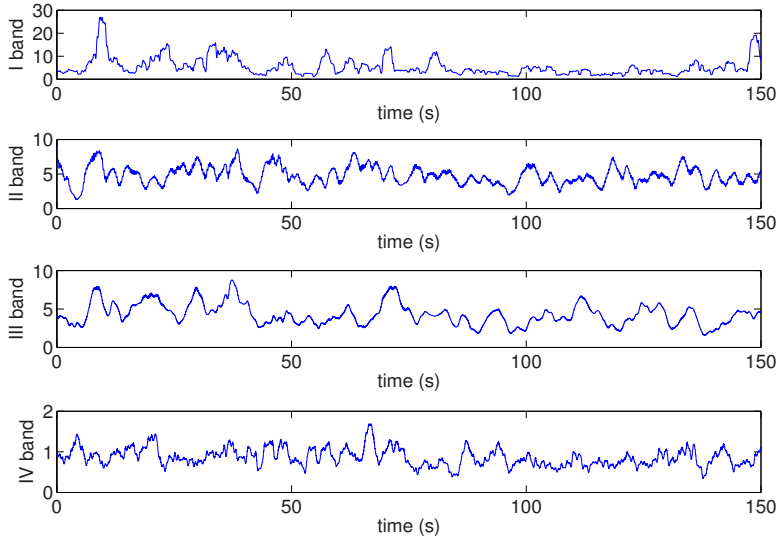


Fig. 7.5. Gabor feature signals $g_l(n)$, for first four subbands, $l=1, 2, 3$ and 4 .

7.3.3 Hidden Markov Model (HMM) and Training

We provide an HMM-based classification technique for BMA recognition. In this technique, each of the BMA classes will be represented by an HMM. Since we are exploring the feasibility of using the HMM for BMA classification using the Gabor features derived in the previous section, we use the standard (also called fully connected or ergodic) HMM with finite mixtures of continuous observation probability density functions as given in [106]. To define the HMM, the number of states and the number of components in the mixture in each of the states are to be specified along with the associated parameters. For simplicity, we choose the same number of states in all the HMMs used for representing various BMA classes. Similarly, we choose the same number of mixture components for all the states. Let us denote the number of states in any HMM as \mathcal{Q} and the number of mixture components in any state of the HMM as \mathcal{M} . The parameters of the HMM are:

- State transition probability $A = \{a_{ij}\}$, $1 \leq i \leq \mathcal{Q}$, $1 \leq j \leq \mathcal{Q}$, where a_{ij} is the state transition probability from i^{th} state to j^{th} state.
- Prior state probability distribution $\underline{\pi} = \{\pi_i\}$, $1 \leq i \leq \mathcal{Q}$, where π_i is the probability of the initial state of the system to be the i^{th} state S_i .
- Observation probability distribution $B = \{b_j\}$, $1 \leq j \leq \mathcal{Q}$, where b_j is a probability distribution for the observations when the system is in j^{th} state. The observation probability distribution for the j^{th} state b_j is modeled by a finite number of mixture components of continuous observa-

tion probability density functions with the mixture weight coefficients c_{jm} , mean vectors \underline{u}_{jm} and covariance matrices Σ_{jm} for m^{th} mixture.

A finite mixture takes the form of the observation probability density b_j for the j^{th} state

$$b_j(G(n)) = \sum_{m=1}^M c_{jm} \mathcal{N}(G(n) | \underline{u}_{jm}, \Sigma_{jm}), \quad (7.18)$$

where $G(n)$ is the observation being modeled, \mathcal{N} is a Gaussian probability density with mean vector \underline{u}_{jm} and covariance matrix Σ_{jm} for the m^{th} mixture component, and c_{jm} are mixture weight coefficients. The mixture weight coefficients c_{jm} , satisfy the conditions:

1. $\sum_{m=1}^M c_{jm} = 1$, $1 \leq j \leq Q$, and
2. $c_{jm} \geq 0$, $1 \leq j \leq Q$, $1 \leq m \leq M$.

In a short form the model is specified as

$$\Lambda = (\underline{\pi}, A, B), \quad (7.19)$$

where $\underline{\pi}$, A , and B are model parameters as defined above.

Let us define $\gamma_n(i)$, the probability of being in state S_i at an instant n given the model Λ and the observation sequence $F(n, N_0)$ defined in Eq. (7.17)

$$\gamma_n(i) = P(q_n = S_i | F(n, N_0), \Lambda), \quad (7.20)$$

where q_n is a variable indicating state at the instant n . Therefore, the probability of being in state S_i at instant n with the m^{th} mixture component accounting for the observation $G(n)$

$$\gamma_n(i, m) = \gamma_n(i) \frac{c_{jm} \mathcal{N}(G(n) | \underline{u}_{jm}, \Sigma_{jm})}{\sum_{m=1}^M c_{jm} \mathcal{N}(G(n) | \underline{u}_{jm}, \Sigma_{jm})}. \quad (7.21)$$

Let us define $\zeta_n(i, j)$, the probability of being in state S_i at instant n and in state S_j at instant $n + 1$, given the model Λ and the observation sequence $F(n, N_0)$

$$\zeta_n(i, j) = P(q_n = S_i, q_{n+1} = S_j | F(n, N_0), \Lambda). \quad (7.22)$$

It has been shown by Baum *et al.* [13] that the probabilities $\gamma_n(i)$, $\gamma_n(i, m)$ and $\zeta_n(i, j)$ as defined in equations (7.20), (7.21) and (7.22), respectively, can be used to reestimate the model parameters from the observation sequence $F(n, N_0)$ and the initial model Λ . They have shown that the reestimated model parameters define a new model $\bar{\Lambda} = (\bar{\underline{\pi}}, \bar{A}, \bar{B})$ which can either be the same as the initial model Λ or can have greater likelihood of the observation sequence $F(n, N_0)$, i. e., $P(F(n, N_0) | \bar{\Lambda}) \geq P(F(n, N_0) | \Lambda)$. The model parameters can be updated by iteratively replacing the initial model Λ by the new model $\bar{\Lambda}$ to increase the likelihood of the given observation sequence $F(n, N_0)$ till

a limiting point at which there is no significant gain in the likelihood. This procedure of parameter reestimation from a given observation sequence and the initial model is known as Baum-Welch reestimation method [106]. The reestimation formula due to this method for prior state probability π_i , state transition probability a_{ij} and the mixture density parameters c_{jm} , \underline{u}_{jm} and Σ_{jm} are

$$\bar{\pi}_i = \gamma_1(i), \quad (7.23)$$

$$\bar{a}_{ij} = \frac{\sum_{n=1}^{N_0-1} \zeta_n(i, j)}{\sum_{n=1}^{N_0-1} \sum_{m=1}^M \gamma_n(i, m)}, \quad (7.24)$$

$$\bar{c}_{jm} = \frac{\sum_{n=1}^{N_0} \gamma_n(j, m)}{\sum_{n=1}^{N_0} \sum_{m=1}^M \gamma_n(j, m)}, \quad (7.25)$$

$$\bar{\underline{u}}_{jm} = \frac{\sum_{n=1}^{N_0} \gamma_n(j, m) \cdot G(n)}{\sum_{n=1}^{N_0} \sum_{m=1}^M \gamma_n(j, m)}, \quad (7.26)$$

$$\bar{\Sigma}_{jm} = \frac{\sum_{n=1}^{N_0} \gamma_n(j, m) \cdot (G(n) - \bar{\underline{u}}_{jm})(G(n) - \bar{\underline{u}}_{jm})^T}{\sum_{n=1}^{N_0} \sum_{m=1}^M \gamma_n(j, m)}. \quad (7.27)$$

Following the details of HMM provided above, we represent each BMA class through an HMM for the classification purpose. Let us add a subscript k to the notations as defined above to define the HMM for k^{th} BMA class as $\Lambda_k = (\underline{\pi}_k, A_k, B_k)$. If a total of c different BMA classes are used to form a classifier then $1 \leq k \leq c$. A part of the set of feature sequences $F(n, N_0)$ defined in Section 7.3.2 for each BMA is reserved for training purpose. For k^{th} BMA class these training sequences will be indicated as $F_k(n, N_0)$. We train the HMM representing k^{th} BMA class using the training data $F_k(n, N_0)$. In this training, the parameters of all the HMM Λ_k , $1 \leq k \leq c$ are derived in order to maximize the likelihood of their corresponding training sequences $F_k(n, N_0)$, $1 \leq k \leq c$ using the Baum-Welch method [106] described above

$$\Lambda_k = \arg \max_{\Lambda} P(F_k(n, N_0) | \Lambda), \quad 1 \leq k \leq c. \quad (7.28)$$

The parameters Λ_k , $1 \leq k \leq c$, obtained after this supervised training will be used for classification of feature sequences reserved for the testing purpose.

7.3.4 Activity Classification

We have seen that in a BMA classifier each of the specified BMA is represented by an HMM having its parameters obtained by the given supervised training using the features from the motion artifact signal. Let c be the number of models corresponding to c different BMA classes and a feature sequence $F(n, N_0)$ is provided for testing, which belongs to any of the c BMA classes indexed by $k = 1, 2, \dots, c$. It is possible to find the likelihood of the given test

sequence $F(n, N_0)$ for being in any of the c BMA classes. Let us denote the likelihood of $F(n, N_0)$ computed using the k^{th} model corresponding to the k^{th} BMA class, with parameters $A_k = (\underline{\pi}_k, A_k, B_k)$ as $P(F(n, N_0)|A_k)$. The BMA class can be recognized using the criterion of the maximum likelihood

$$u = \arg \max_{k, 1 \leq k \leq c} P(F(n, N_0)|A_k), \quad (7.29)$$

where u is the label of the recognized BMA class out of the possible $k = 1, 2, \dots, c$ indices. The given test sequence is now classified to an appropriate BMA class.

7.4 Experimental Results

7.4.1 PCA-based Recognition

The collected ECG data from the subjects is analyzed using the PCA-based technique. The results of the PCA-based analysis are presented here in this section. First, the results of BMA classification in terms of classification rates, accuracy and false alarms are presented. This includes single subject classifiers with subject specific training and multiple subjects classifiers with combined training. Different classifiers are formed using different combinations of BMA classes that we will explain in this section. In the second part, we present an example of motion artifact removal using the class specific PCA-based filtering of the ECG signal. The improvement due to the PCA-based filtering is shown through better localization of detected P and T waves.

BMA Classification

A uniform length of 160 sample point duration is chosen for each ECG beat during the preprocessing steps. The BMA label (ground truth) is known for each of the ECG beats collected. The data set is divided into two parts: one for training the classifiers and the other for classifier testing purposes. The exact details of the population size for each of these two parts for various BMAs are given in Table 7.1. The column ‘Single Subject’ corresponds to the case where the classifier is trained for a particular subject (subject number one in our experiment) and tested on the same subject. The last column corresponds to the case when the classifier is both trained and tested for a collective pool of subjects and not specific for a single subject. The known BMA labels in the test data are used for performance evaluation of the classifier testing and are not available to the classifier itself. The classification test is performed on the sequences of 30 consecutive ECG beats (30 × 160 sample points).

The performance is evaluated based on two parameters: accuracy (P_T) defined as

$$P_T = N_{true}/(N_{true} + N_{missed}), \quad (7.30)$$

Table 7.1. Details of number of ECG beat streams used for training and testing of a particular BMA.

Body movement activity	Single Subject		Multiple Subjects	
	training	testing	training	testing
Sitting still	289	578	2927	5854
Left arm	227	454	2336	4672
Right arm	278	557	2278	4556
Both arms	224	449	1586	3112
Walking	583	1167	4120	8240
Twisting	355	711	2798	5597
Climbing down	268	536	1407	2814
Climbing up	344	688	1879	3759
Total	2568	5140	19331	38604

and false detection rates (P_F) defined as

$$P_F = N_{false}/(N_{true} + N_{false}), \quad (7.31)$$

where N_{true} is the number of true detections, N_{missed} is the number of missed detections and N_{false} is the number of false detections.

We use the following example to explain this. A classifier has three classes namely A1, A2 and A3 and the corresponding number of test signals recorded are 100, 90 and 80. Now, if the classifier detects 95 test signals as class A1 and 10 out of these 95 detections, actually belong to either class A2 or class A3 rather than class A1, then $N_{false} = 10$, $N_{true} = 95 - 10 = 85$ and $N_{missed} = 100 - 85 = 15$.

A hierarchical tree structure of BMA classes is shown in Fig. 7.6. There are five BMA classes in the top layer: (1) sitting still, (2) arm movement, (3) walking and climbing down stairs (W&CD), (4) climbing upstairs and (5) twisting movement at waist. The arm movement is a combined class of three separate movements of (2a) left arm, (2b) right arm and (2c) both arms. Similarly, W&CD is a combination of two BMA subclasses: (3a) walking and (3b) climbing down stairs. These BMA subclasses, shown in the second layer of the graph, demonstrate partial correlation among the corresponding motion artifacts. As a result these subclasses are subject to more false detections. To study this aspect of BMA classification in ECG signals, we construct five different types of BMA classifiers (Table 7.2) formed by various possible combinations of BMA classes/subclasses (Fig. 7.6).

Since an artifact subspace in the given scheme of BMA classification is represented by a corresponding set of eigenvectors, the performance of the classifiers is studied against the number of eigenvectors used to represent the subspace. Fig. 7.7 shows the performances of the classifiers I-V that are trained and tested on data collected from a single subject. Here the training is very specific to an individual subject and the performance shown here is

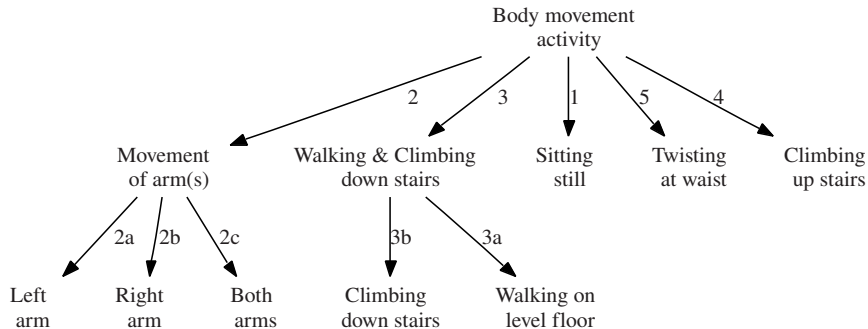


Fig. 7.6. Various BMAs and possible class formation by combining two or more BMAs into a single class. (©2007 IEEE)

Table 7.2. Five different classifiers for subject specific training with various combinations of BMA classes / subclasses in Fig. 7.6. The corresponding classifiers for multiple subjects are VI to X.

Classifier		BMA
Subject specific	Subject independent	
I	VI	1, 2, 3 and 4
II	VII	1, 2, 3a, 3b and 4
III	VIII	1, 2a, 2b, 2c, 3 and 4
IV	IX	1, 2a, 2b, 2c, 3a, 3b and 4
V	X	1, 2a, 2b, 2c, 3a, 3b, 4 and 5

also specific to the same subject. It is noted that the accuracy improves as the number of eigenvectors is increased from one to six, which results in a wider span of the artifact subspace of an individual BMA class. However, the performance saturates with further increase in the number of eigenvectors, since this results in overlapping of the spanned subspaces for different classes.

Due to possible correlation among the eigenfunctions of the specified subclasses, there is a drop in accuracy with increasing number of classes. The P_T value for classifier I (4 classes) is 98%, whereas for classifier V (8 classes) $P_T = 85\%$. Thus it is possible to accurately recognize the BMA from the ambulatory ECG itself, but the degree of accuracy depends on separability of the BMAs.

The complete performances of the above BMA classifiers I, II, III and IV are presented in Fig. 7.8(a), 7.8(b), 7.8(c) and 7.8(d), respectively, showing the confusion matrix for all classes. In all cases six eigenvectors are used for the classification of the data collected from a single subject. In classifier I there are four BMA classes: 1, 2, 3, and 4 (Table 7.2). The accuracy P_T of the classifier I is 98% with a false detection rate $P_F=1.4\%$. This suggests that

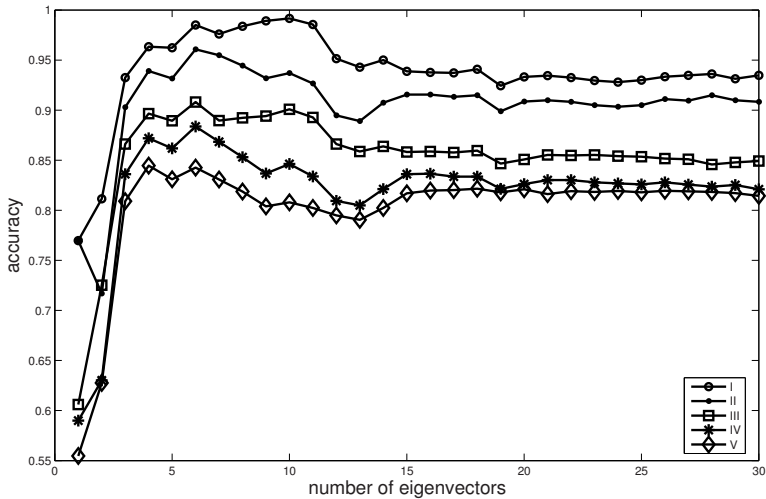
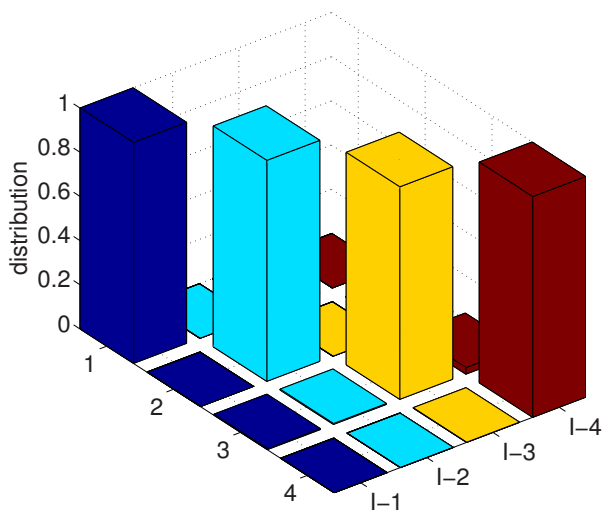


Fig. 7.7. Classification accuracy as a function of number of eigenvectors for the BMA classifiers: I, II, III, IV and V. (©2007 IEEE)

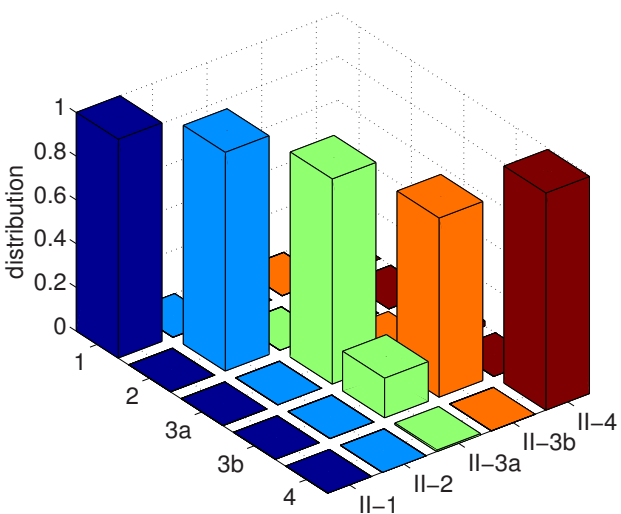
all these four classes of BMAs are very well separable using the PCA-based classification technique.

In BMA classifier II, there are five BMA classes: 1, 2, 3a, 3b, and 4. Here, the activities of walking (3a) and climbing down (3b) stairs are recognized as separate classes. However, there is a moderate amount of confusion between these two classes: 3a and 3b, as shown in Fig. 7.8(b), about 18% of total known labels of climbing down stairs are misclassified as walking and 4% of walking labels are misclassified as climbing down stairs. For these two classes, the average $P_T = 90\%$ and $P_F = 8.5\%$. The average performance for classifier II is $P_T = 96\%$ and $P_F = 4\%$. Further studies will be required to determine if there is a fundamental limitation in separating walking and climbing down. A possible explanation suggests that the corresponding gaits for these two BMAs differ only in the lower limbs and the upper body gait remains similar during both the activities. It is only the upper body gait that matters in generating a particular type of motion artifact.

In BMA classifier III there are six BMA classes: 1, 2a, 2b, 2c, 3, and 4. Here, the movement of left arm (2a), right arm (2b) and both arms (2c) are recognized as separate classes. However, a significant level of confusion exists between these three classes as shown in Fig. 7.8(c). On average, 25% of total known labels of both the classes 2b and 2c are misclassified as 2a, and 12% of total known labels of the 2b are misclassified as 2c. For these three classes, average P_T is 77% and P_F is 17%. The average performance for classifier III is $P_T = 91\%$ and $P_F = 7\%$. This suggests that, for the given

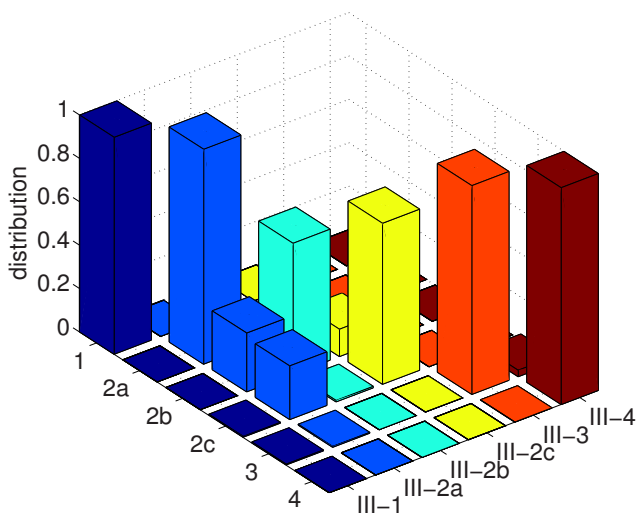


(a)

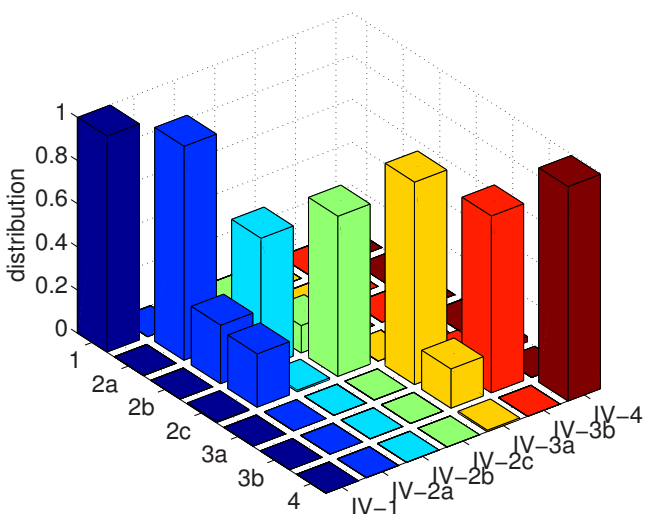


(b)

(See next page for figure caption.)



(c)



(d)

Fig. 7.8. Confusion matrices for BMA detection for classifiers (a) I, (b) II, (c) III and (d) IV. The horizontal axes in each case represent known and recognized BMA classes. The vertical bars represent the classification accuracy. (©2007 IEEE)

lead-II configuration, any movement of the arms (be it left or right) does affect the ECG signal in a similar manner which reduces the differentiability of the corresponding BMAs.

In BMA classifier IV, there are seven BMA classes: 1, 2a, 2b, 2c, 3a, 3b, and 4. Here the BMA (2a) left arm, (2b) right arm and (2c) both arms movement, (3a) walking and (3b) climbing down stairs are recognized as separate BMA classes. The notable aspect about the classifier IV is that all the seven different BMA classes are recognized by a single classifier. The confusion levels between classes are similar to that of classifier III (arm movements) and classifier II (walking and climbing down stairs). The classifier IV demonstrates $P_T = 88\%$ and $P_F = 10\%$, which is worse than the previous cases, due to the larger number of classes considered.

In BMA classifier V, there are now eight BMA classes: 1, 2a, 2b, 2c, 3a, 3b, 4 and 5. As compared to the classifier IV, the performance under the BMA subclasses 2a, 2b and 2c is further deteriorated since a new BMA class of twisting at waist introduced here also involves arm movement. The classifier V has $P_T = 84\%$ and $P_F = 13\%$.

The results given so far (Fig. 7.8) correspond to analyzing the performance of the classifiers on a single subject (subject number one in this case). We now compute the inter-subject variability of the obtained results by computing the classification rates for each classifier trained and tested on individual subjects. This is given in Table 7.3 for the classifiers I-V. It can be seen from the table that the mean accuracy (P_T) and mean false detection rate (P_F) for these classifiers display similar behaviors as discussed earlier. The standard deviation for accuracy is quite low. However, the standard deviation for the false detection rates appears to be on a slightly higher side.

Table 7.3. Inter-subject variability of classification rates (in %) of the subject-specific classifiers over the entire subject population.

Classifier	Accuracy (P_T)		False detection rate (P_F)	
	mean	std. dev.	mean	std. dev.
I	92.44	6.71	5.95	5.38
II	86.81	8.38	9.78	6.64
III	79.85	7.11	15.23	5.52
IV	73.98	8.97	19.06	6.53
V	72.79	7.51	20.20	6.08

The results presented above were for the classifiers I to V, tested with subject specific training. The subject specific training allowed us to shield the classifier from possible inter-personal variability. Hence we now repeat the experiments where principal components are learnt not from an individual subject, but from all subjects available with us. The corresponding classifiers VI to X (see Table 7.2) are trained on 23 different subjects to understand the

impact of inter-personal variability on classifier performance. As mentioned earlier, one third of the available ECG beats from each subject but pooled together to form a common pool of training data have been used for training purposes. The accuracy of classification for various choices of the number of eigenvectors is plotted for the classifiers VI to IX in Fig. 7.9. As compared to the training over a single subject the required number of eigenvectors is much higher and the maximum P_T is only 85%, as expected. The confusion matrices of the classifiers VI to IX using 19 eigenvectors are plotted in Fig. 7.10. The trends of confusions among certain classes, i.e. arm movement classes or walking and climbing down stairs, are similar to that in the subject specific classifiers.

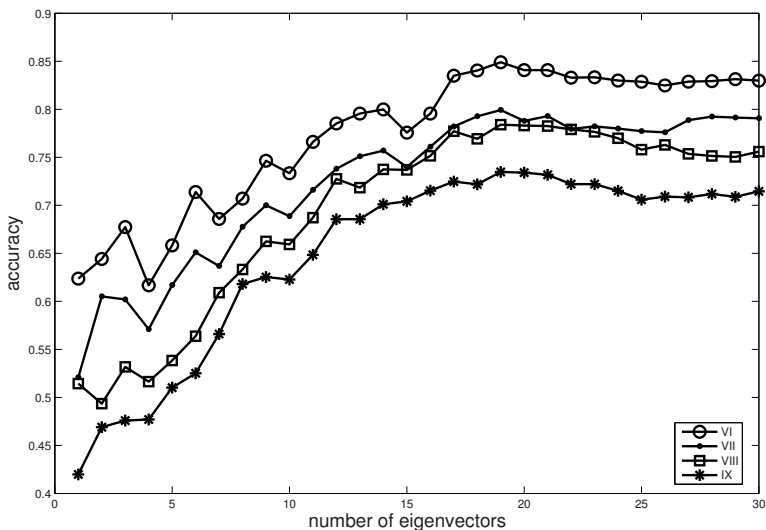
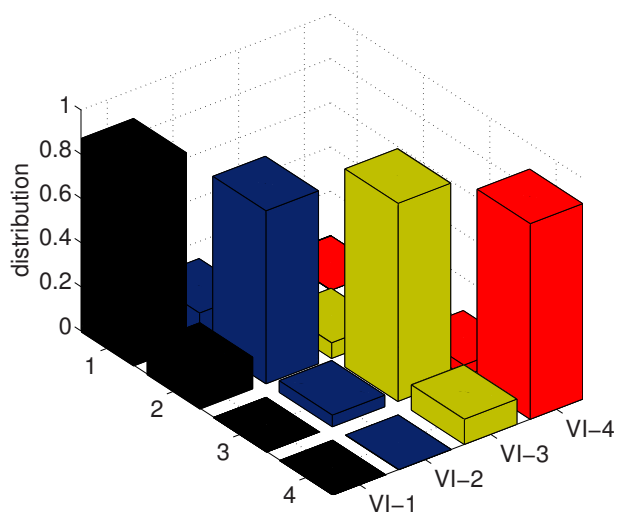
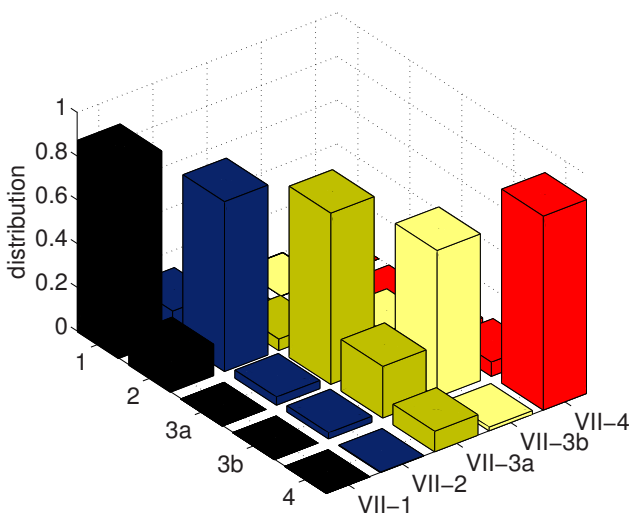


Fig. 7.9. Accuracy of the combined (multi-subject) classifiers as a function of number of eigenvectors used to represent the artifacts when the data is collected from different subjects. Here the classifiers are VI, VII, VIII and IX. (©2007 IEEE)

To study further the effect of inter-personal variation in ECG data, a new classifier, called classifier XI with four BMA classes 1, 2, 3, and 4 is trained on 22 subjects out of the total 23 subjects, leaving each time one designated test subject. This is equivalent to employing a leave-one-out testing method. The performance of classifier X is $P_T(\max.)= 72\%$ and $P_F(\min.)= 26\%$. Thus, it appears that the error signal generated due to inter-personal variation is significant. It is therefore advisable that the classifier be customized for a given user in order to achieve the highest accuracy. However, this should not be a cause of alarm as the W-ECG system is meant to monitor only a specific

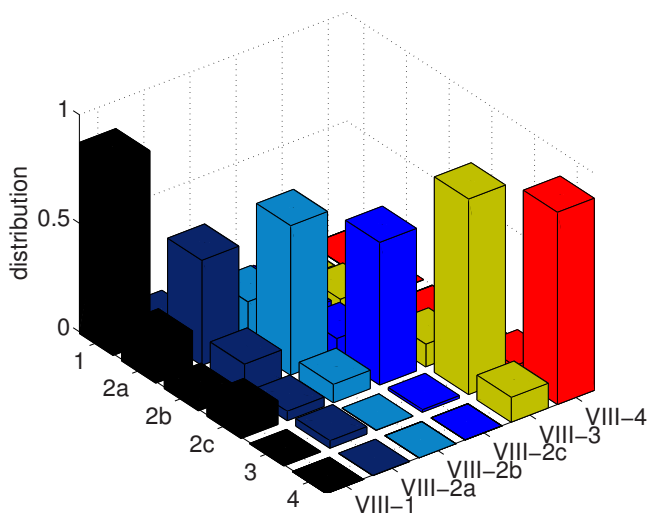


(a)

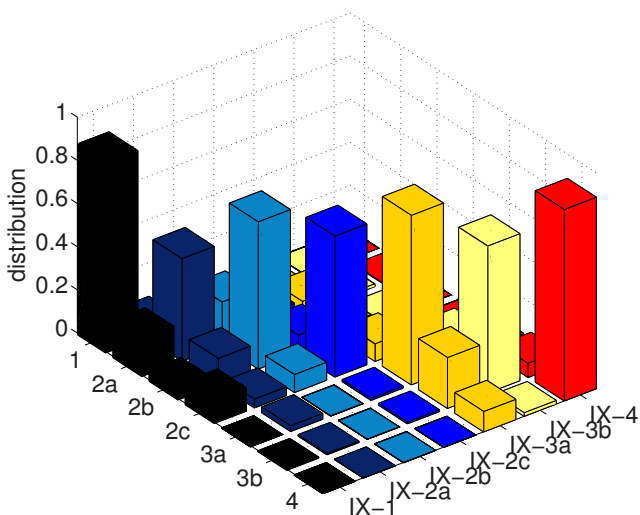


(b)

(See next page for figure caption.)



(c)



(d)

Fig. 7.10. Confusion matrices for BMA detection for multi-subject classifiers (a) VI, (b) VII, (c) VIII and (d) IX. The horizontal axes in each case represent known and recognized BMA classes.

subject at a given time. Hence it should be possible to retrain the classifier for each subject.

Detection of P and T Waves in Presence of BMA

Fig. 7.11(a) shows a sequence of recorded ECG beats in presence of BMA (walking) prior to artifact removal. In Fig. 7.11(b) the component due to motion artifacts as derived by the class specific PCA-based method using the classifier III is shown. In Fig. 7.11(c) the reconstructed ECG signal after subtracting the artifact signal is shown. The ECG signal after the removal of motion artifacts is quite clean even though this has been accomplished with a single lead W-ECG.

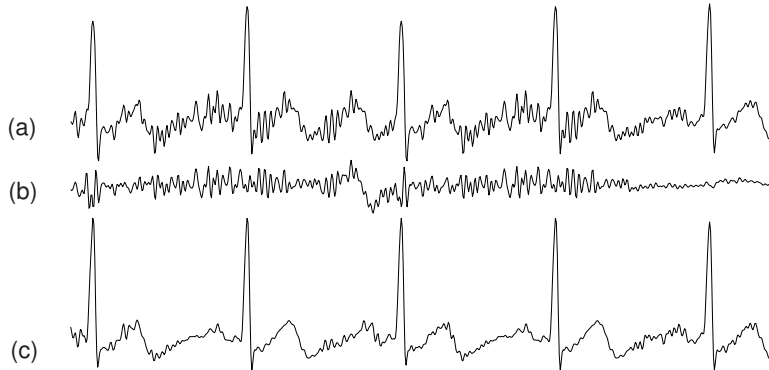


Fig. 7.11. Illustration of artifact removal from ambulatory ECG using the class specific PCA-based filtering. (a) Original ECG signal before any artifact removal, (b) artifact signal derived by the class specific PCA-based method, and (c) reconstructed ECG signal after subtracting the artifact signal. ((C)2007 IEEE)

This artifact removal procedure helps to improve the quality of analysis of ECG signal in presence of BMA as demonstrated here in the detection of P and T waves in the collected ECG data. The P wave is a small and smooth peak that occurs just before the QRS complex due to atrial activity of the heart and the T wave occurs following the QRS complex due to the ventricular activity. In order to detect the P, QRS complex and T waves, we use a combination of two existing techniques in the literature [63, 66, 132]. First, the ECG signal is smoothed by a low-pass filter with a 3dB cut-off at 12Hz as recommended in [66] for P and T wave detection. Then a morphological operator for detecting P and T waves is applied which is inspired by the method

of QRS detection in [132]. Since the R peak position is in the middle, P and T waves are located by searching for maxima in the appropriate windows before and after the R peak position in the output of the morphological filter.

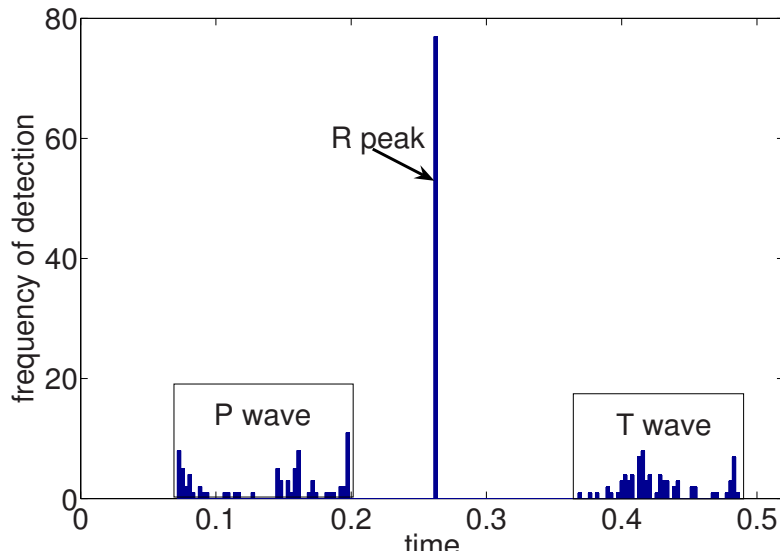
The histograms representing the locations of P and T waves detected in the ECG signal from a particular subject (a part of the ECG is shown in Fig. 7.11), before and after artifact removal, are shown respectively in Fig. 7.12(a) and 7.12(b). It may be noted that since the input beats have already been resampled to have the same number of samples, the samples may correspond to different timings based on the resampling factor used earlier. In order to plot them on an actual time unit, the locations of the detected P and T waves are shown after correcting for the resampling operation. In Fig. 7.12(a), the histogram without the artifact removal is broadly spread out (standard deviations of 46.4ms and 29.8ms, respectively, for P and T locations) while in Fig. 7.12(b) the histogram is much narrower (standard deviations of 8ms and 11.9ms, respectively, for P and T locations). It is noted that a 12Hz pre-filtering is applied to the ECG signal in both the cases prior to detection of P and T waves. This shows that in the presence of BMA induced artifact, the 12Hz lowpass filter as suggested in [66] alone is not sufficient for the accurate localization of P and T waves and the given artifact removal scheme improves the quality of analysis.

7.4.2 HMM-based Recognition

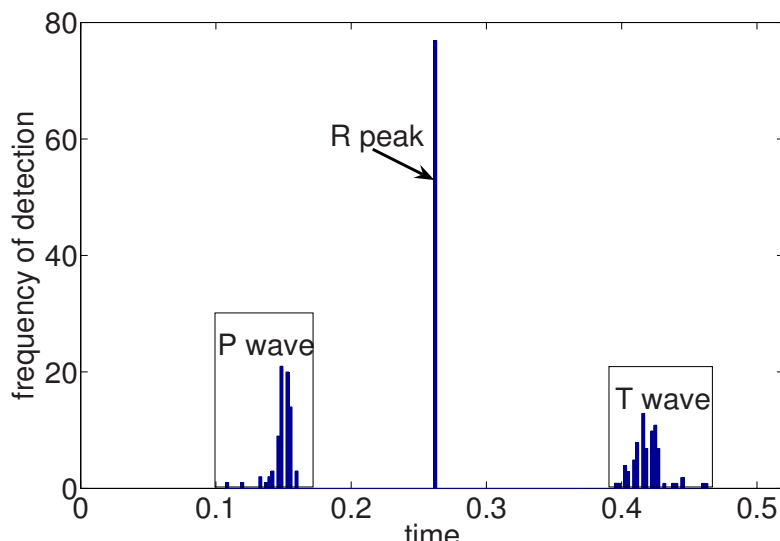
Here we present the results of HMM-based BMA recognition from the ambulatory ECG signal. The ‘sitting still’ is considered here as a representative class of the ECG data for which there is no BMA present and hence it is free from any motion artifact. This signal is taken as the representative of the reference signal while using the adaptive filter proposed earlier to estimate the component due to the cardiac cycle in presence of motion artifact. The methodology explained in the previous section is adopted for training various BMA classifiers with different combinations of BMA classes as listed in Table 7.2. Here we concentrate only on the subject specific cases only.

We use 80% of the available data for each individual subject for training purposes, and the remaining 20% of the data is used for testing purposes.

First, we explore the HMM-based method for BMA recognition for testing the accuracy of classification with subject specific training. The BMA classifiers I to V as described in Table 7.2 are trained using the data from an individual subject. The following set of parameters is used in the feature extraction step: $\alpha=1.5$, $f_0=1\text{Hz}$, $L=10$, and $W=484$ (equivalent to 2s of the data length at $f_s=242\text{Hz}$). The classifiers are trained using the appropriate number of HMMs using the supervised learning method given in Section 7.3.3. The number of states $Q=4$ and number of mixture components $M=3$ are chosen for this experiment. The trained classifiers are used for recognition of BMA from the test sequences collected from the same subject according to the technique given in Section 7.3.4. Here the length of each test sequences is chosen to



(a)



(b)

Fig. 7.12. Histograms of location estimates of P and T waves with respect to the location of R wave (a) when motion artifacts were present and (b) after artifact removal. The horizontal axes represents actual time in seconds. (©2007 IEEE)

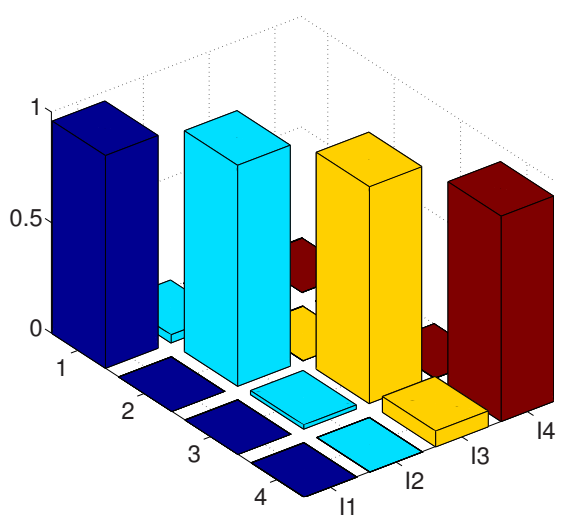
be $N_0=1200$ (approximately equivalent to 5 seconds of ECG recording). The accuracy of classification P_T is calculated using Eq. (7.30). This experiment of the subject specific training is repeated for all subjects individually and with the same parameter values as described above. The aggregate of confusion matrices for classifiers I to IV, showing the accuracy of the classifier as well as amount of misclassification to other classes over the actual vs. recognized BMA classes are presented in Fig. 7.13 for these experiments for the subject specific training. The confusion matrix for the classifier I with subject specific training is shown in Fig 7.13(a). There are four BMA classes in the classifier I: 1. sitting still, 2. movements of arm(s), 3. walking on level floor and climbing down on stair combined (W&CD), and 4. climbing up stairs. There are two most significant confusions: 5.3% of ‘sitting still’ are recognized as movement of arm(s) and 4.6% of climbing up stair are recognized as W&CD. Most of the other confusions among the BMA classes are much less than 1%. The aggregate accuracy of this classifier is 97.6%.

The confusion matrix for the classifier II with subject specific training is shown in Fig 7.13(b). There are five BMA classes in the classifier II : 1. sitting still, 2. movements of arm(s), 3a. walking on level floor, 3b. climbing down on stair, and 4. climbing up stairs. Here the two BMA classes indicated as 3a and 3b, are separated as opposed to the classifier I in which they were combined into W&CD class. The most significant confusion occurs at 5.6% of the climbing down stairs being recognized as walking on level floor, which is expected because of the similarity of the two BMAs. The aggregate accuracy of this classifier is 97.1%.

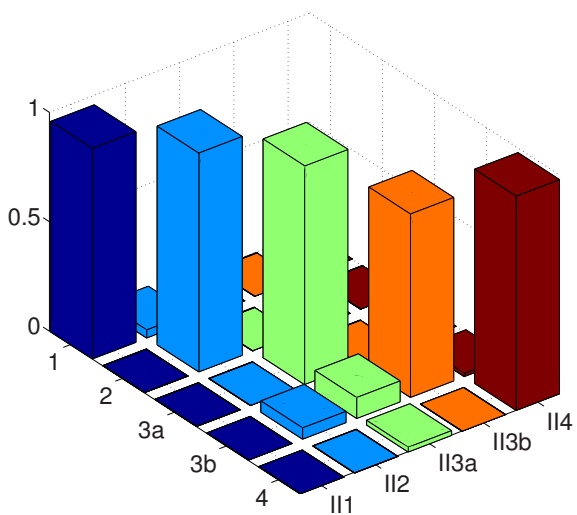
The confusion matrix for the classifier III with subject specific training is shown in Fig 7.13(c). There are six BMA classes in this classifier. Here three BMA classes are indicated as 2a, 2b and 2c, corresponding to the movements of left, right and both arm(s), respectively. Here 10% of each of the movements of left and right arm are recognized as movements of both arms. Apart from these, 10%, 3% and 6% of 2a, 2b and 2c, respectively, are recognized as W&CD. The result shows a significant difficulty in recognizing movements of left arm, right arm and both arms as three different classes. The aggregate accuracy of the classifier III is 92.3% which is substantially less than the previous two classifiers.

The confusion matrix for the classifier IV with subject specific training is shown in Fig 7.13(d). There are seven BMA classes in the classifier IV. Here the three movements of left, right and both arm(s) indicated as 2a, 2b and 2c, respectively, are separated along with 3a and 3b BMA classes. The types of confusions mentioned above for the classifiers II and III, are also seen in this classifier, hence the accuracy drops to 90.5%. However, this can be considered quite significant with a view of having the ability to classify so many BMAs as different classes using a single-lead of ECG.

In order to explore the ability of the BMA recognition scheme to handle a larger number of BMAs, we introduce one more class of twisting at waist

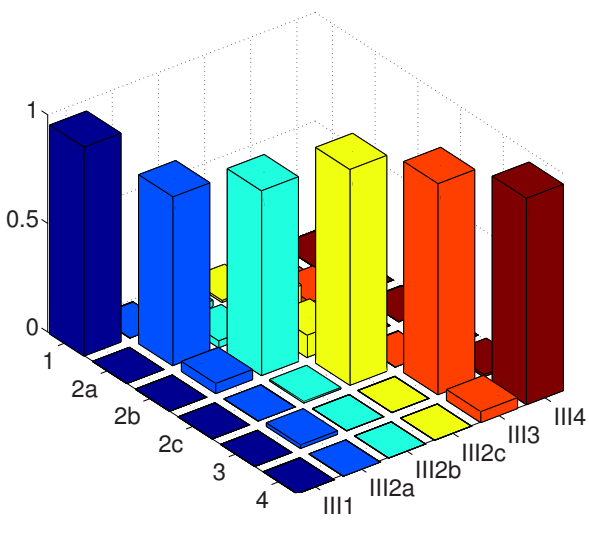


(a)

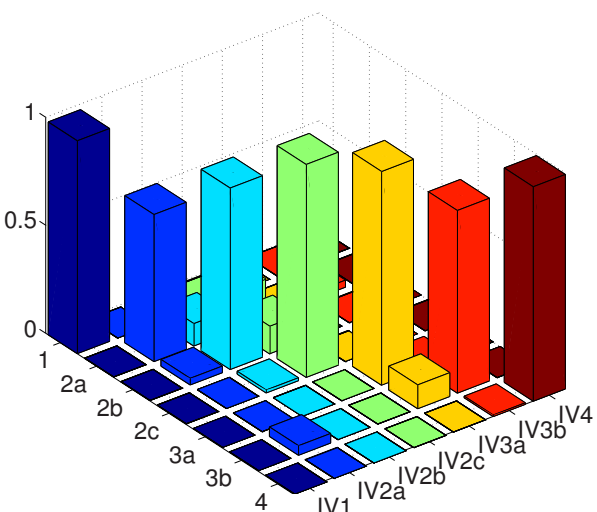


(b)

(See next page for figure caption.)



(c)



(d)

Fig. 7.13. Confusion matrices for BMA recognition using HMM for classifiers (a) I, (b) II, (c) III and (d) IV under subject specific training. The horizontal axes in each case represent known and recognized BMA classes. The notation IV2b means - class label 2b (right arm movement) for the classifier IV.

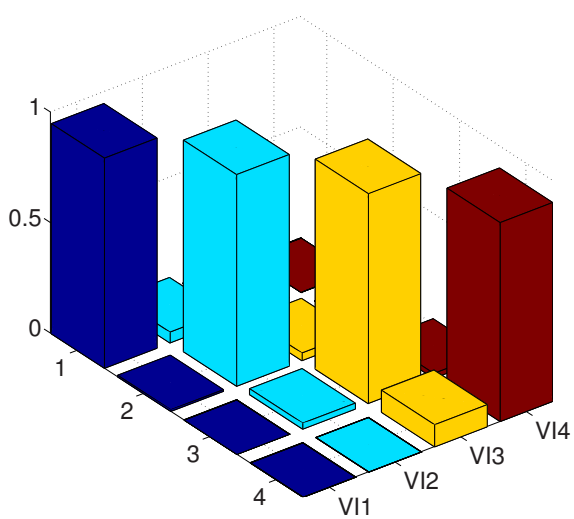
activity. The classifier V has eight BMA classes including the previously considered seven different BMA classes. The accuracy of the classifier V is 88.6%.

Table 7.4. Accuracies of BMA classifiers I to V for a single subject with different numbers of states and mixture components in HMM.

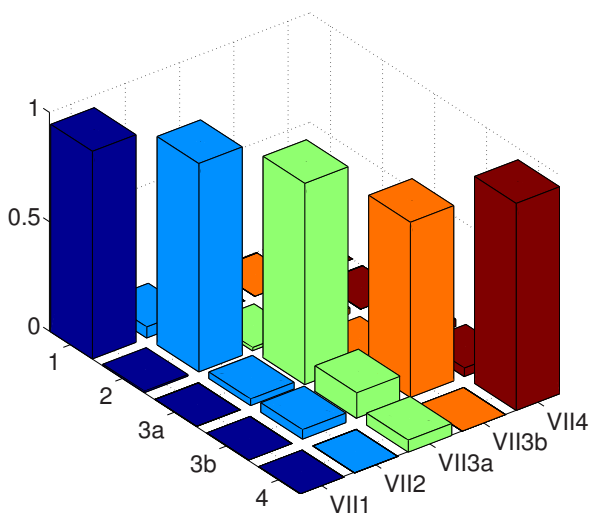
BMA Classifier	accuracy (%)			
	$\mathcal{Q} = 3, \mathcal{M} = 3$	$\mathcal{Q} = 3, \mathcal{M} = 4$	$\mathcal{Q} = 4, \mathcal{M} = 3$	$\mathcal{Q} = 4, \mathcal{M} = 4$
	98.6	98.0	97.8	97.1
I	96.9	97.4	97.9	94.6
II	90.8	92.9	91.8	90.2
III	92.2	91.5	89.8	88.9
IV	91.9	90.2	89.1	89.8
V				

Since we do not know exactly what are the best numbers of states and mixture components to choose for the HMM in the classifiers, we have selected the same combination of numbers of states and mixtures to represent each of the BMA classes. We have tried four different such combinations, e.g., $(\mathcal{Q} = 3, \mathcal{M} = 3)$, $(\mathcal{Q} = 3, \mathcal{M} = 4)$, $(\mathcal{Q} = 4, \mathcal{M} = 3)$ and $(\mathcal{Q} = 4, \mathcal{M} = 4)$, for all the five classifiers I to V. The remaining parameters are all as specified above for the subject specific classifiers I to V. The recognition accuracies for the classifiers I to V for the four different combinations of $(\mathcal{Q}, \mathcal{M})$ are presented in Table 7.4. We found that there is no further gain in terms of classification accuracy with more number of states or mixture components.

To verify the ability of classifiers I to V for handling inter-personal variability, a combined training over multiple subjects is provided to the corresponding multi-subject classifiers, VI to X. We train the classifiers using the training data collected from all the subjects. With this combined training the classifiers are tested against possible inter-personal variations in motion artifact signals for the same BMA. We had carried out similar experiments for PCA-based method also. The aggregate confusion matrices for the BMA classifiers VI to IX using HMM are shown in Fig. 7.14. Here also, like the subject specific training, the confusion takes place among the BMA classes of movements of left, right and both arm(s). Similarly, there are confusions taking place among walking and climbing up/down stairs classes. The classifiers VI to X for the combined subjects training have accuracies of 94%, 91.8%, 87%, 86.2% and 85%, respectively. It is observed, as in the previous case of PCA-based BMA classification, that the HMM-based method performs better if the subject specific training is provided. Though the accuracies obtained with the combined training as compared to those with subject specific training are on lower side, the deterioration in the HMM-based method is less than that using the PCA-based method discussed in the previous section.

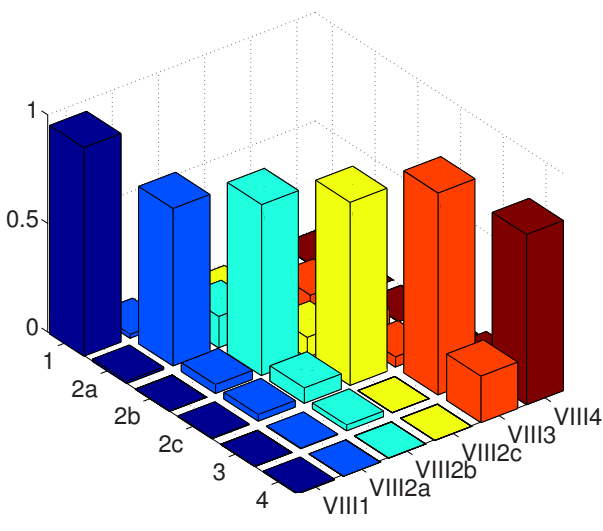


(a)

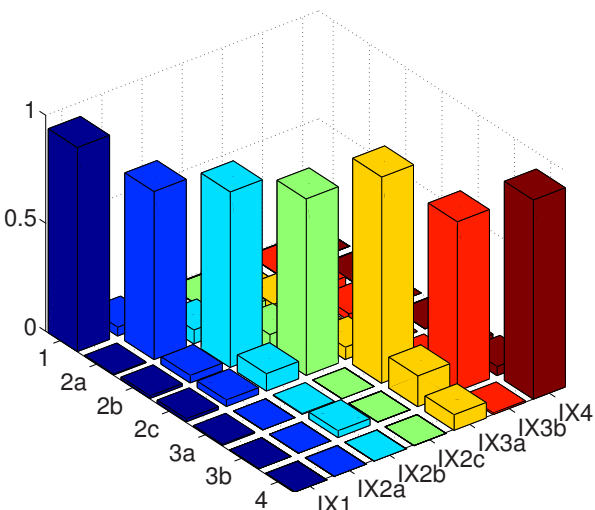


(b)

(See next page for figure caption.)



(c)



(d)

Fig. 7.14. Confusion matrices for BMA recognition using HMM for classifiers (a) VI, (b) VII, (c) VIII and (d) IX under combined training. The horizontal axes in each case represent known and recognized BMA classes.

In this chapter, we have discussed two techniques for BMA recognition from the motion artifacts in the ECG signal. Now we compare the accuracy of BMA classification for the HMM-based method with that of the PCA-based method. The average accuracies obtained on the data set considered in this experiment with the classifiers I to V are presented in Table 7.5 for both HMM-based and PCA-based methods. It is observed that the HMM-based method has higher accuracy of classification than that of the PCA-based method for all classifiers I to V and in both the cases with subject specific training and with combined training for all subjects. It is also noted that the standard deviation in the accuracy across the different individual subjects in case of subject specific training, is very small for the HMM-based method. Thus the HMM-based method is more consistent over the entire subject population. The comparison of accuracies with combined subjects training for both the techniques shows that the HMM-based technique works very well even with the inter-personal variations in the ECG. The HMM-based method is less sensitive to the inter-personal variations and it can handle such variation very well as opposed to the PCA-based method.

Table 7.5. Comparison of accuracies of BMA classifiers I to X for the subject specific (I-V) and combined (VI-X) training for PCA and HMM based methods. Accuracy for subject specific recognition is presented in terms of mean and standard deviation across all subjects.

method	accuracy (%)	BMA Classifier				
		I	II	III	IV	V
HMM-based subject specific	mean	97.1	96.7	91.8	89.9	88.0
	std. dev.	2.0	2.3	0.7	1.0	1.7
PCA-based subject specific	mean	93.7	88.8	82.5	77.4	75.1
	std. dev.	6.5	9.2	3.9	8.9	7.8
		VI	VII	VIII	IX	X
HMM-based subjects combined	mean	94.0	91.8	87.0	86.2	85.0
PCA-based subjects combined	mean	84.9	79.9	78.4	73.5	65.8

We have also analyzed the effect of the length of the test sequence $F(n, N_0)$ on the BMA recognition using the HMM-based classifiers. For all the classifiers I to V we find that the recognition accuracy improves with the increasing length of the test input from $N_0=300$ samples (≈ 1.24 s) to $N_0=1200$ samples (≈ 4.96 s). The mean accuracy across the subjects along with the vertical bars indicating the standard deviation versus the length of the test sequence is plotted in Fig. 7.15. In order to achieve a good accuracy of BMA classification using the HMM-based method a reasonable choice of length of the test sequence is found to be about 5s.

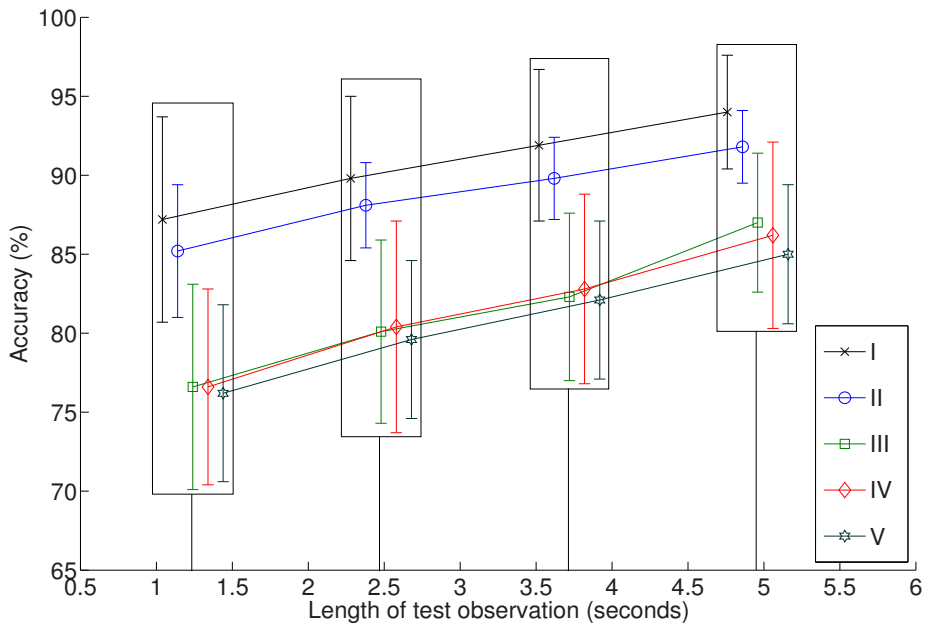


Fig. 7.15. Accuracy vs. length of the test sequence for the BMA classifiers I to V. Height of the vertical bars at each of the coordinates indicates one standard deviation above and below at that point. Five plots correspond to five different classifiers I-V.

7.5 Discussion

In this chapter we have studied classifiability of various BMAs like sitting still, movement of arms, walking and climbing stairs up and down, using the motion artifacts present in ECG signals. It is observed that different BMAs have different separations among them and this determines the accuracy of classification. For example, while climbing up stairs is recognized with a good accuracy ($P_T = 99\%$), there exists a moderate confusion between walking and climbing down stairs and a significant confusion among the movements of left, right and both arms. When we merge two overlapping classes such as walking and climbing down stairs into a single BMA class, the performance expectedly improves. It would be of interest to study the confusion level if the pace of walking/climbing downstairs is increased. Similarly, confusion levels in the case of vigorous arm movement will be of interest. Currently, we have refrained from such activities that may impose stress on the heart, a condition we wanted to preclude in this preliminary study on BMA recognition from motion artifacts.

The performance is the best when the classifier is provided subject specific training, meaning that personal training is recommended rather than generic training on multiple subjects.

In order to be able to use the given PCA-based method, we had to resort to resampling of the ECG beats to match the dimensionality, which may introduce certain artifacts in the QRS complex. Another possible option is to do zero padding to match the dimension. However, this would introduce artifacts in the signal representing BMA that is prevalent over the entire beat duration. In order to avoid that we suggested the use of HMM-based classification.

We have shown that the time localized spectral features of the motion artifact signal can be used for BMA recognition. We have achieved better recognition rates using the HMM-based method as compared to PCA-based method. We have also given a scheme using an adaptive filter for separating motion artifact signal from the ECG which can be used for the estimation of the cardiac cycles in the ECG signal contaminated by the motion artifact. We have found that a 5s long recording is ideal for BMA recognition. A smaller length of the data results in a reduced accuracy, while a longer length of the data will add to the system delay.

We have also experimented on the effect of varying the number of states and mixture components for the HMM. However, a much more elaborate evaluation is needed to ascertain what would be the correct HMM model for classification purposes.

For the given supervised learning technique, the available ground truth is in terms of labels that qualitatively describe activities (e.g. walking gently). However, a more precise labeling of BMA in terms of speed and rigorousness is likely to provide a better understanding of the impact of the resultant motion artifacts. This may be achieved by attaching a network of motion sensors to the body and recording the motion signals synchronously with the ECG signal. In the next chapter we will study the impact of levels of BMA on motion artifact generation quantitatively by using the ground truth from the acceleration signals captured from the moving body parts.

Impact of Ambulation

In previous chapters we have discussed methods for detecting and recognizing different body movement activities (BMAs) from the analysis of the ECG signal acquired under ambulation. The ECG signals have been analyzed to show that the motion artifacts induced by various BMAs can actually be classified into different types which allows recognition of BMA from the ECG itself. The methods discussed so far deal with the commonplace BMAs performed at a normal pace. The constant normal pace of activity allowed us to exclude more complicated situations arising out of variations in the pace levels of the same BMA. However, in real life, different pace levels of any commonplace BMAs are usually described as slow, normal and fast. This kind of variations in the body movement kinematics may also have some impact on the generation of the motion artifacts in the ECG signal. In this chapter, our purpose is to determine the impact of body movement kinematics on the extent of ECG motion artifact by defining a notion called impact signal. The impact signal is derived from the ambulatory ECG signal itself. Two approaches have been adopted in this chapter to validate the basic hypothesis that the impact signal does provide a good measure of the pace of ambulation. One of them involves measuring local acceleration using motion sensors at appropriate body positions, in conjunction with the ECG, while performing routine activities at different pace levels. The other method consists of ECG acquisition during treadmill testing at controlled speeds for fixed durations. Ambulatory ECG signals and the required data about the pace of the activity have been acquired from healthy subjects as well as patients with suspected cardio-vascular disorders. In case of patients, the treadmill tests were carried out under the supervision of a cardiologist. We demonstrate that the impact signal shows a proportional increase with the increasing activity levels. The measured accelerations obtained are also found to be well correlated with the impact signal. The impact analysis thus indicates the suitability of the proposed method for quantification of body movement kinematics from the ECG signal itself, even in the absence of any accelerometer sensors. Such a quantification would also

help in automated documentation of patient activity levels, which could aid in better interpretation of ambulatory ECG.

8.1 Introduction

Ambulatory ECG analysis is adversely affected by motion artifacts induced due to body movements. Knowledge of the extent of motion artifacts could facilitate better ECG analysis. The context of ambulation in ECG analysis plays an important role particularly for monitoring with wearable ECG recorders (W-ECG) for which the patient ambulation is quite unencumbered. During monitoring with W-ECG an accurate diary of physical activities is maintained to facilitate better analysis of the ECG ‘in context’ [43]. It is difficult to provide exact details of the physical activities just by describing a physical activity qualitatively in words and the time stamping of various events by a human user may be quite inaccurate. This difficulty has been solved partially by developing W-ECG systems with evidence based patient activity monitoring in [17, 43, 86, 145]. These systems incorporate accelerometers with ECG recording apparatus, in order to provide information about patient activity levels. However, any exact analysis of the impact of the activity levels as recorded by the accelerometers on the ECG has not been studied yet. Since the primary goal of W-ECG is to monitor ECG signal, it is required to derive a quantitative measure of the quality of the ECG signal rather than just the activity levels being monitored by the accelerometer signals. Here we quantitatively investigate the precise impact of various levels of BMA on the generation of motion artifacts in the ECG signal.

We have shown in Chapter 6, that it is possible to detect the onsets of body movements, or transitions from one movement to another, from the ECG signal itself using a recursive principal component analysis (RPCA) based method. This is based on the fact that different types of body movements affect the skin electrode interface differently. In this chapter, we first define a notion called impact signal which is derived from this RPCA and demonstrate through a number of experiments that the proposed impact signal can be applied for impact analysis of body movement activity (BMA), and consequently, for determining different levels of body movements from the ECG signal itself. We show that it is a measure of induced motion artifact on the ECG signal.

For quantifying subject activities, we perform two different sets of experiments: one using the treadmill test, and the other using commercially available accelerometers. The treadmill test, a benchmark in stress testing for cardiac patients, is calibrated in terms of energy expenditure for standard test protocols, like the Bruce protocol. The output from triaxial accelerometers on the human body have been quantified as a function of energy expenditure in [16], and hence the activity level of a subject. Accelerometric measurements and treadmill speeds have been shown to be well correlated in [31]. Accelerometry

has been used for studies of body movements in [81, 82, 83]. We report our observations on the magnitude of the impact signal in relation to the walking speed of the subject in the treadmill test, as well as the recorded accelerations while performing various types of body movements at three different pace levels: slow, normal and fast. We note that slow body movements may induce motion artifacts of smaller magnitude whereas quick body movements are likely to induce larger motion artifacts. At rest, there are usually no motion artifacts at all. Thus different levels of body movements may have different impact on the motion artifacts and hence on the ambulatory ECG signal. We thus show that BMA levels can be quantified from the ECG signal itself using the impact signal, without using any sophisticated motion sensors. In other words, we demonstrate that it is, indeed, possible to have a truly unencumbered ambulatory cardiac monitoring system without the use of multiple inputs from accelerometers tethered to the body, with activity detected from just a single lead of the ECG. This is useful for development of a simple, low cost, ECG monitoring system which can automatically provide information about BMA from the ECG signal.

The chapter is organized as follows. We describe a method for deriving the impact signal in Section 8.2. In Section 8.3, it is explained how we synchronized the free running clocks of two different systems, the W-ECG equipment and the motion sensor system. The results obtained from various experiments with treadmill and motion sensors are presented in Section 8.4. We discuss about the experimental results and conclusions in Section 8.5.

8.2 Derivation of Impact Signal

We use the RPCA error signal as derived in Section 6.2, at every R peak locations from the analysis of appropriately time warped ECG beats. We repeat the RPCA based algorithm here for the ease of reading.

Since we use PCA based method which is sensitive to feature alignment, it is required that the input data vectors have the same dimension. The ECG beats are therefore time synchronized with respect to R peak in each beat, and resampled to a fixed length of M_0 samples, to account for possible heart rate variability (HRV). The value of M_0 is chosen based on the normal heart beat duration and the given sampling rate of the ECG recorder. In our experiments presented here, we encountered the heart rate variations from 64 to 160 (under the stress test) beats per minute. The R peaks in the ECG signals are detected using a modified Pan-Tompkins algorithm [96] as discussed in Chapter 6. The current ECG beat length is estimated as the duration between the current R peak and the previous one.

In order to estimate the principal components, the covariance matrix C_i is recursively computed from the i^{th} length normalized and mean subtracted ECG beat $\underline{r}(i)$ as

$$C_i = \sum_{k=1}^i \alpha^{(i-k)} \underline{r}(k) \underline{r}^T(k) = \alpha C_{i-1} + \underline{r}(i) \underline{r}^T(i), \quad (8.1)$$

where α , $0 < \alpha < 1$ is the *forgetting factor*. A set of top L eigenvectors of the covariance matrix C_i at i^{th} ECG beat is derived using Eq. (8.1). Let $E_i = [\underline{e}_{i1} \underline{e}_{i2} \dots \underline{e}_{iL}]_{M_0 \times L}$ be the set of top L eigenvectors arranged in a non-ascending order of magnitudes of the corresponding eigenvalues. To quantify the variation in the ECG signal due to motion artifacts, we obtain from the next ECG beat $\underline{r}(i+1)$ the component that lies in the span $\{\underline{e}_{i1}, \underline{e}_{i2}, \dots, \underline{e}_{iL}\}$. The error in approximation

$$\epsilon(i) = |\underline{r}(i+1) - (E_i E_i^T) \underline{r}(i+1)| \quad (8.2)$$

provides a measure of the level of motion artifact in the ECG, i.e. the impact of body movement in ambulatory ECG signal. The error $\epsilon(i)$ defined in Eq. (8.2) is called the impact signal for the i^{th} beat. The impact signal could be non-uniform on the time scale due to the beat to beat variations in the heart rate. The exact time instant of the impact signal can be calculated from the R peak location corresponding to the beat index i in the ECG signal. Then it is possible to compare the impact signal with the accelerometer signals at same time instances.

8.3 Synchronization of Impact and Motion Data

We have explained how we acquire the motion data from accelerometers in Chapter 5. We again reiterate the fact that for the impact signal, we use the index ‘ i ’ to denote time axis, while we use the index ‘ n ’ to denote time while measuring acceleration. This is due to the fact that

1. the impact is measured at every heart beat duration of which is variable and
2. the sampling frequencies for the ECG and the motion sensors are different.

The two indices are related in time as $n = \kappa(i)$, where κ is a function of the time instances of occurrence of each QRS complex in the input ECG. In order to synchronize the acceleration and impact signals, we need to calculate the cross-correlation ρ between them.

To compensate for non-uniform sampling rate of the impact signal $\epsilon(i)$, the impact signal is upsampled to 242Hz (sampling frequency of the W-ECG) using a cubic spline interpolation. For comparison between the impact signal and the acceleration signals, the interpolated impact signal is downsampled to 25Hz (sampling frequency of the motion sensor). This two stage process is required because the impact signal is non-uniformly sampled on the time scale as the RR interval may vary with time for an individual. As the motion sensor and ECG acquisition starting times could be slightly different, it is also essential to have an automatic means to calculate the time delay between them.

The location of the peak of the cross-correlation between the acceleration data $\beta_k(n)$ [see Chapter 5 for definition of $\beta_k(n)$] and the time warped impact signal $\epsilon(n)$ is used as a measure of this time delay to synchronize the ECG and motion sensors. Having synchronized these two different types of sensors, the index function $\kappa(i)$ can be easily computed from the warped impact signal. The usefulness of the function $\kappa(i)$ will be clear in the next section when the data from two different sensors are compared at a given instant of time.

8.4 Experimentations

Continuous lead-II ECG signals are recorded as described in Sections 5.4 and 5.6 for the direct motion sensing and the treadmill experiments involving the variations in the pace levels of the BMA. The results for these two types of experiments are reported separately. Data are collected from healthy subjects as well as patients with cardiac disorders. In case of patients, ectopicity in QRS complexes are manifested as major spikes in the impact signal, as mentioned in Chapter 6. To obtain a correct estimate of the impact in these cases, ectopics have to be separated from the input data stream by standard preprocessing techniques discussed in the literature [20, 65, 97]. In [65], an adaptive, model based technique is provided for estimation of width and shape parameters of the QRS complex. Autoregressive modeling of envelopes of coefficients of discrete cosine transform of the QRS complex is discussed in [97]. Application of a neural network for classification of normal and abnormal ECG beats is given in [20]. Having detected the ectopic beat, one may discard abnormal spikes in the impact signal. However, owing to the inability in handling frequent ectopics, the method is not found to work well in subjects where ventricular bigeminy is observed, i.e. one normal QRS complex followed by an ectopic one, alternately.

8.4.1 Experiments on the Treadmill

In the experiment involving the treadmill, our endeavor is to find a relation between the impact signal and the treadmill speed for quantification of the impact signal. Most subjects take some time to adjust to the movement on the treadmill during the first stage of the exercise due to the sudden and jerky start, which consequently affects their gait for reactive stabilization, and results in increased motion artifacts. Subsequently, the subject adjusts to the motion of the treadmill and this steady state behavior is studied in this chapter. We report our findings for healthy subjects and cardiac patients separately as below.

Case I (Healthy Subjects)

Data from healthy volunteers are acquired with different treadmill speeds at zero inclination. Once the subject is settled on the treadmill, the impact

signal ϵ shows an increase in amplitude with increasing treadmill speed. This is illustrated in Fig. 8.1, in which are plotted the mean impact signal m_j , along with the standard deviation σ_j , for j^{th} treadmill speed. This clearly demonstrates that as the human motion activity increases, it can be easily captured from the impact signal derived from the ECG signal itself. The discrepancy in the plot at the beginning is due to jerky start of the treadmill as explained earlier. The variance of the strength of impact signal at a given treadmill speed, shown in this plot, makes a very interesting observation. We observe that, for the j th speed

$$m_j + \sigma_j < m_{j+1} - \sigma_{j+1}.$$

If for a given speed of the treadmill, the impact signal is assumed to be Gaussian distributed, this would mean that, given the measure of the impact signal ϵ , one can correctly identify the treadmill speed in more than 68% cases as the area of a Gaussian probability density function within the range $[m - \sigma, m + \sigma]$ is about 0.68. Given that we work with a single lead ECG recorder, this can be considered quite an accurate measurement technique. Computing the cross-correlation between the impact signal and the treadmill speeds yields a typical correlation coefficient of $\rho = 0.95$, which also indicates a strong collinearity among them.

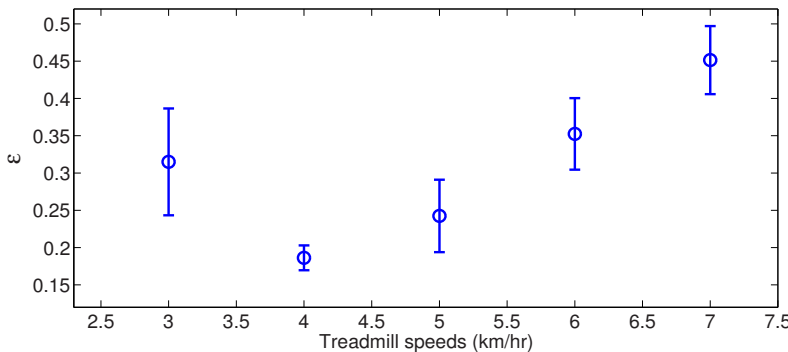


Fig. 8.1. Illustration of the relation between the impact signal and treadmill speeds for a subject walking at different speeds on a treadmill. The large dot represents the mean value of the impact signal (ϵ), with the vertical bars representing the standard deviations around the mean. The horizontal axis is the treadmill speed in km/hr. The first stage on the treadmill shows a larger value of ϵ , due to the initial discomfort of the subject on the treadmill.

Case II (Cardiac Patients)

Patients who undertook the stress test could barely complete three stages of the Bruce protocol. The impact signal for one such subject is shown in

Fig. 8.2(a). As in case of normal subjects, ϵ increases with increasing treadmill speed. From the plot of mean impact signal m_j in Fig. 8.2(b), we find that

$$m_j + \sigma_j < m_{j+1} - \sigma_{j+1}$$

described in Case I, again holds true. The discrepancy in the value of ϵ in the first stage as explained earlier is also observed here. This suggests that the impact signal provides a good estimate of treadmill speed irrespective of whether the QRS complexes of the subjects are normal or abnormal. There is a small treadmill inclination associated with the Bruce protocol, which increases gradually with every stage. We ignore this inclination, as magnitude of this slope is very small at the first few levels of the protocol.

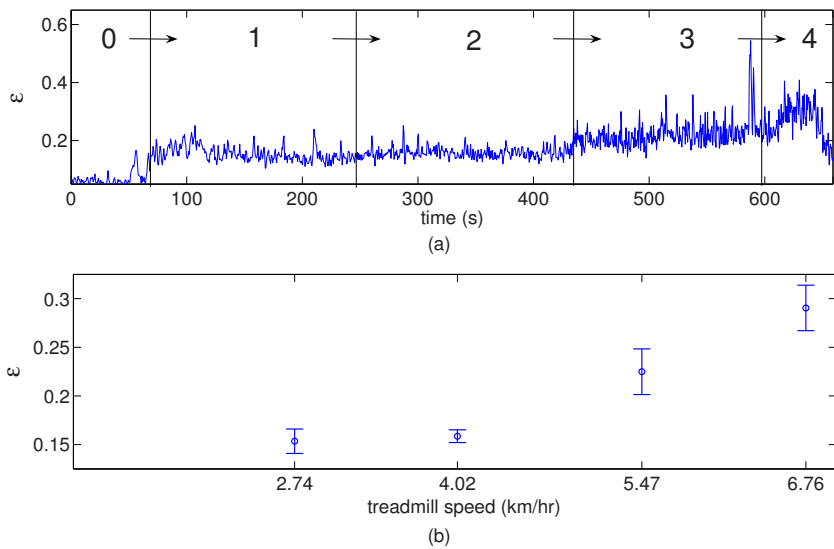


Fig. 8.2. Plots of the impact signal ϵ for a cardiac patient whose treadmill test is terminated after 30 seconds into the fourth stage of the Bruce protocol. The first stage in both plots shows a comparatively large value of ϵ , due to the initial adjustment issues of the subject on the treadmill. (a) Plot of ϵ vs. time in seconds on the treadmill. The corresponding stages are indicated by numbers at the top, with ‘0’ indicating resting conditions. (b) Plot illustrating the relation between ϵ and treadmill speeds. The large dot represents the mean value of the ϵ , with the vertical bars representing the standard deviations.

The treadmill exercise involves putting the heart through a certain amount of stress, with peak heart rates touching 150 beats per minute. Such a stress may result in temporary morphological changes in the ECG, more so in case of patients with an ischemic heart disease [32]. The nearly linear trend of the

impact signal with respect to the treadmill speed despite these morphological variations can be explained by the fact that these changes are gradual compared to the motion artifact, and the RPCA method adapts itself to gradual variations. From this we conclude that the impact signal provides a good estimate of activity levels even when the heart is subjected to high levels of stress.

8.4.2 Experiments with Motion Sensors

In our experiment with motion sensors, since our objective is to evaluate the applicability of ambulatory ECG monitoring, some typical BMAs are chosen as explained in Section 5.4. The impact signal is derived from the ECG signal described in Section 8.2, while the acceleration signals are analyzed according to the procedure given in Section 8.3. The goal here is to determine a relationship between the impact signal $\epsilon(i)$ with the kinematic measures like acceleration $\beta_k(n)$ and displacement $\gamma_k(n)$.

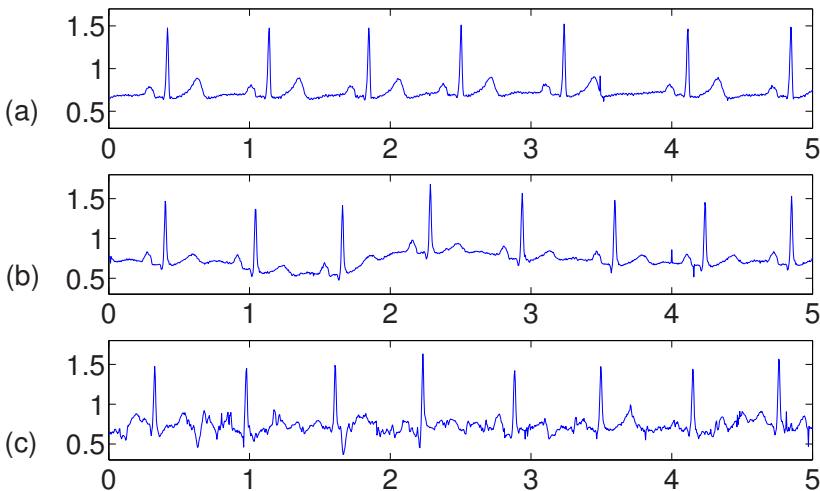


Fig. 8.3. Illustration of ECG signal for a normal subject while different ambulation activities. (a) sedentary ECG signal without any body movement, (b) ambulatory ECG signal of the same subject while moving his left arm, (c) ambulatory ECG signal of the same subject while walking. The horizontal axes are time in seconds in all plots shown.

Before we quantify the effect of ambulation on the acquired ECG, we illustrate the effect by plotting the ECG traces for a normal subject with and without the body movement in Fig. 8.3. The sample ECG under a sedentary

condition without any body movement is shown in Fig. 8.3(a). The corresponding ECG trace for the same subject while moving his left arm is shown in Fig. 8.3(b). Fig. 8.3(c) shows the effect of walking for the same subject. It is quite clear from the plots that the corresponding ECG traces are very different in terms of ambulation artifacts.

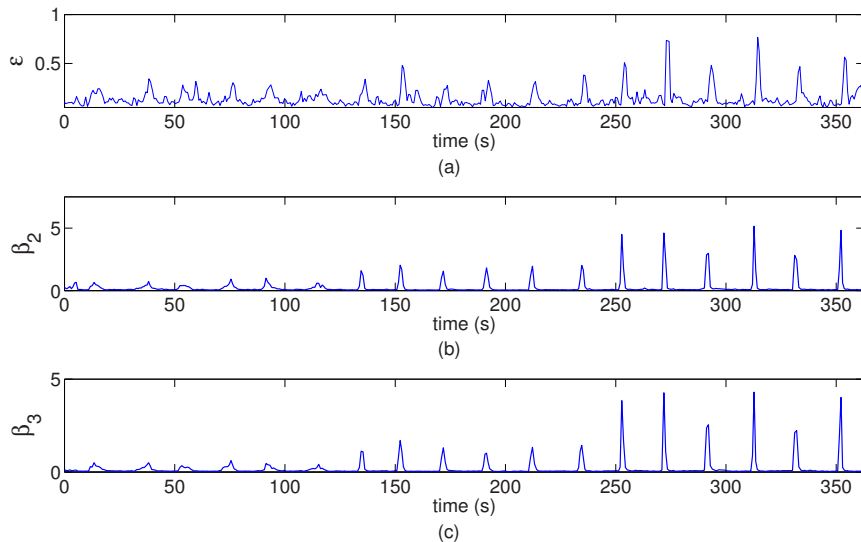


Fig. 8.4. Illustration of impact signal ϵ for change in posture alternating between sitting down and standing up three times each with three different levels: slow (0-120s), medium (120-240s) and fast (240-360s). (a) Impact signal derived from the ambulatory ECG signal, norm of acceleration (m/s^2) for sensor attached at (b) right leg, and (c) frontal waist. (©2007 IEEE)

First, we look at the impact of posture changes, requiring subjects to sit down and stand up alternately at three different intensity levels: slow, medium and fast, with a motion pause of nearly 20 seconds in between. The impact signal for a subject due to these posture changes is shown in Fig. 8.4(a), while the corresponding accelerations $\beta_k(n)$ are shown in Fig. 8.4(b-c). We observe that the magnitude of the impact signal follows the pattern of the acceleration $\beta_k(n)$, i.e., low, medium and high, indicating that the impact signal is a quantitative measure of the levels of the body movement similar to acceleration. From the plot of the impact signal, the exact instants when the posture changes were effected can be identified very easily. This can be verified from the accelerometer data.

Next we analyze the act of climbing up and down on a staircase of 36 steps, again at three different intensity levels. A rest period of 30 seconds is allowed

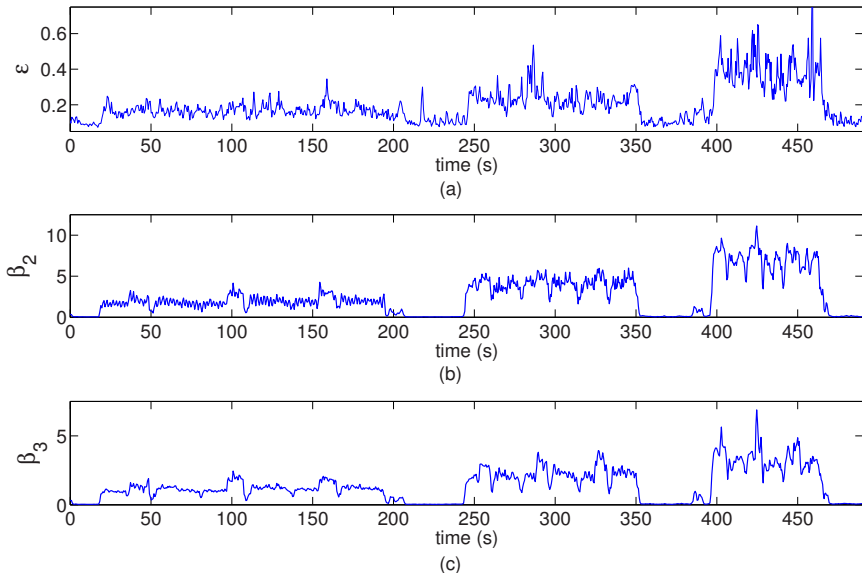


Fig. 8.5. Illustration of impact signal ϵ for climbing stairs with three different paces: slow (18-206s), medium (244-352s) and fast (395-470s). (a) Impact signal derived from the ambulatory ECG signal, norms of acceleration (m/s^2) for sensor attached at (b) right leg, and (c) frontal waist. (©2007 IEEE)

after finishing each level. The impact signal $\epsilon(n)$ for this activity for a subject and the corresponding acceleration signals $\beta_k(n)$ are shown in Fig. 8.5. From the amplitudes of signals in the figure and their time spans it is apparent that the impact signal does quantify the different levels of body movement while climbing stairs. For slow motion, both the impact signal and the acceleration measures are less in magnitude. They both increase proportionately as the pace increases.

We now consider rotation of the torso at the waist, with both hands firmly at the hips (so that they do not move with respect to the trunk), at three different intensities: slow, medium and fast, with a little rest in between. The impact signal $\epsilon(n)$ for a subject and corresponding accelerations $\beta_k(n)$ from the motion sensors placed at right leg and frontally at the waist are shown in Fig. 8.6. The relative variation in amplitude across the three paces of movement remains similar for all motion sensors. Specifically, the twisting body movement is well represented by the sensor placed on the waist, and the corresponding impact on ambulatory ECG is evident from the amplitudes of the impact signal for the three different levels of motion activity.

Next, we look at the impact of the extent of body movement on the ECG signal. Arm movements have a larger extent as compared to usual leg and waist movements, as the shoulder joint is one of the most freely movable joints in the human body with a large range of motion (ROM). Hence we consider

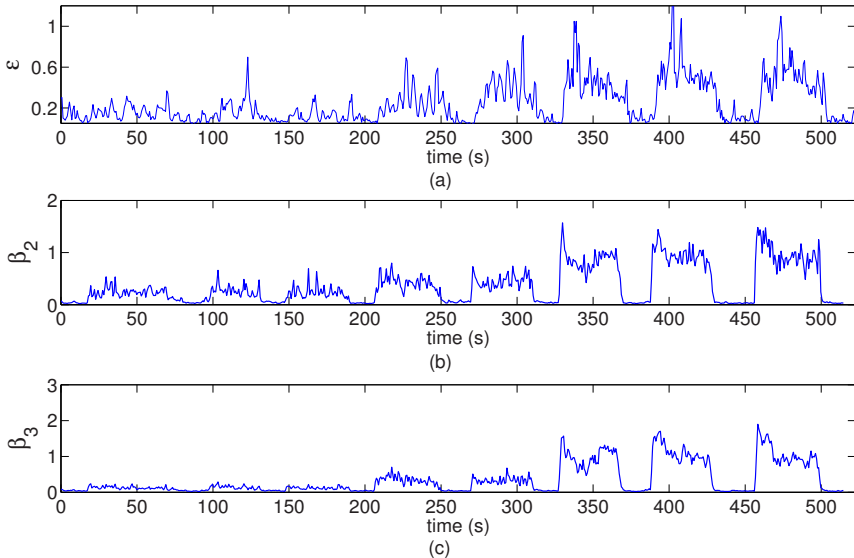


Fig. 8.6. Impact signal ϵ while twisting the torso at the waist with three different paces: slow (17–191s), medium (206–312s), and fast (326–500s). (a) Impact signal derived from the ambulatory ECG signal, norms of acceleration (m/s^2) for sensor attached at (b) right leg, and (c) frontal waist. The troughs intervening the high magnitude regions correspond to the resting time between consecutive action phases. (©2007 IEEE)

arm movement with flexion at the shoulder joint parallel to the sagittal plane of the body. For this purpose, the subject is asked to swing one of the arms to different angular extents: very small ($\pm 10^\circ$ from rest), small ($\pm 30^\circ$), moderate ($+60^\circ$ to -45°) and wide ($+90^\circ$ to maximum ROM angle backward). Approximately the same pace is maintained throughout the different extents of arm movement, with the other arm kept at rest by the side of the body. An instance of the impact signal $\epsilon(n)$ for this activity involving the right arm, with corresponding acceleration signal $\beta_1(n)$ and displacement signals $\delta_1(n)$ [see Chapter 5 for definition] of the sensor placed on the right arm are shown in Fig. 8.7. Except in the case of very small extent of movement, the magnitudes of acceleration for the other extents are nearly at the same level. There is a discernible increase in the amplitudes of the corresponding impact signal, associated with the increasing displacement levels. That shows the impact of extents, e.g. very small, small, moderate and wide movements of right arm on the ECG signal. Hence, it is not just the pace (as quantified by the acceleration) that determines the motion artifacts, the extent of motion (such as stride length, etc.) also plays an important role in determining the impact of the body movement on the ECG data. A similar exercise is also performed with the left arm. However, for the lead-II configuration, the impact signal is

not as sensitive to left arm movements as compared to right arm movements, as reported previously. It may be useful to adopt a different lead configuration for this case.

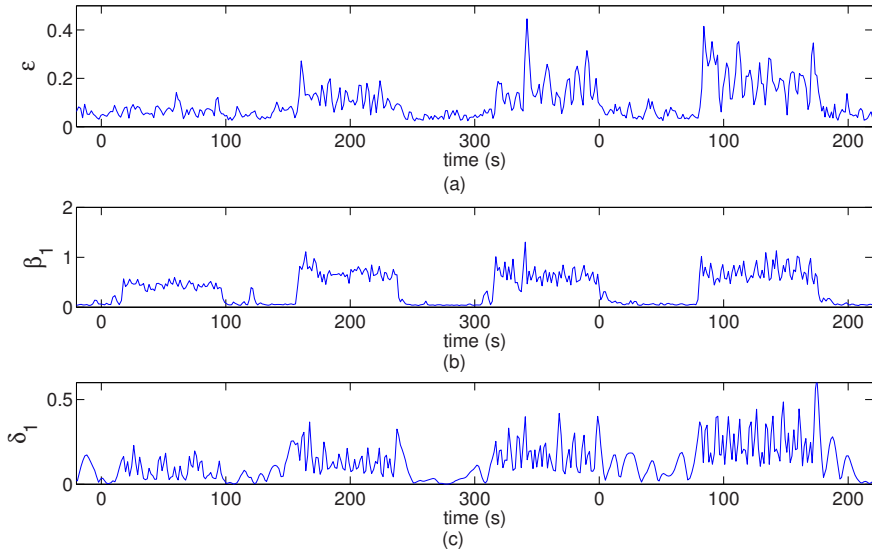


Fig. 8.7. Illustration of impact signal ϵ for right arm movement with four different extents with similar pace (very small:8–48s, small:78–120s, moderate:156–200s, wide:340–388s). (a) Impact signal derived from the ambulatory ECG signal, (b) norm of acceleration (m/s^2) for sensor attached at right arm, and (c) norm of displacement (m) for the sensor attached at right arm.

Now we study the combined effect of the pace of motion and the extent of the body movement on the acquired ECG data. Analysis of the impact for different strides (extents) and speeds of walking also indicates an increase in the amplitude of impact signal with the increase in acceleration. In addition, one also observes that for the same pace of the stride, a longer stride results in increased motion artifacts. A shorter but quicker stride may result in the same walking speed as a longer but slower stride. Looking at this from the perspective of the treadmill experiment, and considering that impact signal $\epsilon(n)$ is almost proportional to treadmill speed (see Fig. 8.1), this is an expected result. An illustration of the impact of walking is given in Fig. 8.8. The plot shows that an increased stride length (or extent of motion) has a greater impact on the generation of motion artifact than the pace of activity. The increased stride length while walking automatically requires an increased movement of arms for reactive stabilization of the body and hence the skin at electrode contact is involved in further stretching and contraction.

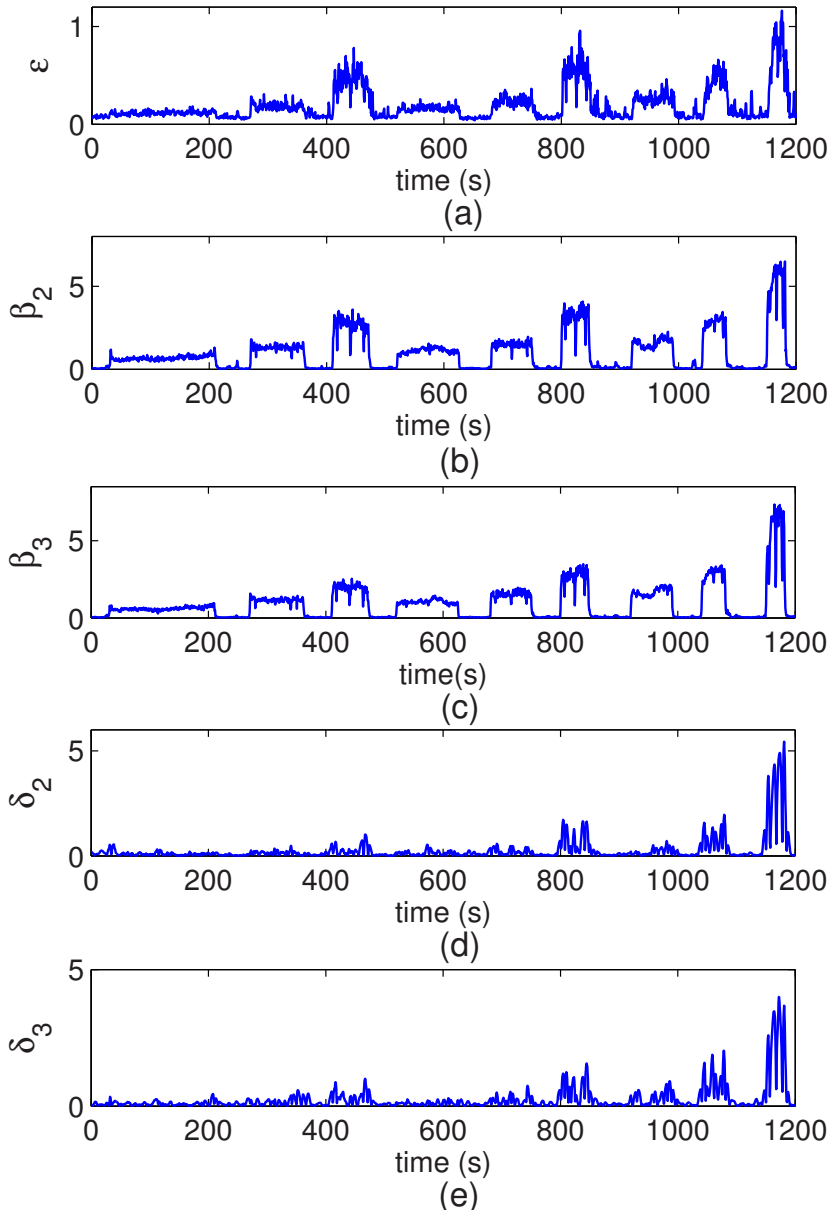


Fig. 8.8. Illustration of impact signal ϵ for walking with three different stride-lengths: 1, 2 and 3 ft. and at three different speeds: slow (1 ft: 25-207s, 2 ft: 265-358s and 3 ft: 405-470s), medium (1 ft: 515-621s, 2 ft: 675-747s and 3 ft: 795-843s) and fast (1 ft: 915-987s, 2 ft: 1035-1078s and 3 ft: 1145-1180s). (a) Impact signal derived from the ambulatory ECG signal, norms of acceleration (m/s^2) for sensor attached at (b) right arm, and (c) frontal waist, displacement as a function of time, captured by the motion sensor placed at (d) right arm, and (e) frontal waist. For (a), (b) and (c): ©2007 IEEE.

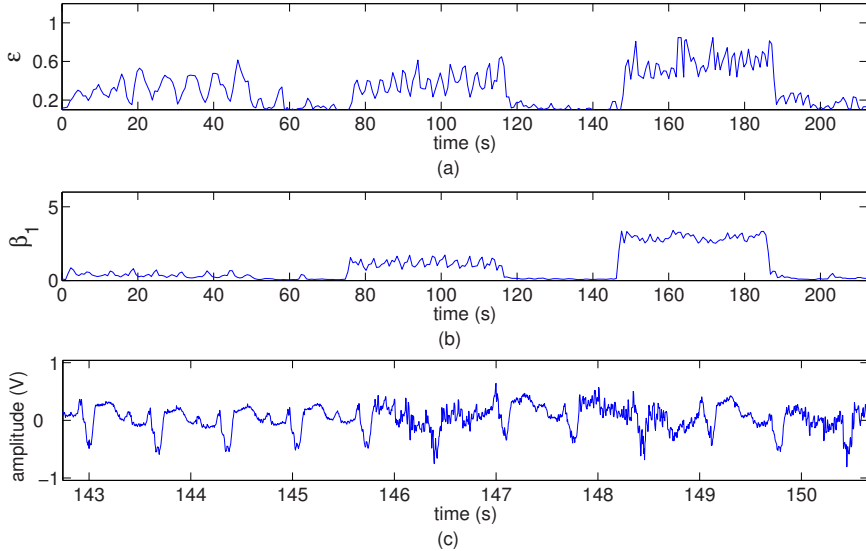


Fig. 8.9. Illustration of the impact signal ϵ of a cardiac patient for right arm movements at three different speeds : slow (0-50s), medium (75-120s) and fast (144-190s). (a) Impact signal derived from the ambulatory ECG signal, (b) norm of acceleration (m/s^2) for sensor attached at right arm, (c) a snapshot of the ECG signal recorded during this activity. Note the abnormal QRS morphology.

The motion sensor experiment also involves patients with cardiac disorders and anomalous QRS complexes. Since there is no existing protocol as yet and this experiment is not conducted under medical supervision, it is ensured that the overall intensity levels of the activity are lower for the selected patients to avoid undue physical stress. Fig. 8.9(a-c) shows the results for the movement of right arm as in Section 5.4 at three different speeds from a patient with a prosthetic aortic valve and a left bundle branch block (LBBB). From the ECG, we can observe that the QRS duration is more than twice that of a normal subject, the R wave amplitude is smaller than normal, and the S wave is predominant. However, the resulting trends are similar to that of healthy subjects. The RPCA method is largely unaffected by the vastly different QRS morphology in case of the cardiac patient data. Motion artifacts being an external influence at the superficial level of the skin, it must have similar effects on the ECG for both healthy subjects as well as those with cardiac abnormalities.

In our next attempt to analyze the acquired data, we remove the time dependence and plot the impact signal as a function of the instantaneous acceleration. This should ideally remove the human bias as we no longer know when a particular acceleration takes place and what the subject is actually trying to do at that instant. The scatter plot of the impact signal for the

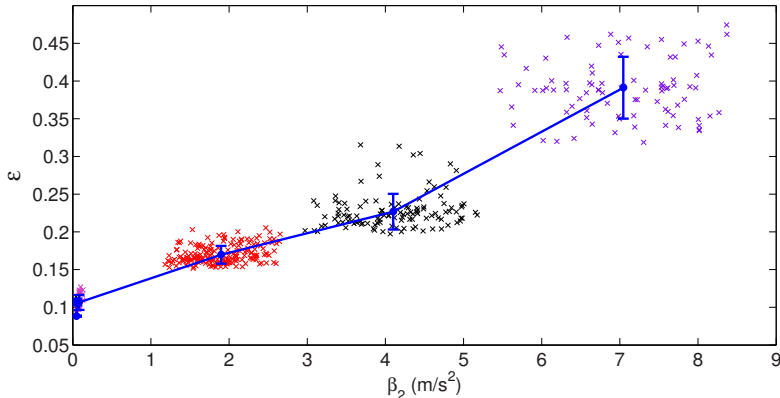


Fig. 8.10. Scatter plot of the magnitude of the impact signal ϵ as a function of norm of instantaneous acceleration while climbing stairs for the sensor attached at the right leg. Note the well defined clusters around the large dots, which represent the mean value of ϵ over 15 beats. The trend appears to be more or less linear, and the vertical bars, representative of the standard deviation of ϵ , indicate separability of acceleration levels at a resolution of nearly $0.2g$.

experiment on climbing stairs vs. norm of acceleration in Fig. 8.10 shows the presence of well defined clusters corresponding to different magnitudes of acceleration, underlining the fact that ϵ is a proper representative of activity levels. It is also clear that mean values of ϵ provide better estimates of activity levels than instantaneous values, although instantaneous values of the impact signal provide a fairly accurate indication of initiation or cessation of activity periods.

An alternative representation of the impact signal and the corresponding norm of instantaneous acceleration after temporal smoothing are illustrated in Fig. 8.11 and Fig. 8.12, associated with the activities of walking and twisting of torso, respectively. The linear relationship shows that the impact signal can be used for quantification of motion. Comparing Fig. 8.11 and Fig. 8.12, we note from the range of the impact signal that a smaller acceleration at the waist due to stretching of the body while twisting, causes a similar impact on the skin electrode interface, as a larger acceleration at the leg while walking. At zero acceleration, a finite value of error (≈ 0.1) is observed, analogous to background noise, which can be attributed to the beat to beat variability in the human ECG even at rest.

Plotting the cross-correlation between the acceleration signal $\beta_k(n)$ and the impact signal $\epsilon(n)$ indicates a strong correlation between the two quantities in time, with a typical correlation coefficient of 0.80. The location of the peak on the correlation plot also proves to be a good estimate of the time delay between the starting of motion and ECG data, as verified from the video recording of the experiment. As mentioned in Section 5.4.2, this is used in

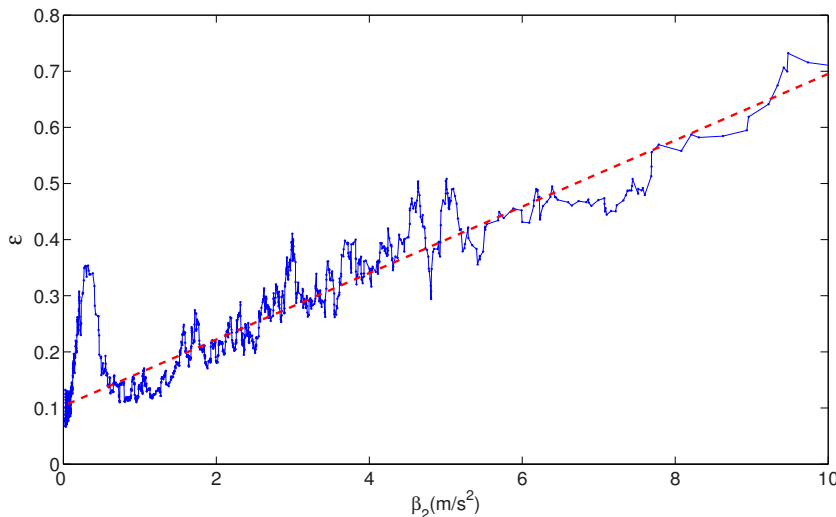


Fig. 8.11. Plot of the magnitude of the impact signal ϵ as a function of norm of instantaneous acceleration while walking for the sensor attached at the right leg. This indicates that as the activity level goes up, so does the motion artifact. The trend appears to be a linear one. (©2007 IEEE)

all plots to time synchronize the acceleration and impact signals. One of the plots showing cross-correlation between the acceleration signal and the impact signal while climbing stairs is shown in Fig. 8.13. In order to synchronize with the ECG data, we observe from the plot that the accelerometer data must be time shifted forward by 9.6s.

Presented in Table 8.1, is a summary of the global mean (μ) and standard deviation (σ) of the coefficient of cross-correlation (ρ) and slope (ω) of the line best fitting impact ϵ against acceleration data β , for climbing stairs and walking when experimented on different subjects. The cross-correlation values are high, while the low values of the standard deviation of ρ indicate less inter-personal variation. In other words, the impact signal is well correlated for most of the subjects. Standard deviation values for slope ω are marginally higher, indicating higher interpersonal variability in this regard. This implies that the method requires individual specific calibration for more accurate quantification of patient activity levels.

8.5 Discussions

We have studied the impact of body movements on generation of motion artifacts in ambulatory ECG recordings, and reported our observations on the

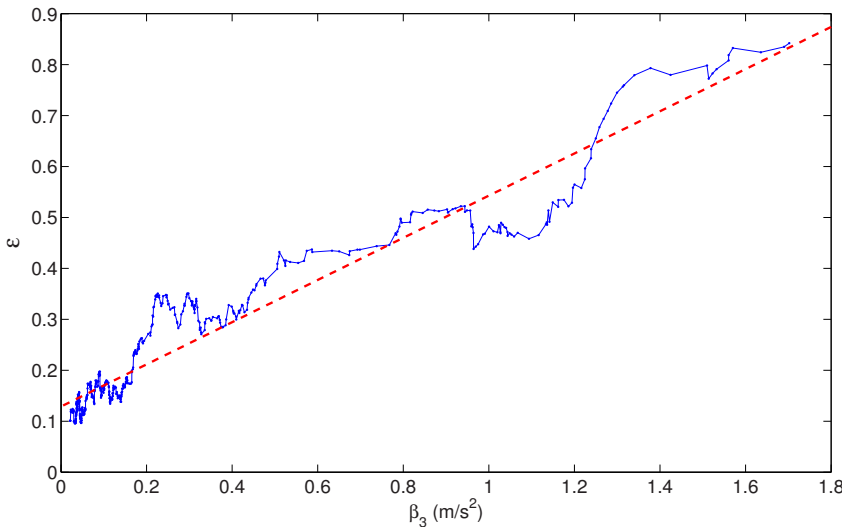


Fig. 8.12. Plot of the magnitude of the impact signal ϵ as a function of norm of instantaneous acceleration for the twisting at waist movement for the sensor attached frontally at the waist. Note that the acceleration values are much smaller (about 0.1-0.2g) compared to the previous plot as the movement at the waist is much slower than that at the leg. (©2007 IEEE)

Table 8.1. Means (μ) and standard deviations (σ) of the coefficients, ρ and ω for climbing up stairs and walking across different subjects. The columns hand, thigh and waist signify the placement of the motion sensor.

Coefficients	Correlation (ρ)			Slope (ω)			
Activity	Hand	Thigh	Waist	Hand	Thigh	Waist	
Climb	μ	0.8226	0.8090	0.8150	0.1337	0.0655	0.1297
	σ	0.0195	0.0161	0.0176	0.0368	0.0222	0.0408
Walk	μ	0.8517	0.8027	0.7985	0.1989	0.1548	0.1779
	σ	0.0278	0.0628	0.0512	0.0599	0.0675	0.0471

quantification of body movements using the impact signal. The amplitude of the impact signal is shown to be very well correlated with the accelerations at the limb locations, a fact that is verified by analyzing the signal amplitudes in time synchronization. The impact signal also shows a linear trend with the treadmill speed in case of the stress test, further validating the idea of motion quantification from the ECG data itself. The results from the treadmill experiment also indicate that the impact analysis is able to successfully adapt

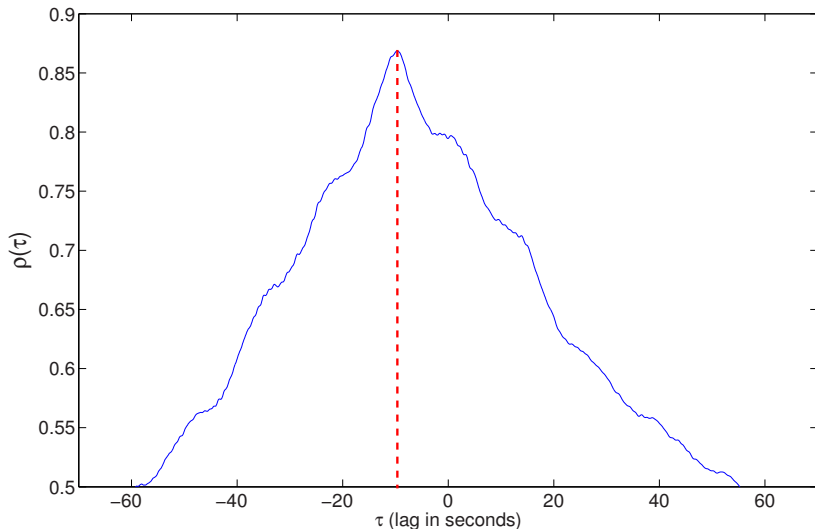


Fig. 8.13. Plot of the cross-correlation between the acceleration signal β and the impact signal ϵ as a function of lag (τ) in seconds for the activity of climbing stairs. The dashed line indicates the maximum correlation, which also gives the time lag between the two signals for the purpose of synchronization. The plot takes triangular shape as expected since the two signals have inherent rectangular shape due to step changes in the levels. (©2007 IEEE)

to stress induced morphological ECG variations, and can be applied even at high activity levels.

The impact signal has been presently used for measuring an extraneous activity superimposed on regular heart activity, be it normal or abnormal. Data sets from both healthy subjects and cardiac patients have been obtained to corroborate our hypothesis. Quantification of the impact signal from cardiac patients requires further analysis pertaining to detections for ectopicity and rhythm disturbances. We observe that the impact signal is unaffected by abnormal QRS morphologies, if they are regular and periodic. However, the method does not work in case of abnormalities like ventricular bigeminy where ectopics occur very frequently. Also, we have restricted ourselves to subjects with normal posture and gait, and results may be different in case of individuals with defects in gait. An indication of this fact is the discrepancy observed in the first stage of the treadmill test, where an abnormal gait results due to difficulty in adjusting to the jerky start of the treadmill. For the chosen lead configuration, it is found that movements of right arm have a greater impact as compared to similar movements of the left arm.

We have limited our studies to single lead (lead-II) observations. However, additional activities could be analyzed if more than one ECG leads are available.

Conclusions

The work presented in the previous chapters is focused on deriving ambulation information from the motion artifact induced due to physical activities in wearable ECG systems (W-ECG). Various methodologies required to achieve that have been discussed in details. We have also provided hardware and calibration details. The experimental protocol is defined for acquisition of data. Finally we have presented results of different experiments. The conclusions derived from this work and scopes for future work in the same area are now discussed in this chapter.

9.1 Conclusions

In this monograph, we have studied the impact of body movement activities (BMA) on the ambulatory ECG signal. Motion artifact in ECG signal induced due to BMA is considered here as a source of useful information related to the physical activities of the subject. The presented work was initiated in view of increasing demand and popularity of W-ECG for ambulatory cardiac monitoring. One such W-ECG, called *locket* and developed at IIT Bombay, is used for collecting the ECG signals during subject ambulation with some specific types of BMA. The ideas generated and hypothesis like “BMA recognition is possible from ECG signal itself” have been verified from the analysis of the real life ECG signals.

The motivation for BMA recognition from ECG signal comes from the fact that if the motion artifacts can be well understood from BMA point of view then it can help us in better interpretation of automated analysis of ECG signal. Since every BMA is performed in a different manner, BMA specific analysis of motion artifact should be possible. We have shown that it is possible to recognize the motion artifact from BMA specific view point.

In Chapter 6, we have shown that the changes in BMA due to activity transition can be detected from the ECG signal itself. This is useful for temporal segmentation of ECG signal. The method used for this task is an

unsupervised learning approach based on recursive principal component analysis (RPCA) of the ECG beats and hence can be implemented on computer based W-ECG. The BMA segmented ECG signal can be useful for automated analysis of ECG signal.

In Chapter 7, we exploit differences in motion artifacts due to different BMAs for recognition of a particular BMA from the ECG signal itself. The possibility of BMA recognition using motion artifacts is verified with a supervised learning approach based on principal component analysis (PCA) of the ECG beats. Several commonplace BMAs such as movements of arm(s), walking, climbing, etc. are recognized from the ECG signal itself. We have attempted various class combinations for improving the recognition rates and formed five different BMA classifiers based on that. We have searched for the most suitable number of principal components for the BMA recognition in order to achieve a high accuracy in recognition and to reduce the computational complexity and found that 6 to 8 eigenvectors would be a good choice for recognition of the BMAs considered in our studies. We also investigated the impact of inter personal variability on this method and found that the subject specific training gives better performance in terms of accuracy in classification. Since the goal of the study is to develop a pervasive monitoring system for individual cardiac patients, initial study suggests that the training of the system should be individually tuned. We have also discussed a BMA specific PCA-based filtering method for removal of the induced motion artifact due to the particular BMA without affecting the morphologies of P and T waves in the cardiac cycle. The performance of the PCA-based filtering is verified by locating P and T waves using an automated method with and without using the proposed filtering. The improvement due to the filtering is shown using the histograms of detected P and T wave locations.

In Chapter 7, we have also re-validated the concept of BMA recognition from motion artifacts using a parametric, supervised learning technique based on a hidden Markov model (HMM). We have suggested the use of an HMM to represent each BMA class, trained from the Gabor features derived from the motion artifact signals corresponding to that particular BMA class. We have also suggested an adaptive filtering technique for separating the motion artifact signal for that purpose. Separation of the estimated cardiac component of the ECG from the composite signal is required to prevent the HMM classifier from working with the artifact signal under the heavy bias of the cardiac component, thus improving the classification accuracy. We have used a fully connected HMM with a few number of states and Gaussian mixture components. BMA classifiers with various class combinations as we found in the earlier PCA-based method are used for recognition of the specific BMA. The recognition rates are found to be better than that in the PCA-based method. We have also studied the effects of length of the test data and selection of number of states and number of mixture models. We have found a length of 5s for the test data to be sufficient for achieving a high level of accuracy in BMA recognition. A smaller length will result in a decreased accuracy and a

longer length will add to further delay without much improvement. The effects of number of states and the actual number of mixture components have been studied for a limited number of combinations and require a more detailed investigation. However, we have shown that it is possible to achieve a very good performance even with a very few states (3-4) and mixture components (3-4) for all the BMA classes. The effect of increasing these numbers remains to be investigated but it will surely increase the complexity while learning the model parameters.

Finally in Chapter 8, we have investigated a different aspect of deriving BMA information from the ECG signal. We derived a measure of motion artifact called impact signal from the ECG signal itself using the RPCA method discussed previously for detection of BMA transitions. The impact signal is validated using acceleration signals acquired from the motion sensors placed on various parts of the body for measurement of the level of BMA. Three different levels of certain commonplace BMAs are considered. The levels are also quantitatively described in terms of acceleration values at different positions on the body. We have shown that the impact signal derived from the ECG signal can be used for measuring the level of a BMA without requiring any extra motion sensors. This is demonstrated by showing the relation between the impact signal and the acceleration signal in terms of their cross-correlation coefficients and the slope of best fitting line. We have also tested the possibility of applying RPCA to ECG signal with different types of QRS morphologies, collected from patients with known cardiac abnormalities. We have found that the method works well irrespective of the QRS morphology provided that the pattern itself is regularly repetitive without serious disturbances in rhythm. The rhythm disturbances or infrequent arrhythmia are manifested as very large values of impact signal and hence can be detected by a simple analysis of RR intervals as well as by using some standard method of arrhythmia classification.

9.2 Scopes for Future Work

In this monograph some of the very preliminary but useful methods for deriving BMA information from ECG signal for wearable ECG monitoring are devised. These methods are found to be suitable even for a single-lead ECG recorder. The lead-II configuration was adopted for the investigation of the feasibility of the BMA recognition from ECG signal. Both the proposed PCA-based and HMM-based methods should work for any lead configuration. However, from the experiments we have observed that the induced motion artifact due to any specific BMA is sensitive to placement of electrodes. For example, the lead-II configuration is more sensitive to right arm movements than that to the similar left arm movements because of the proximity of the electrode to the right arm. This kind of sensitivity of a specific lead to a specific type of BMA can provide more useful information of the BMA in a multiple lead sys-

tem. Therefore, in future we plan to study impact of various types of BMA on different ECG lead configurations. We hope to increase the confidence levels in recognition of BMA using the analysis of multiple ECG leads. It should also be possible to use more sophisticated methods to take advantage of redundant and independent components of information in multiple lead ECG signals.

After achieving a satisfactory level of accuracy in identifying all usual BMAs, it should be possible to conduct some ergonomic studies regarding the routine of physical activities of the cardiac patient wearing ECG recorders without requiring any sophisticated motion sensors. This will help to increase the utility of the W-ECG for personal health monitoring.

Every method discussed here requires detection of R peaks in ECG signal as a preprocessing step. In this work, R peak detection was not a challenging problem and performed in an automated way and accurately even in the presence of motion artifacts due to the various BMAs performed by the subjects. Therefore, it should be possible to use the proposed algorithms as it is for practical applications. However, it is of interest to know how can the R peak detection be made more robust using ECG signals in conjunction with the motion artifact information available from multiple leads. This should be possible because we anticipate that the ECG signal recording in only few of the available ECG leads would be contaminated severely and hence the signals from other less affected ECG leads can be used for detecting the R peaks.

We have discussed an HMM based technique for BMA recognition in Chapter 7 which shows very promising results. However, we need to fully investigate issues related to feature selection, types of HMM and numbers of states and mixture components to further improve in terms of accuracy and computational efficiency. Are the Gabor features the right feature? It requires a thorough investigation to come out with the correct feature set which can capture the distinguishing characteristics of the motion artifacts. Another interesting study would be to relate the hidden states with the dynamics of the body motion. Finally, it is to be recalled that all BMA recognition efforts have been restricted to cases where the heart is not stressed due to activity. With the induced stress, the cardiac component of the signal will also undergo changes. Suitable modifications in the methodology are required to deal with such cases.

In this monograph, the BMA recognition and impact analysis of ECG signal are considered as two separate aspects. It remains to be investigated how both the analyses can be done more efficiently in a unified manner. Moreover, the method of the impact analysis has been tested successfully up to the third level of the Bruce tread-mill test protocol, that is up to approximately a walking speed of 5.5 kmph whereas the BMA recognition is tested at relaxed or normal pace levels of BMA. However, challenges in practical applications of these methods are required to be studied. For example, different types of motorized vehicles have different levels of vibrations and hence can affect the comfort of the patient as well as W-ECG recordings differently. This kind of motion studies can also be useful and can be done in future work. Similarly,

impact of movement on ECG signals and motion artifact generation during sport activities can also be studied. We have used the reconstruction error after appropriate RPCA updating as the measure of impact. Although this yields quite interesting results, this is quite an ad-hoc measure. Is there a better measure of the impact? A detailed study is required in this regard.

Thus we see that the studies related to motion artifact in ECG signals during ambulatory monitoring have wide scopes for future work. Further investigations in this area will definitely improve the analysis and the utility of wearable ECG recorders.

References

1. *User Guide and Specifications USB-6008/6009*. National Instruments.
2. *MSP430F1491 Data Sheet*. Texas Instrument, 2004.
3. *Secure Digital Card*. <http://en.wikipedia.org/wiki>, 2008.
4. V. X. Afonso, W. J. Tompkins, T. Q. Nguyen, and S. Luo. ECG Beat Detection using Filter Banks. *IEEE Trans. on Biomedical Engineering*, 46(2):192–202, Feb. 1999.
5. V. X. Afonso, W. J. Tompkins, T. Q. Nguyen, K. Michler, and S. Luo. Comparing Stress ECG Enhancement Algorithms with an Introduction to a Filter Bank based Approach. *IEEE Engineering in Medicine and Biology Magazine*, 15(3):37–44, May/June 1996.
6. Y. Al-Assaf. Surface Myoelectric Signal Analysis: Dynamic Approaches for Change Detection and Classification. *IEEE Trans. on Biomed. Engg.*, 53(11):2248–2256, Nov. 2006.
7. J. A. Van Alste and T. S. Schilder. Removal of Baseline Wander and Power-line Interference from the ECG by an Efficient FIR filter with a Reduced Number of Taps. *IEEE Trans. on Biomed. Engg.*, 32(12):1052–1060, Dec. 1985.
8. M. Astrom, J. Garcia, P. Laguna, O. Pahlm, and L. Sornmo. Detection of Body Position Changes using the Surface Electrocardiogram. *Medical and Biological Engineering and Computing*, 41(2):164–171, March 2003.
9. M. Astrom, J. Garcia, P. Laguna, and L. Sornmo. ECG based Detection of Body Position Changes. *Signal Processing Report*, SPR-48:1–34, November 2000.
10. M. Astrom, E. C. Santos, L. Sornmo, P. Laguna, and B. Wohlfart. Vectorcardiographic Loop Alignment and the Measurement of Morphologic Beat-to-Beat Variability in Noisy Signals. *IEEE Trans. on Biomedical Engineering*, 47(4):497–506, April 2000.
11. M. Bahoura, M. Hassani, and M. Hubin. DSP Implementation of Wavelet Transform for Real Time ECG Waveforms Detection and Heart Rate Analysis. *Computer Methods and Programs in Biomedicine*, 52(1):35–44, January 1997.
12. J. Bartosik, O. Pahlm, L. Edenbrandt, J. Svensson, W. K. Haisty, and G. S. Wagner. Reconstruction of the Standard 12-Lead ECG from Recordings using Nonstandard Activity-compatible Proximal Limb Lead Positions. *Journal of Electrocardiology*, 28(1):33–38, Jan. 1995.

13. L. E. Baum, T. Petrie, G. Soules, and N. Weiss. A Maximization Technique Occurring in the Statistical Analysis of Probabilistic Functions of Markov Chains. *The Annals of Mathematical Statistics*, 41(1):164–171, Feb. 1970.
14. H. C. Bazett. An Analysis of the Time Relations of Electrocardiograms. *Heart*, 7:353–370, 1920.
15. P. O. Borjesson, O. Pahlm, L. Sornmo, and M-E. Nygards. Adaptive QRS Detection Based on Maximum A Posteriori Estimation. *IEEE Trans. on Biomedical Engineering*, 29(5):341–351, May 1982.
16. C. V. C. Bouten, K. T. M. Koekkoek, M. Verduin, R. Kodde, and J. D. Janssen. A Triaxial Accelerometer and Portable Data Processing Unit for the Assessment of Daily Physical Activity. *IEEE Transactions On Biomedical Engineering*, 44(3):136–147, March 1997.
17. J. R. Boyle, M. K. Karunanithi, T. J. Wark, W. Chan, and C. Colavitti. An Observational Trial of Ambulatory Monitoring of Elderly Patients. In *12th International Conference on Biomedical Engineering (ICBME)*, Singapore, Dec. 2005.
18. C. L. Chang, K. P. Lin, T. H. Tao, T. Kao, and W. H. Chang. Validation of Automated Arrhythmia Detection for Holter ECG. In *IEEE EMBS-1998*, pages 101–103, 1998.
19. P. Chazal, M. O'Dwyer, and R. B. Reilly. Automatic Classification of Heartbeats Using ECG Morphology and Heartbeat Interval Features. *IEEE Trans. on Biomedical Engineering*, 51(7):1196–1206, July 2004.
20. H. S. Chow, G. B. Moody, and R. G. Mark. Detection of Ventricular ectopic beats using Neural Networks. In *Computers in Cardiology*, pages 659–662, Durham, NC, USA, Oct. 1992.
21. C. H. H. Chu and E. J. Delp. Impulsive Noise Suppression and Background Normalization of Electrocardiogram Signals using Morphological Operators. *IEEE Trans. on Biomedical Engineering*, 36(2):262–273, February 1989.
22. D. A. Coast, R. M. Stern, G. G. Cano, and S. A. Briller. An Approach to Cardiac Arrhythmia Analysis using Hidden Markov Models. *IEEE Trans. on Biomedical Engineering*, 37(9):826–836, Sept. 1990.
23. T. Desel, T. Reichel, S. Rudischhauser, and H. Hauer. A CMOS Nine Channel ECG Measurement IC. In *IEEE ASIC-96*, pages 115–118, China, 1996.
24. R. O. Duda, P. E. Hart, and D. G. Stork. *Pattern Classification*, 2nd ed. Wiley Interscience, New York, NY, 2001.
25. W. A. H. Engelse and C. Zeelenberg. A Single Scan Algorithm for QRS-Detection and Feature Extraction. In *Computers in Cardiology*, pages 37–42, 1979.
26. F. Enseleit and F. Duru. Long-Term Continuous External Electrocardiographic Recording: A Review. *Europace*, 8:255–266, April 2006.
27. O. J. Escalona, R. H. Mitchell, D. E. Balderson, and D. W. G. Harron. Fast and Reliable QRS Alignment Technique for High-Frequency Analysis of Signal-Averaged ECG. *Medical and Biological Engineering and Computing*, 31(1):S137–S146, July 1993.
28. R. J. Gibbons et al. ACC/AHA 2002 Guideline Update for Exercise Testing. *American College of Cardiology Foundation and American Heart Association*, 2002.
29. P. A. D. Fabbro and C. A. D. Reis Filho. An Integrated CMOS Instrumentation Amplifier with Improved CMRR. In *IEEE SICSD'02*, pages 57–61, Brazil, 2002.

30. C. L. Fancourt and J. C. Principe. On the use of Neural Networks in the Generalized Likelihood Ratio Test for Detecting Abrupt Changes in Signals. In *IJCNN*, pages 243–248, Como, Italy, 2000.
31. R. Fensli, T. Faersnes, C. Hadland, and T. Gundersen. Wearable Activity Sensor based on Triaxial Accelerometer. In *Scandinavian Conference in Health Informatics, SHI*, Aalborg, Denmark, 2005.
32. G. F. Fletcher, G. J. Balady, E. A. Amsterdam, B. Chaitman, R. Eckel, J. Fleg, V. F. Froelicher, A. S. Leon, I. L. Pina, R. Roxanne, D. A. Simons-Morton, M. A. Williams, and T. Bazzarre. Exercise Standards for Testing and Training: A Statement for Healthcare Professionals From the American Heart Association. *Circulation*, 104:1694–1740, 2001.
33. Nobel Foundation. *Nobel Lectures in Physiology or Medicine, 1922-1941*. World Scientific, 1999.
34. K. Freeman and A. Singh. P Wave Detection of Ambulatory ECG. In *IEEE Engineering in Medicine and Biology Conference*, pages 647–648, Orlando, Florida, USA, 1991.
35. G. M. Friesen, T. C. Jannett, M. A. Jadallah, S. L. Yates, S. R. Quint, and H. T. Nagle. A Comparision of the Noise Sensitivity of Nine QRS Detection Algorithms. *IEEE Trans. on Biomedical Engineering*, 37(1):85–98, January 1990.
36. D. Gabor. Theory of Communication. *J. IEE (London)*, 93(26):429–457, November 1946.
37. J. Garcia, M. Astrom, J. Mendive, P. Laguna, and L. Sornmo. ECG-based Detection of Body Position Changes in Ischemia Monitoring. *IEEE Trans. on Biomedical Engineering*, 50(6):677–685, June 2003.
38. G. H. Golub and C. F. Van Loan. *Matrix Computations*, 3rd ed. Johns Hopkins University Press, Baltimore and London, 1996.
39. P. S. Hamilton. A Comparison of Adaptive and Nonadaptive Filters for Reduction of Power-line Interference in the ECG . *IEEE Trans. on Biomedical Engineering*, 43(1):105–109, January 1996.
40. P. S. Hamilton, M. G. Curley, R. M. Aimi, and C. Sae-Hau. Comparison of Methods for Adaptive Removal of Motion Artifact. In *Computers in Cardiology*, pages 383–386, Cambridge, MA, USA, Sept. 2000.
41. P. S. Hamilton and W. J. Tompkins. Quantitative Investigation of QRS Detection Rules Using the MIT/BIH Arrhythmia Database. *IEEE Trans. on Biomedical Engineering*, 33(12):1157–1165, Dec. 1986.
42. B. R. Hayes-Gill, A. C. Cardoso, N. Meinke, J. A. Crowe, B. Francon, and A. Harrison. A Generic ASIC and DSP based Ambulatory Electrophysiological Recorder. In *IEE Colloquium on Data Logging of Physiological Signals*, pages 9/1–9/3, London, Nov. 1995.
43. J. Healey and B. Logan. Wearable Wellness Monitoring Using ECG and Accelerometer Data. In *Proceedings of the 2005 Ninth IEEE International Symposium on Wearable Computers (ISWC'05)*, pages 220–221, Osaka, Japan, Oct. 2005.
44. N. J. Holter. New Method for Heart Studies. *Science*, 134:1214–1220, Oct. 1961.
45. N. J. Holter and J. A. Generelli. Remote Recording of Physiological Data by Radio. *Rocky Mountain Medical Journal*, 46(9):747–751, Sept. 1949.

46. P-W. Hsia, J. M. Jenkins, Y. Shimoni, K. P. Gage, J. T. Santinga, and B. Pitt. An Automated System for ST Segment and Arrhythmia Analysis in Exercise Radionuclide Ventriculography. *IEEE Trans. on Biomedical Engineering*, 33(6):585–593, June 1986.
47. C-T. Hsieh, G-L. Hsieh, E. Lai, Z-T. Hsieh, and G-M. Hong. A Holter of Low Complexity Design Using Mixed Signal Processor. In *Proceedings of the 5th IEEE Symposium on Bioinformatics and Bioengineering (BIBE'05)*, pages 316–319, Minneapolis, USA, 2005.
48. Y. H. Hu, W. J. Tompkins, J. L. Urrusti, and V. X. Afonso. Applications of Artificial Neural Networks for ECG Signal Detection and Classification. *J. Electrocardiology*, 26:66–73, 1993.
49. F. Jager, R. G. Mark, and G. B. Moody. Analysis of Transient ST Segment Changes During Ambulatory Monitoring. In *Computers in Cardiology*, pages 453–456, Los Alamitos, 1991.
50. F. Jager, R. G. Mark, and G. B. Moody. Characterization of Transient Ischemic and Non-ischemic ST Segment Changes. In *Computers in Cardiology*, pages 721–724, Vienna, Austria, Sept. 1995.
51. F. Jager, R. G. Mark, G. B. Moody, and S. Divjak. Analysis of Transient ST Segment Changes during Ambulatory Monitoring using the Karhunen-Loeve Transform. In *Computers in Cardiology*, pages 691–694, Durham, NC, USA, Oct. 1992.
52. F. Jager, G. B. Moody, and R. G. Mark. Detection of Transient ST Segment Episodes during Ambulatory ECG Monitoring. *Computers and Biomedical Research*, 31(5):305–322, Oct. 1998.
53. F. Jager, G. B. Moody, A. Taddei, and R. G. Mark. Performance Measures for Algorithms to Detect Transient Ischemic ST Segment Changes. In *Computers in Cardiology*, pages 369–372, Los Alamitos, 1991.
54. R. Jane, P. Laguna, N. V. Thakor, and P. Caminal. Adaptive Baseline Wander Removal in the ECG: Comparative Analysis with Cubic Spline Technique. In *Computers in Cardiology*, pages 143–146, Durham, NC, USA, 1992.
55. R. Jane, S. Olmos, P. Laguna, and P. Caminal. Adaptive Hermite Models for ECG Data Compression: Performance and Evaluation with Automatic Wave Detection. In *Computers in Cardiology*, pages 389–392, London, UK, Sept. 1993.
56. R. Jane, H. Rix, P. Caminal, and P. Laguna. Alignment Methods for Averaging of High Resolution Cardiac Signals: A Comparative Study of Performance. *IEEE Trans. on Biomedical Engineering*, 38(6):571–579, June 1991.
57. T. Jernberg, B. Lindahl, M. Hogberg, and L. Wallentin. Effects on QRS-Waveforms and ST-T-Segment by Changes in Body Position During Continuous 12-Lead ECG: A Preliminary Report. In *Computers in Cardiology*, pages 461–464, Lund, Sweden, Sept. 1997.
58. S. Jesus and H. Rix. High Resolution ECG Analysis by an Improved Signal Averaging Method and Comparision with a Beat-to-Beat Appraoch. *J. Biomedical Engineering*, 10:25–32, 1988.
59. S. Kadambé, R. Murray, and G. F. Boudreaux-Bartels. Wavelet Transform-based QRS Complex Detector. *IEEE Trans. on Biomedical Engineering*, 46(7):838–848, July 1999.
60. G. Kavaiya. *How to Achieve Maximum Portable Functionality with Minimal Space*. <http://www.portabledesign.com>, 2008.

61. H. A. Kestler, F. Schwenker, J. Wohrle, V. Hombach, G. Palm, and M. Hoher. Combined Assessment of Beat-to-Beat Micro-Variability and Signal-Averaged ECG parameters. In *IEEE CC 2001*, pages 28:73–28:76, 2001.
62. M. Khalil and J. Duchene. Uterine EMG Analysis: A Dynamic Approach for Change Detection and Classification. *IEEE Trans. on Biomed. Engg.*, 47(6):748–756, June 2000.
63. B-U. Kohler, C. Hennig, and R. Orglmeister. The Principles of Software QRS Detection. *IEEE Engineering in Medicine and Biology*, pages 42–57, Jan.-Feb. 2002.
64. E. Laciár, R. Jane, and D. H. Brooks. Improved Alignment Method for Noisy High-Resolution ECG and Holter Records using Multiscale Cross-correlation. *IEEE Trans. on Biomedical Engineering*, 50(3):344–353, March 2003.
65. P. Laguna, R. Jane, and P. Caminal. Adaptive Feature Extraction for QRS Classification and Ectopic Beat Detection. In *Computers in Cardiology*, pages 613–616, Venice, 1991.
66. P. Laguna, R. Jane, and P. Caminal. Automatic Detection of Wave Boundaries in Multilead ECG Signals: Validation with the CSE Database. *Computers and Biomedical Research*, 27(1):45–60, 1994.
67. P. Laguna, N. V. Thakor, P. Caminal, R. Jane, H-R. Yoon, A. B. Luna, V. Martí, and J. Guindo. New Algorithm for QT Interval Analysis in 24-Hour Holter ECG: Performance and Applications. *Medical and Biological Engineering and Computing*, 28(1):67–73, January 1990.
68. K. Lasanen and J. Kostamovaara. A 1-V CMOS Preprocessing Chip for ECG Measurements. In *IEEE BioCAS-04*, pages S1.2–1 – S1.2–4, Singapore, 2004.
69. C. Levkov, G. Mihov, R. Ivanov, I. Daskalov, I. Christov, and I. Dotsinsky. Removal of Power-line Interference from the ECG: a Review of the Subtraction Procedure. *BioMedical Engineering OnLine*, 4, August 2005.
70. C. Li and C. Zheng. QRS Detection by Wavelet Transform. In *IEEE Engineering in Medicine and Biology Conference*, pages 330–331, San Diego, CA, USA, 1993.
71. C. Li, C. Zheng, and C. Tai. Detection of ECG Characteristic Points using Wavelet Transforms. *IEEE Trans. on Biomedical Engineering*, 42(1):21–28, January 1995.
72. W. Li, H. H. Yue, S. Valle-Cervantes, and S. J. Qin. Recursive PCA for Adaptive Process Monitoring. *Journal of Process Control*, 10(5):471–486, Oct. 2000.
73. S. Luo and W. J. Tompkins. Experimental Study: Brachial Motion Artifact Reduction in the ECG. In *Computers in Cardiology*, pages 33–36, Vienna, Austria, Sept. 1995.
74. S. Mallat and W. L. Hwang. Singularity Detection and Processing with Wavelets. *IEEE Trans. on Information Theory*, 38(2):617–643, March 1992.
75. J. Malmivuo and R. Plonsey. *BioElectromagnetism-Principles and Applications of Bioelectric and Biomagnetic Fields*. Oxford University Press, New York, 1995.
76. P. Maragos and R. W. Schafer. Morphological Systems for Multidimensional Signal Processing. *Proceedings of the IEEE*, 78(4):690–710, April 1990.
77. R. G. Mark, G. B. Moody, and W. H. Olson. Real-Time Ambulatory Arrhythmia Analysis with Microcomputer. In *Computers in Cardiology*, pages 57–62, 1979.

78. J. P. Martinez, R. Almeida, S. Olmos, A. P. Rocha, and P. Laguna. A Wavelet-Based ECG Delineator: Evaluation on Standard Databases. *IEEE Trans. on Biomedical Engineering*, 51(4):570–581, April 2004.
79. J. P. Martinez, S. Olmos, and P. Laguna. Evaluation of a Wavelet-Based ECG Waveform Detector on the QT Database. In *Computers in Cardiology*, pages 81–84, Cambridge, MA, USA, Sept. 2000.
80. R. Martins, S. Selberherr, and F. Vaz. A CMOS IC for Portable EEG Acquisition Systems. *IEEE Trans. on Instrumentation and Measurement*, 45(5):1191–1195, October 1998.
81. M. J. Mathie, B. G. Celler, N. H. Lovell, and A. C. F. Coster. Classification of Basic Daily Movements using a Triaxial Accelerometer. *Medical and Biological Engineering and Computing*, 42(5):679–687, September 2004.
82. M. J. Mathie, A. C. F. Coster, N. H. Lovell, and B. G. Celler. Detection of Daily Physical Activities using a Triaxial Accelerometer. *Medical and Biological Engineering and Computing*, 41(3):296–301, May 2003.
83. M. J. Mathie, A. C. F. Coster, N. H. Lovell, and B. G. Celler. Accelerometry: Providing an Integrated, Practical Method for Long-Term, Ambulatory Monitoring of Human Movement. *Physiological Measurement*, 25(2):R1–R20, April 2004.
84. G. McGlinchey, S. Pietkiewicz, R. Frank, P. Schmidt-Andersen, and F. Hansen. A Programmable Medical Data Acquisition System. In *IEEE CICC*, pages 9.4/1–9.4/6, USA, 1988.
85. A. C. MettingVanRijn, A. Peper, and C. A. Grimbergen. High Quality Recording of Bioelectric Events. I: Interference Reduction, Theory and Practice. <http://www.biosemi.com/publications/artikel3.htm>, Nov. 2005.
86. J. Muhlsteff, R. Schmidt O. Such, M. Perkuhn, H. Reiter, J. Lauter, J. Thijss, G. Musch, and M. Harris. Wearable Approach for Continuous ECG and Activity Patient Monitoring. In *26th IEEE EMBC*, pages 2184–2187, San Francisco, CA, USA, Sept 2004.
87. C.W. Mundt, K.N. Montgomery, U.E. Udoh, V.N. Barker, G.C. Thonier, A.M. Tellier, R.D. Ricks, R.B. Darling, Y.D. Cagle, N.A. Cabrol, S.J. Ruoss, J.L. Swain, J.W. Hines, G.T.A. Kovacs, and W. Carsten. A Multiparamatere Wearable Physiologic Monitoring System for Space and Terrestrial Applications. *IEEE Trans. on Information Technology in Biomedicine*, 9(3):382–391, Sept. 2005.
88. I. S. N. Murthy and G. S. S. Durga Prasad. Analysis of ECG from Pole-Zero Models. *IEEE Trans. on Biomedical Engineering*, 39(7):741–751, July 1992.
89. S. Nag and M. Shojaei-Baghini. *12-Lead Portable ECG Recorder, Project Report*. Department of Electrical Engineering, IIT-Bombay, 2006.
90. S. Nag and M. Shojaei-Baghini. Multi Channel Electrocardiogram Using Custom Analog Chip. In *PICA-2006*, 2006.
91. K. A. Ng and P. K. Chan. A CMOS Analog Front-End IC for Portable EEG/ECG Monitoring Applications. *IEEE Trans. on Circuits and Systems I*, 52(11):2335–2347, Nov. 2005.
92. V. S. Nimbargi. *Characterization of ECG Motion Artifacts using Wavelet Transform and Neural Networks, M. Tech, Thesis*. School of Biosciences & Bioengineering, Indian Institute of Technology Bombay, Powai, Mumbai, 2004.
93. V. S. Nimbargi, V. M. Gadre, and S. Mukherji. Characterization of ECG Motion Artifacts using Wavelet Transform and Neural Networks. In *Indian*

- Conference on Medical Informatics and Telemedicine*, Kharagpur, West Bengal, India, 2005.
94. M. Okada. A Digital Filter for the QRS Complex Detection. *IEEE Trans. on Biomedical Engineering*, 26(12):700–703, December 1979.
 95. O. Pahlm and L. Sornmo. Software QRS Detection in Ambulatory Monitoring - A Review. *Medical and Biological Engineering and Computing*, 22:289–297, July 1984.
 96. J. Pan and W. L. Tompkins. A Real-Time QRS Detection Algorithm. *IEEE Trans. on Biomedical Engineering*, 32(3):230–236, March 1985.
 97. J. S. Paul, M. R. S. Reddy, and V. J. Kumar. Automatic Detection of PVC's using Autoregressive Models. In *19th IEEE EMBC*, pages 68–71, 1997.
 98. T. Pavlidis. Waveform Segmentation Through Functional Approximation. *IEEE Trans. on Computers*, 22(7):689–697, July 1973.
 99. T. Pawar, N. S. Anantakrishnan, S. Chaudhuri, and S. P. Duttagupta. Impact Analysis of Body Movement in Ambulatory ECG. In *29th IEEE EMBC*, pages 5453–5456, Lyon, France, August 2007.
 100. T. Pawar, N. S. Anantakrishnan, S. Chaudhuri, and S. P. Duttagupta. Transition Detection in Body Movement Activities for Wearable ECG. *IEEE Trans. on Biomedical Engineering*, 54(6):1149–1152, June 2007.
 101. T. Pawar, N. S. Anantakrishnan, S. Chaudhuri, and S. P. Duttagupta. Impact of Ambulation in Wearable-ECG. *Springer, Annals of Biomedical Engineering*, 36(9):1547–1557, September 2008.
 102. T. Pawar, S. Chaudhuri, and S. P. Duttagupta. Analysis of Ambulatory ECG Signal. In *28th IEEE EMBC*, pages 3094–3097, New York City, New York, USA, Aug.-Sept. 2006.
 103. T. Pawar, S. Chaudhuri, and S. P. Duttagupta. Body Movement Activity Recognition for Ambulatory Cardiac Monitoring. *IEEE Trans. on Biomedical Engineering*, 54(5):874–882, May 2007.
 104. S. C. Pei and C. C. Tseng. IIR Multiple Notch Filter Design based on Allpass Filter. *IEEE Transactions on Circuits and Systems II: Analog and Digital Signal Processing*, 44(2):133–136, February 1997.
 105. I. Provaznik and J. Holcik. Adaptive Recurrent System for Noise Cancellation and Arrhythmia Detection. In *IEEE Engineering in Medicine and Biology*, pages 1270–1271, Baltimore, MD, USA, Nov. 1994.
 106. L. R. Rabiner. A Tutorial on Hidden Markov Models and Selected Applications in Speech Recognition. *Proceedings of the IEEE*, 77(2):257–286, Feb. 1989.
 107. Y. N. Rao and J. C. Principe. Time Series Segmentation using a Novel Adaptive Eigendecomposition Algorithm. *Journal of VLSI Signal Processing*, 32(1-2):7–17, August 2002.
 108. R. J. Riedel. High-Throughput Amplifier and Analog-to-Digital Converter. *Hewlett-Packard Journal*, 9:16–20, October 1994.
 109. A. Ruha, J. Kostamovaara, and S. Saynajakangas. A CMOS Micropower Heart Rate Indicator. In *IEEE ASIC Seminar and Exhibit*, pages P10–4.1–P10–4.6, USA, 1989.
 110. A. Ruha, S. Sallinen, and S. Nissila. A Real-Time Microprocessor QRS Detector System with a 1-ms Timing Accuracy for the Measurement of Ambulatory HRV. *IEEE Trans. on Biomedical Engineering*, 44(3):159–167, March 1997.
 111. J. S. Sahambi, S. N. Tandon, and R. K. P. Bhatt. Using Wavelet Transforms for ECG Characterization. An On-line Digital Signal Processing System. *IEEE Engineering in Medicine and Biology Magazine*, 16(1):77–83, Jan-Feb 1997.

112. H. M. Schepers, H. F. J. M. Koopman, and P. H. Veltink. Ambulatory Assessment of Ankle and Foot Dynamics. *IEEE Transactions On Biomedical Engineering*, 54(5):895–902, May 2007.
113. J. J. Segura-Juarez, D. Cuesta-Frau, L. Samblas-Pena, and M. Aboy. A Microcontroller-based Portable Electrocardiograph Recorder. *IEEE Trans. on Biomedical Engineering*, 51(9):1686–1690, September 2004.
114. G. R. Shaw and P. Savard. On the Detection of QRS Variations in the ECG. *IEEE Trans. on Biomedical Engineering*, 42(7):736–741, July 1995.
115. Z. Shinar, A. Baharav, and S. Akselrod. R Wave Duration as a Measure of Body Position Changes during Sleep. In *Computers in Cardiology*, pages 49–52, Hannover, Germany, Sept. 1999.
116. M. Shojaei-Baghini, R. K. Lal, and D. K. Sharma. An Ultra Low-Power CMOS Instrumentation Amplifier for Biomedical Applications. In *IEEE BioCAS-04*, pages S1.1–1–S1.1–4, Singapore, Dec. 2004.
117. M. Shojaei-Baghini, R. K. Lal, and D. K. Sharma. A Low-Power and Compact Analog CMOS Processing Chip for Portable ECG Recorders. In *IEEE ASSCC'05*, Hsinchu, Taiwan, Nov. 2005.
118. M. Shojaei-Baghini, R. K. Lal, and D. K. Sharma. An Ultra Low-Power Current-Mode Integrated CMOS Instrumentation Amplifier for Personal ECG Recorders. *World Scientific Journal of Circuits, Systems and Computers*, 17(6), 2008.
119. E. Skordalakis. Recognition of the Shape of the ST Segment in ECG Waveforms. *IEEE Trans. on Biomedical Engineering*, 33(10):972–974, October 1986.
120. E. Soria-Olivas, M. Martinez-Sober, J. Calpe-Maravilla, J. F. Guerrero-Martinez, J. Chorro-Gasco, and J. Espi-Lopez. Application of Adaptive Signal Processing for Determining the Limits of P and T Waves in an ECG. *IEEE Transactions On Biomedical Engineering*, 45(8):1077–1080, August 1998.
121. L. Sornmo. A Model-Based Approach to QRS Delineation. *Computers and Biomedical Research*, 20:526–542, 1987.
122. L. Sornmo. Vectorcadiographic Loop Alignment and Morphologic Beat-to-Beat Variability. *IEEE Trans. on Biomedical Engineering*, 45(12):1401–1413, December 1998.
123. L. Sornmo, O. Pahlm, and M-E. Nygards. Adaptive QRS Detection: A Study of Performance. *IEEE Trans. on Biomedical Engineering*, 32(6):392–401, June 1985.
124. Y. Suzuki. Self-organizing QRS-Wave Recognition in ECG Using Neural Networks. *IEEE Trans. on Neural Networks*, 6(6):1469–1477, November 1995.
125. N. V. Thakor and J. G. Webster. Ground-Free Recording with Electrodes Two ECG. *IEEE Trans. on Biomedical Engineering*, 27(12):699–704, December 1980.
126. N. V. Thakor and J. G. Webster. Electrode Studies for the Long-Term Ambulatory ECG. *Medical and Biological Engineering and Computing*, 23(2):116–121, March 1985.
127. N. V. Thakor, J. G. Webster, and W. J. Tompkins. Design, Implementation, and Evaluation of a Microcomputer-based Portable Arrhythmia Monitor. *Medical and Biological Engineering and Computing*, 22(2):151–159, March 1984.
128. N. V. Thakor, J. G. Webster, and W. J. Tompkins. Estimation of QRS Complex Power Spectra for Design of a QRS Filter. *IEEE Trans. on Biomedical Engineering*, 31(11):702–706, November 1984.

129. N. V. Thakor, Y. Zhu, and K. Pan. Ventricular Tachycardia and Fibrillation Detection by a Sequential Hypothesis Testing Algorithm. *IEEE Trans. on Biomedical Engineering*, 37(9):837–843, September 1990.
130. N. V. Thakor and Y-S. Zhu. Applications of Adaptive Filtering to ECG Analysis: Noise Cancellation and Arrhythmia Detection. *IEEE Trans. on Biomedical Engineering*, 38(8):785–794, August 1991.
131. D. A. Tong, K. A. Bartels, and K. S. Honeyager. Adaptive Reduction of Motion Artifact in the Electrocardiogram. In *IEEE Engineering in Medicine and Biology*, pages 1403– 1404, 2002.
132. P. E. Trahanias. An Approach to QRS Complex Detection using Mathematical Morphology. *IEEE Trans. on Biomedical Engineering*, 40(2):201–205, Feb. 1993.
133. J. K. Udupa and I. Murthy. Syntactic Approach to ECG Rhythm Analysis. *IEEE Trans. on Biomedical Engineering*, 27(7):370–375, July 1980.
134. V. Vaid. *A Silicon Locket for ECG Monitoring, M. Tech, Thesis*. Department of Electrical Engineering, Indian Institute of Technology Bombay, Powai, Mumbai, 2003.
135. H. J. L. M. Vullings, M. H. G. Verhaegen, and H. B. Verbruggen. ECG Segmentation using Time-Warping. *Advances in Intelligent Data Analysis*, pages 275–285, 1997.
136. S. G. Wadia and A. Ambasta. *SiLoc Documentation, Internal Report*. Department of Electrical Engineering, IIT-Bombay, 2004.
137. J. G. Webster. Reducing Motion Artifacts and Interference in Biopotential Recording. *IEEE Trans. on Biomedical Engineering*, 31(12):823–826, December 1984.
138. J. G. Webster. *Medical Instrumentation-Application & Design*. John Wiley & Sons, New York, 3rd edition, August 1998.
139. J. G. Webster. *Medical Instrumentation-Application & Design*. John Wiley & Sons, New York, 4th edition, 2003.
140. S. J. Weisner, W. J. Tompkins, and B. M. Tompkins. A Compact, Microprocessor-based ECG ST-Segment Analyzer for the Operating Room. *IEEE Trans. on Biomedical Engineering*, 29(9):642–649, September 1982.
141. B. Widrow and S. D. Stearns. *Adaptive Signal Processing*. Prentice-Hall, Englewood Cliffs, NJ, 1985.
142. R. F. Yazicioglu, P. Merken, R. Puers, and C. Van Hoof. A $60 \mu\text{W}$ $60\text{nV}/\text{rootHz}$ Readout Front-End for Portable Biopotential Acquisition Systems. *IEEE Trans. on Solid State Circuits*, 42(5):1100–1110, May 2007.
143. C. J. Yen. Analog Integrated Circuit Design for the Wireless Bio-signal Transmission System . In *IEEE AP-ASIC-99*, pages 345–346, Korea, 1999.
144. C. J. Yen, W. Y. Chung, M. C. Chi, and S. H. Lee. A 0.75-mW Analog Processor IC for Wireless Biosignal Monitor. In *IEEE ISLPED-03*, pages 443–448, Korea, 2004.
145. T. Yoshimura, Y. Yonezawa, H. Maki, H. Ogawa, I. Ninomiya, and W. M. Caldwell. An ECG Electrode-Mounted Heart Rate, Respiratory Rhythm, Posture and Behavior Recording System. In *26th IEEE EMBC*, pages 2373–2374, San Francisco, CA, USA, Sept. 2004.
146. W. Zong, G. B. Moody, and D. Jiang. A Robust Open-Source Algorithm to Detect Onset and Duration of QRS Complexes. In *Computers in Cardiology*, pages 737–740, Thessaloniki, Greece, Sept. 2003.

Index

- acceleration signal, 13, 57
- accelerometer, 57, 124
- activity classification, 90, 99
- activity level, 57
- activity recognition, 79
- adaptive recurrent filter, 22, 93
- adaptive threshold, 68
- ambulatory ECG signal, 10
- ambulatory monitoring, 9
- analog to digital converter, 29
- angular shift, 23
- anti-aliasing filter, 85
- arrhythmia, 66, 145
- arrhythmia classification, 82
- arrhythmia monitoring, 16
- artifact signature, 63
- ASIC design, 33
- atrial activity, 18, 110
- atrial depolarization, 3
- atrial extra systole, 68, 75
- augmented lead, 2
- automatic gain control, 18
- bandpass filter, 67
- baseline correction, 17
- baseline signal, 3
- baseline wandering, 5, 16
- beat alignment, 20, 85
- biopotential signal, 27
- biphasic function, 19
- bluetooth, 57
- BMA, 10, 25
- BMA information, 11
- BMA label, 54
- BMA recognition, 11, 54, 55, 79
- BMA transition, 79
- body movement activity, 10, 25, 47, 53, 79
- body stretching, 55
- Bruce protocol, 61, 124, 128
- buffer overflow, 69
- calibration, 46
- cardiac abnormality, 79
- cardiac cycle, 3, 63
- cardiac disorder, 1
- cardiac monitoring, 1, 15
- cardiac patient, 56
- cardiac signal, 10, 66
- cardio-vascular disorders, 123
- clock generator, 42
- common mode noise, 28
- common mode rejection ratio, 32
- commonplace BMA, 54
- composite ECG signal, 9, 10
- composite mean, 20
- composite median, 20
- computer aided analysis, 9
- confusion matrix, 102
- convergence rate, 94
- correlation, 83
- correlation matrix, 84
- coupling capacitance, 28
- covariance matrix, 12, 69, 87
- cross-correlation, 20, 50, 126
- current balancing technique, 34
- dc bias, 10

- dc bias correction, 86
 detection of R peak, 85
 device temperature, 83
 dextrocardia, 55
 diaphragm, 74
 differential amplifier, 32
 differential mode signal, 28
 dimensionality reduction, 88
 direction cosines, 59
 discrete cosine transform, 19, 127
 discrete Fourier transform, 48
- ECG beat, 3, 82
 ECG electrode, 2
 ECG signal, 1
 ectopic beat, 75
 eigenvector, 12
 electrocardiogram, 1, 15
 electrocardiography, 15
 electrode, 1
 electrolyte gel, 30
 electrometer, 15
 electromyograph, 5, 22
 EMG noise, 58
 EMG signal, 22
 equivalent impedance, 6
 error signal, 21
 experimental protocol, 11, 53
- false detection rate, 101
 fibrillation condition, 18
 finite impulse response, 85
 foam pad electrode, 2
 forgetting factor, 69, 126
- Gabor feature, 92
 Gabor filter, 12, 92, 95
 galvanometer, 15
- half-cell potential, 30
 heart axis, 65
 Hermite function, 19
 hidden Markov model, 12, 81, 91, 97,
 144
 HMM, 12
 Holter monitor, 27
- impact analysis, 11, 54
 impact of ambulation, 123
- impact of BMA, 11
 impact signal, 13, 59, 123, 126, 145
 impedance variation, 22
 impulse response, 22, 93, 95
 inflection point, 19
 input impedance, 46
 instantaneous motion, 60
 instrumentation amplifier, 28
 inter-subject variability, 106
 ischemia, 23
 ischemia monitoring, 65, 81
 isoelectric level, 3, 19, 83, 86
- Karhunen-Loeve transform, 23, 81
 kinematics, 123
- least mean squares algorithm, 93
 leave-one-out testing, 107
 left bundle branch block, 75, 136
 local acceleration, 123
 local mean subtraction, 59
 locket, 7, 10, 45
- magneto-resistive sensor, 23
 magnitude spectrum, 48
 matched filter, 18
 maximum likelihood criterion, 12, 92
 microcontroller, 29, 42
 monolithic implementation, 34
 morphological operator, 17, 110
 motion artifact, 1, 5, 10, 63, 80
 motion artifact removal, 12, 91
 motion artifact signal, 10
 motion sensing, 57
 motion sensor, 13, 54, 123
 motion tracker, 57
 moving average filter, 16
 muscle stiffness, 58
 myoelectric signal, 65
- neural network, 81
 noise cancellation, 21
 non-parametric classification, 81
 non-volatile memory, 42
 notch filter, 18, 22
- P wave, 3
 Pan-Tompkins method, 67
 parametric classification technique, 81
 PCA, 12

- PCA-based filtering, 81
personal healthcare device, 27
phase margin, 37
polyphase implementation, 85
posture change, 71
powerline interference, 5, 83
pre-cordial lead, 2
principal component analysis, 12, 81, 144
prosthetic aortic valve, 75
proximal limb lead, 24
pseudo-periodic signal, 16
- QRS complex, 3, 4, 16
QRS detection, 13, 67
QRS morphology, 56
- R wave, 4
reactive stabilization, 127
reconstruction error, 90
recursive principal component analysis, 11, 64, 67
reference signal, 94
repolarization of ventricles, 18
resampling, 69
RPCA, 11
RR interval, 18, 51, 70
- sampling frequency, 54
sensor noise, 10
signal conditioning, 30
signal to noise ratio, 84
Silicon Locket, 28
singularity detection, 17
skin humidity, 83
slew rate, 46
- ST segment, 4, 16
state transition probability, 97
stress test ECG, 61
structuring element, 17
suction electrode, 2
superposition, 10
supervised learning, 12, 79, 88
- T wave, 3, 4, 16
temporal segmentation, 11
time delay neural network, 65
time synchronization, 126
transconductance amplifier, 33
transition detection, 54, 55
trapezoidal rule, 59
treadmill test, 60, 124, 127
- USB interface, 42
- variable length filter, 22
vectorcardiograph, 81
ventricular activity, 17, 110
ventricular bigeminy, 127
ventricular depolarization, 4
ventricular extra systole, 75
- W-ECG, 7, 24, 53
wavelet coefficient, 17
wavelet transform, 81
wearable ECG, 1
wearable ECG recorder, 15
Wilson's central terminal, 2
wireless interface, 57
wireless link, 42
- zero padding, 121